CYCLIC OXIDATION AND BREAKAWAY CORROSION

OF

STAINLESS STEELS IN SO_2 +AIR ATMOSPHERE

CYCLIC OXIDATION AND BREAKAWAY CORROSION OF STAINLESS STEELS IN SO_2 +AIR ATMOSPHERE

By

WEIGUO YANG

M.Eng. (University of Science and Technology Beijing)

A Thesis
Submitted to the School of Graduate Studies
In Partial Fulfillment of the Requirements
For the Degree
Master of Applied Science

McMaster University

MASTER OF APPLIED SCIENCE (2003)　McMASTER UNIVERSITY
(Materials Science and Engineering)　Hamilton, Ontario

TITLE: **Cyclic Oxidation and Breakaway Corrosion of Stainless Steels in SO_2+Air Atmosphere**

AUTHOR: Weiguo Yang, M.Eng. (University of Science and Technology Beijing)

SUPERVISORS: Dr. K. S. Coley
Dr. M. B. Ives

NUMBER OF PAGES: xv, 124

ABSTRACT

In sulfuric acid production plants, stainless steels used in the hot gas converters are subject to both thermal cycling (temperature fluctuation and shutdown) and SO_2+air or SO_3 +air gas mixture. In this study, a discontinuous cyclic oxidation test was designed to simulate the corrosion of stainless steels in SO_2+air gas mixture that is often encountered in the plants. Two commercial stainless steels, 304H (UNS. S30409)(common construction material used in hot gas converter, low Silicon content) and A611 (UNS. S30601) (high Silicon content) were used for testing, and 24-hour cyclic oxidation was conducted in 7%SO_2+air gas mixture at 420°C, 620°C, and 720°C. The exposed samples were examined by SEM (Scanning Electron Microscope) and XRD (X-Ray Diffraction).

At all test temperatures, in both air and SO_2 containing atmosphere, A611 showed a good corrosion resistance and no breakaway corrosion. Silicon was found to be concentrated at the scale/metal interface that is assumed to be in the form of a layer of silica. The good corrosion resistance of A611 is attributed to the silica layer at the interface that both improves the adherence of scale and acts as a barrier to diffusion.

However, for 304H alloy, although at 420°C the alloy was protected under thermal cyclic condition, at both 620°C and 720°C, breakaway corrosion occurred after only two 24hour-thermal cycles. The partial spallation of the scale contributes to the higher weight gain at 620 °C while complete spallation results in a lower weight gain at 720 °C. Due to the partial spallation and therefore the penetration of molecular SO_2, a rapid interface recession was observed at 620 °C leaving no obvious internal oxidation & sulfidation occurring within the alloy; a clear internal oxidation&sulfidation region was found close to the interface at 720 °C. A possible spalling & breakaway corrosion mechanism of 304H is proposed. Also the oxide-metal interface adherence of 304H and A611 is discussed.

ACKNOWLEDGMENTS

I would like to express my gratitude to my supervisors, Dr. Coley and Dr. Ives, for their constant guidance and advice during this work.

I also wish to thank:

McMaster University, the Department of Materials Science & engineering, and Walter W. Smeltzer Corrosion Laboratory for the provision of financial support, and to John Rodda for his assistance during the experiment.

Finally, I would like to thank my wife and daughter for their understanding and strong support during the hard times

TABLE OF CONTENTS

LIST OF FIGURES AND TABLES

CHAPTER 1

INTRODUCTION

High temperature corrosion is often encountered in such areas as high temperature processes in chemical, mineral & metallurgical industries, coal gasification, heat-loaded parts of nuclear reactors, aerospace & gas turbines, diesel engines, pulp and paper, waste incinerators, etc. High temperature corrosion may have various detrimental effects. Due to the loss of material, corrosion reduces the load-bearing capability of constructional materials; considerable material may be lost or wasted in hot working of metals; reaction chambers to which a particular reaction or process is confined may break down.

Most commercial stainless steel or heat resistant steels contain a sufficient amount of chromium, as an alloying element, to ensure the formation of an adherent and compact scale of Cr_2O_3, necessary to protect the alloy from oxidation at high temperatures. However, as the scale grows, it may become susceptible to cracking & spalling due to the formation of other non-adhesive oxides/ spinels, and the development of stresses. Three main sources of scale stress are significant in scale failure [1]:

- External stresses due to the deformation of substrate /scale, e.g., by substrate creep
- Thermally induced stresses resulting from temperature changes and different coefficients of thermal expansion for substrate and scales
- Stresses resulting from oxide growth

Thermal stresses are often larger in absolute value than growth stresses and external stresses [1-2], and therefore thermal stresses often play the most significant role in the failure of protective oxide layers. In practical high temperature technical applications, stainless steels or heat-resistant alloys are often subject to a number of heating-cooling cycles or temperature fluctuations throughout their service life. The cycle may be of a few hours duration as in aircraft turbines, or may be hundreds or even thousands of hours as in the case of industrial power generation plant [2-4].

Typical thermal cycling for gas turbines is shown Table1.1. Repeated cracking & spalling can ultimately lead to the formation of non-protective oxides as the substrate becomes depleted in chromium (Cr), and this leads to "breakaway corrosion" which has considerable practical consequences. By developing an understanding of the steps leading to the breakaway process, it is greatly helpful to understand the corrosion mechanism. This understanding may help develop a procedure for predicting breakaway, or at least for recognizing its precursors at an early stage [5].

Table1.1. Typical duty cycle for various gas turbine engines [3]

Gas Turbine Application	Duty cycle (hour)		
	Minimum	Mean	Maximum
Aero gas turbine (civil)	1	2	8
Aero gas turbine (Military)	1	2	4
Industrial turbine (Base power generation)	500	2000	8000
Industrial turbine (Peak power generation)	2	4	12

Stainless steels (e.g.Alloy 304H) are the current common construction materials in hot gas converters for sulphuric acid production. In these converters the chemical reaction SO_2+$2O_2$=$2SO_3$, occurs, catalyzed by V_2O_5, and therefore the stainless steels are exposed to SO_2, SO_3 and O_2. In this case, the high temperature corrosion of stainless steels involves oxidation and sulfidation /sulfation because of the presence of SO_2 and SO_3, making the corrosion process complex. Also, operating temperatures in these plants are not absolutely well controlled and always have some fluctuation (Figure 1.1); shutdown and restart often occur in plants (shown in table1.2). Thus, stainless steels used in hot gas converters are not only exposed to SO_2/SO_3/ O_2 gas mixtures, but are subject to thermal cycling (heating–cooling cycle).

Previous studies on high temperature corrosion in SO_2/ SO_3/ O_2 gas mixture mainly focused on pure metals (Fe,Cr,Ni) [6-16], and some Ni-based alloys [11-12,17-19] and Fe-based alloys [20-21], and were under isothermal condition. Most studies of cyclic oxidation of alloys have been in air or pure oxidizing atmosphere at high temperature [1-4,22-29]. The cyclic oxidation of alloys in SO_2-containing atmosphere has been rarely reported. Basu et al [30] studied

Table 1.2. Frequency of shutdown in sulfuric acid production plants [31]

Plant	Number of Shutdowns	Duration of Cold Events
Falconbridge	8	46 days total
Cominco	3	2 of 8 days, 1 of 222 days
INCO	2	2 of 2 weeks

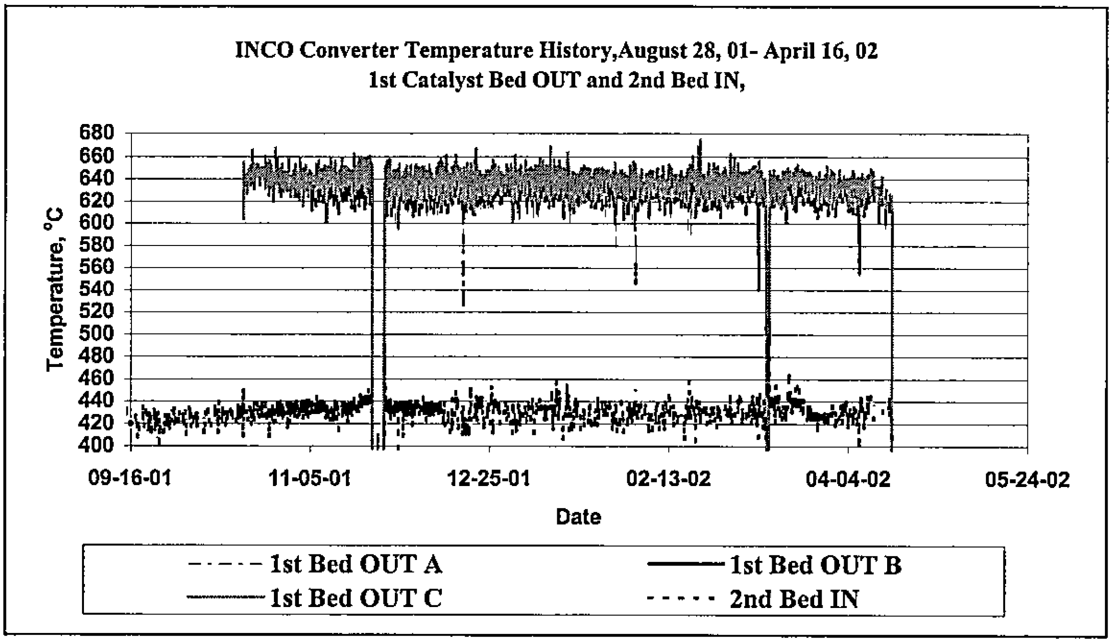

Figure 1.1 INCO gas converter temperature history [31]: For the exit from the 1st and 2nd catalyst beds. This represents the temperature experienced by the hot gas heat exchanger

the cyclic oxidation (20hr-thermal cycle) of Fe-18Cr-20Ni-1.5Mn alloys in a SO_2+O_2 atmosphere, but the content of oxygen was very low (only 50ppm). Thus, the cyclic oxidation of commercial stainless steels in SO_2+O_2 gas mixtures has been rarely reported, and there is almost no report in the literature about the cyclic oxidation of commercial stainless steels in SO_3+O_2 atmosphere (SO_3 is the major sulfur containing species).

From a practical point of view, it is important to gain an insight into the cyclic oxidation behaviour of stainless steels in SO_2+O_2 or SO_3+O_2 gas mixtures in order to understand the corrosion mechanism, especially the breakaway corrosion mechanism of stainless steels in this atmosphere.

This study seeks to investigate cyclic oxidation behaviour of stainless steels (alloys 304H and A611) in SO_2+ air atmosphere and SO_3+air atmosphere, and therefore to provide evidence for developing, improving and selecting materials used in these atmospheres.

CHAPTER 2

LITERATURE REVIEW

2.1 Formation and Growth of Protective Oxide Scales

The preferential or selective oxidation of alloying components such as chromium or aluminum to form continuous external compact scales Cr_2O_3, Al_2O_3 respectively, is an important means of achieving oxidation protection in practical alloys.

The growth of the protective scales usually follows a parabolic rate law or something approximately a parabolic rate law as described by the Wagner equation. The basic assumptions of the Wagner Theory [32-33]: (1) Reactions at the oxide/gas and oxide/metal interfaces are considered to be sufficient rapid for local equilibrium to be established at the interfaces; (2) the lattice diffusion of the reacting atoms or ions or the transport of electrons through the completely dense scale (Figure 2.1) is rate controlling in the overall oxidation reaction.

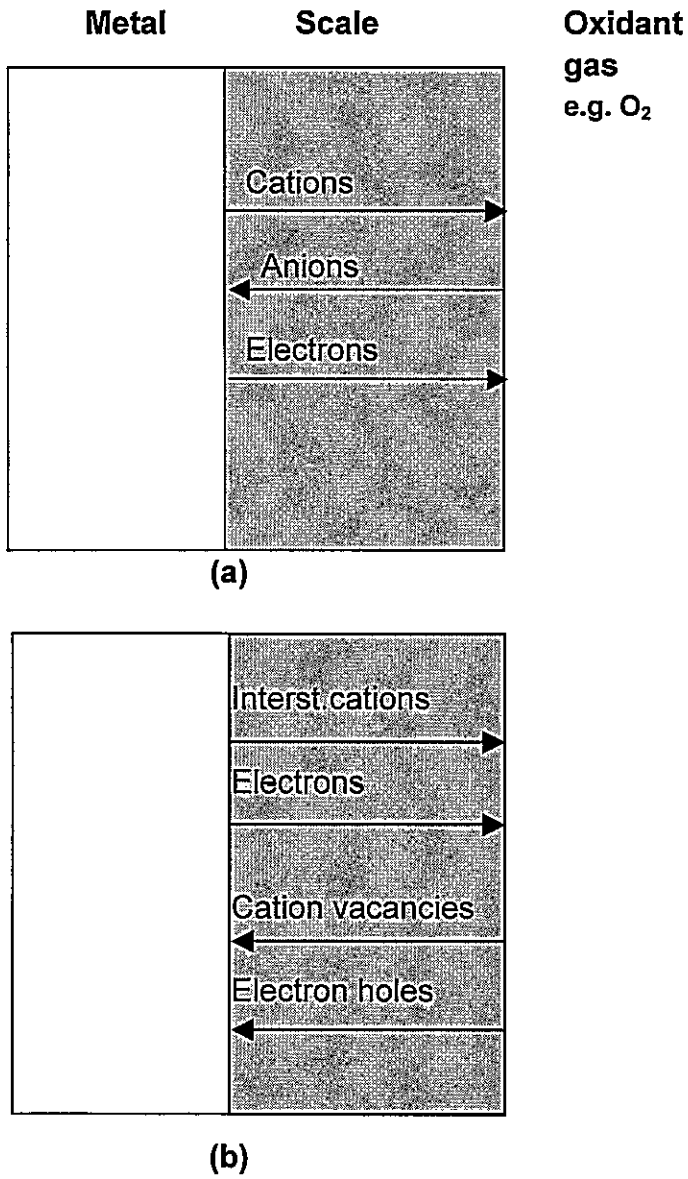

Figure 2.1 (a)Transport process through a dense, single-phase scale growing by lattice diffusion. Transport of reaction atoms or ions or of electrons is rate determining; (b) Transport processes in growing scales in terms of lattice and electronic defects, e.g. of metal vacancies and interstitial ions and of electrons and electron holes [32].

Based on above assumptions, the differential and integrated forms of the parabolic rate equation are given by [32-33]

$$\frac{dx}{dt} = k_p' \frac{1}{x} \qquad (2\text{-}1) \qquad \text{and} \qquad x^2 = 2k_p' t + C = k_p t + C \qquad (2\text{-}2)$$

Where x—the oxides thickness; t--- time; k_p' (or k_p)-- parabolic rate constant; C—integration constant

Wagner derived the expression of parabolic rate constant [33] for the growth of scale (and thereby for k_p') in terms of the self-diffusion coefficients of the metal and oxygen ions, D_M and D_O [33]:

$$k_p' = \frac{1}{2} C_O \int_{P_{O_2}^i}^{P_{O_2}^o} (D_O + \frac{z_c}{z_a} D_M) d \ln P_{O_2} \qquad (2\text{-}3)$$

C_O – Concentration of oxygen in the oxide;

Z_c --- valences of cations;

Z_a --- valences of anions;

$P_{O_2}^o$ ---Partial pressure of oxygen at oxide/gas interface;

$P_{O_2}^i$ ---Partial pressure of oxygen at oxide/metal interface;

Although Wagner considered that the electrons and ions (or corresponding defects) migrate independently of each other, and also assumed that local equilibria exists within the oxide, within the accuracy of experimental results, Wagner theory gives an adequate description of simple metal-gas reactions at high temperature [32]. However at lower temperatures grain boundary diffusion has to be included to obtain reasonable prediction for all but the most defective oxides. For highly protective oxides Wagner theory tends to predict slower corrosion than that occurs in practice [32]. The overall effective diffusion coefficient is expressed as a weighted sum of those for lattice and grain boundary diffusion [32]:

$$D_{eff}=D_l(1-f)+D_bf \qquad (2-4)$$

Where f is the fraction of the total number of diffusion sites that are situated in the boundaries. But, even this method still tends to predict greater protectiveness than occurs for the most protective oxides [32].

2. 2 Degradation & Spallation of Protective Oxide Scales

Breakdown of a protective oxide film (Cr_2O_3, Al_2O_3) is more prone to occur under practical situations involving thermal cycling, where the alloy component is subject to a number of heating-cooling cycles throughout its service life. The cycle may be of a few hours duration, as in aircraft turbines, or may be hundreds or even thousands of hours as in the case of ground based power turbines [2-4]. Since there is a difference in coefficient of thermal expansion between oxide and metal (table 2.1), thermal stresses are induced during a temperature variation (cooling from the process temperature) [22].

The induced thermal stress can cause cracking and eventual spalling of the scale. The thermal stress relates to ΔT, the difference in thermal expansion coefficients of metal and oxide, and the thickness of oxide scale. The expression of thermal stress is as follows [34]:

$$\delta_{ox} = \frac{E_{ox}\Delta T(\alpha_{ox} - \alpha_m)}{(1-\nu)(1+\frac{E_{ox}t_{ox}}{E_m t_m})} \quad (\mathrm{Nm}^{-2}) \qquad (2\text{-}5)$$

where :

δ_{ox} --Stress in oxide

E_{ox} --Elastic modulus of oxide

ΔT --Difference between oxidizing temperature and temperature to which sample is cooled

α_{ox} -- Coefficient of thermal expansion of oxide

α_m -- Coefficient of thermal expansion of metal

E_m -- Elastic modulus of metal

ν --Poisson ratio (assumed to be the same for both phases)

Table 2.1. Linear thermal expansion coefficients of some metal/oxide systems [32]

System	Oxide Coefficient	Temperature Range (^oC)	Metal Coefficient	Temperature Range (^oC)	$\Delta\alpha = \alpha_{ox} - \alpha_m$
Fe/FeO	12.2×10^{-6}	100~1000	15.3×10^{-6}	0~900	-3.1×10^{-6}
Fe/Fe_2O_3	14.9×10^{-6}	20~900	15.3×10^{-6}	0~900	-0.4×10^{-6}
Fe/Cr_2O_3	7.3×10^{-6}	100~1000	15.3×10^{-6}	0~900	-8×10^{-6}
Fe/NiO	17.1×10^{-6}	20~1000	15.3×10^{-6}	0~900	1.8×10^{-6}
Ni/NiO	17.1×10^{-6}	20~1000	17.6×10^{-6}	0~1000	-0.5×10^{-6}
Co/CoO	15.0×10^{-6}	20~900	14.0×10^{-6}	0~350	1×10^{-6}
Cr/Cr_2O_3	7.3×10^{-6}	100~1000	9.5×10^{-6}	0~1000	-2.2×10^{-6}
Cu/Cu_2O	4.3×10^{-6}	20~750	18.6×10^{-6}	0~800	-14.3×10^{-6}

t_{ox}—Thickness of oxide

t_m—Thickness of metal

For thin oxides relative to the metal substrate, the equation can be simplified to give [34]:

$$\delta_{ox} = \frac{E_{ox}\Delta T(\alpha_{ox} - \alpha_m)}{(1-\nu)} \qquad (2\text{-}6)$$

Compressive stress is usually induced in oxide during cooling [34-35]. The relaxation of stresses by creep deformation of the oxide scale or the metal becomes difficult, and therefore cracking and spalling will take place. Two distinct routes for spalling of a compressively stressed oxide were proposed by H. E. Evans [34-35] (shown in Figure 2.2):

Route 1: Initial failure occurs by compressive shear cracking. Further cooling of the sample results in differential contraction strains which drive wedges of the adjacent oxide layer under the segment bounded by the shear cracks and thus produce gradual decohension at the interface.

Route 2: Compressive straining initiates buckling of the oxide over areas of poor adherence. When through thickness cracks form in regions of high tensile stress within the oxide, spalling occurs.

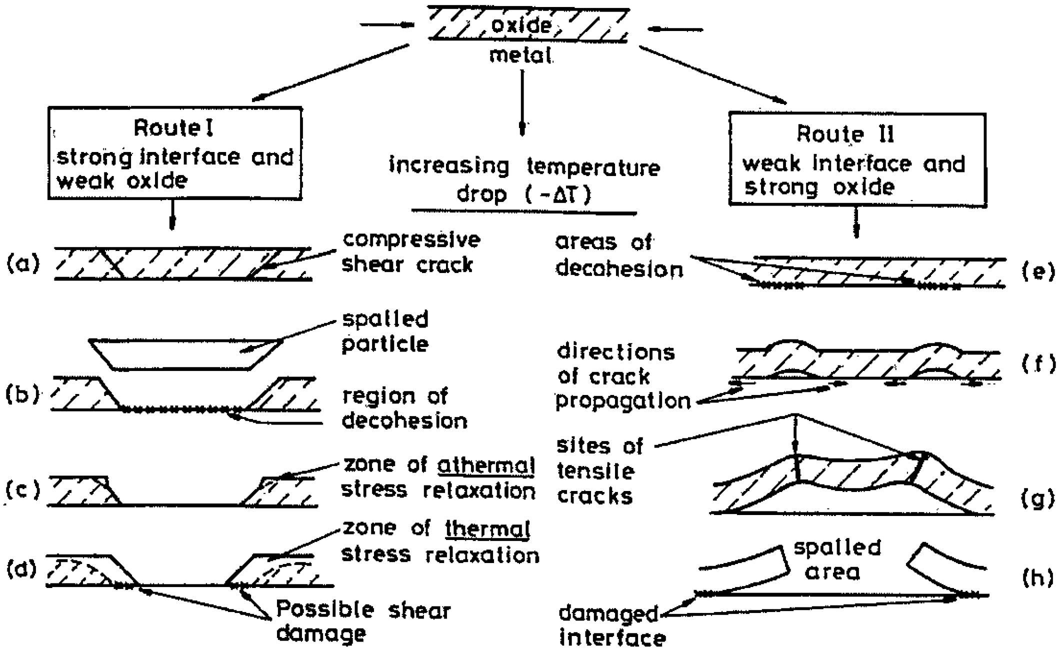

Figure 2.2 Cracking & spalling model [34-35]

Actually, the initiation event does not release spallation from the entire alloy surface and increasingly high oxide strain energy must be provided by the temperature drop, ΔT, to produce further spalling. The key reason for this is that no unique value of critical strain energy, W^*, for spalling can apply to the entire specimen. Rather, there is a variation across the surface such that some areas will spall at low W^*, whereas others will require high values. This situation is illustrated schematically in Figure 2.3

Moon and Lee [23] quantified the fraction, F, of spalled scale resulting from a temperature drop, ΔT, by the expression

$$F = \left[\frac{w_g (\Delta T)^2}{\beta} \right]^m \qquad (2\text{-}7)$$

where:

w_g— weight gain during oxidation(related to the scale thickness) before spalling

m— a positive number which depends on the mechanical properties of the scale

β— a constant that is dependent on the strength of adhension at the alloy-scale interface

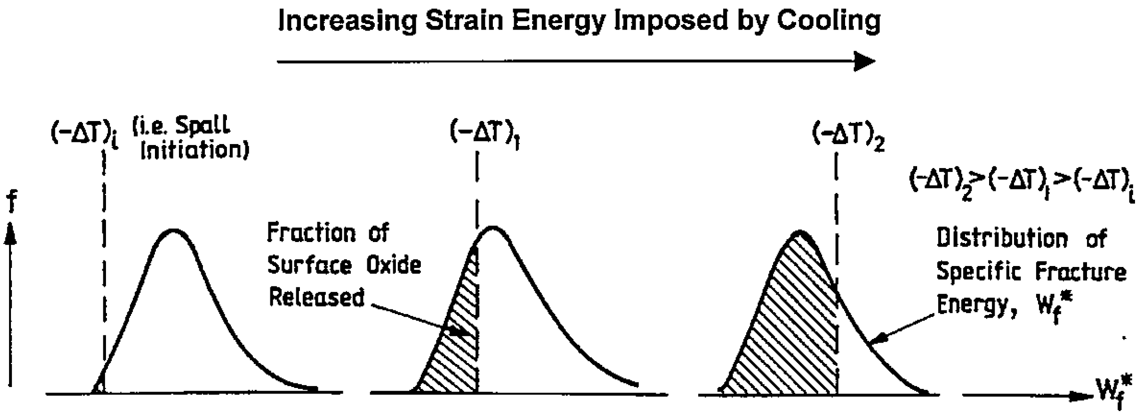

Figure 2.3 Schematic representation of how spatial variation in critical strain energy for spalling determines fraction of oxide spalled during cooling [34]

It is clear that the extent of scale spalling increases with an increase in either or both scale thickness and temperature drop. The difference in the spalling behavior of alloys at a given temperature is directly attributable to the composition-dependent parameters *m* and *β*.

2.3 Breakaway Corrosion of Cr_2O_3 Forming Alloys

High resistance to oxidation of stainless steels is generally associated with the formation of chromic oxide, Cr_2O_3. When stainless steels are exposed to an oxygen-containing atmosphere they will develop a chromia scale (Cr_2O_3). This oxide grows at a very slow rate, since cation diffusion, which is thought to be the process controlling growth of thin scale, is very slow. Lower chromium stainless steels may form $FeFe_{2-x}Cr_xO_4$ with x approaching 2 [36-37], and under certain conditions this spinel oxide may also be relatively protective [36-37]. It is probably true to say that the formation and maintenance of Cr_2O_3 provides the most protective situation. However, even under iso-thermal conditions, the initial presence of Cr_2O_3 scale does not guarantee high oxidation resistance as a function of time. According to Wood [36-37], a number of possible changes can take place in the oxidation behavior with time (Figure 2.4). Under mild oxidizing conditions the protective Cr_2O_3 scale might be maintained, with its growth kinetics

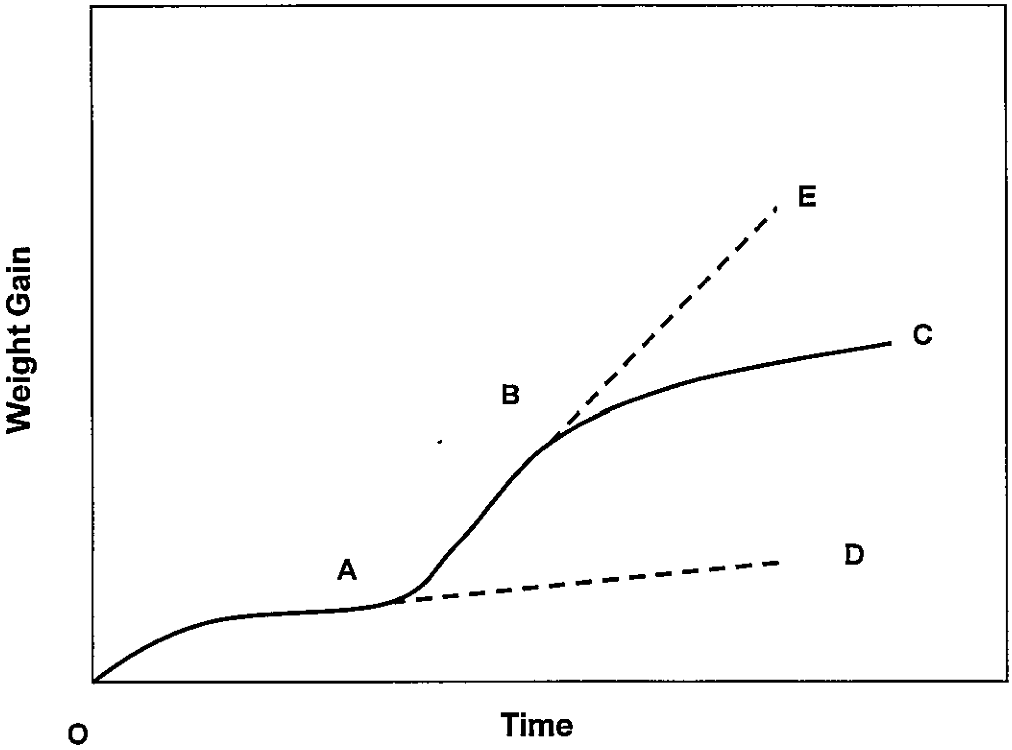

Figure 2.4 Typical oxide growth curves for the oxidation of Fe-Cr alloys and stainless steels [36-37]

approximating a parabolic relationship curve OAD. Yet under more severely oxidizing condition oxide growth may initially follow curve OA, but at some point a sudden increase in growth rate may occur, as indicated by segment AB. This is known as " breakaway", and its occurrence is dependent on alloy composition, environment, and time. Depending on alloy composition and environmental conditions, the rapid oxidation may continue, as indicated by segment ABE, or the oxidation rate may again decrease, as shown by segment BC. This breakaway corresponds to the formation of a duplex scale consisting of an inner layer of spinel oxide (such as $FeCr_2O_4$) and an outer layer of ferric oxide (Fe_2O_3).

Two different mechanisms for the formation of iron-rich oxides nodules have been proposed:

(1) "The diffusional theory "[37-38] proposes that Fe and possibly Ni enter the Cr_2O_3 film and transform it to a spinel structure. Evans et al [39] classified this as Intrinsic Chemical Failure (InCF).

(2) "The cracking theory" [37-38] deals with the stresses that can develop during oxide growth. These stresses can cause the oxide to crack so that the

underlying matrix is exposed, allowing iron-rich oxides to grow. Evans et al [39] classified this as Mechanically Induced Chemical Failure (MICF). Mechanical damage to the protective oxides can be repaired by self-healing if prior exposure has not reduced the Cr level below the critical concentration for healing [39].

Under thermal cycling conditions, the induced thermal stress is often larger in absolute value than growth stresses and external stresses [1-2], and therefore thermal stress greatly contributes to the failure of protective oxide layer. Thermal stress causes cracking & spalling. The damaged areas can be repaired by a self-healing process before solute (Cr,Al) near the alloy surface is depleted to a critical concentration, the minimum concentration required for the formation of a external protective oxide layer. However, repeated spalling & self-healing eventually leads to the depletion of solute (Cr,Al) and therefore the formation of non-protective oxides. Thus, breakaway corrosion takes place. This situation is illustrated schematically in Figure 2.5. Compared to isothermal oxidation, cyclic oxidation could cause rapid breakaway corrosion depending on the spalling and self-healing process.

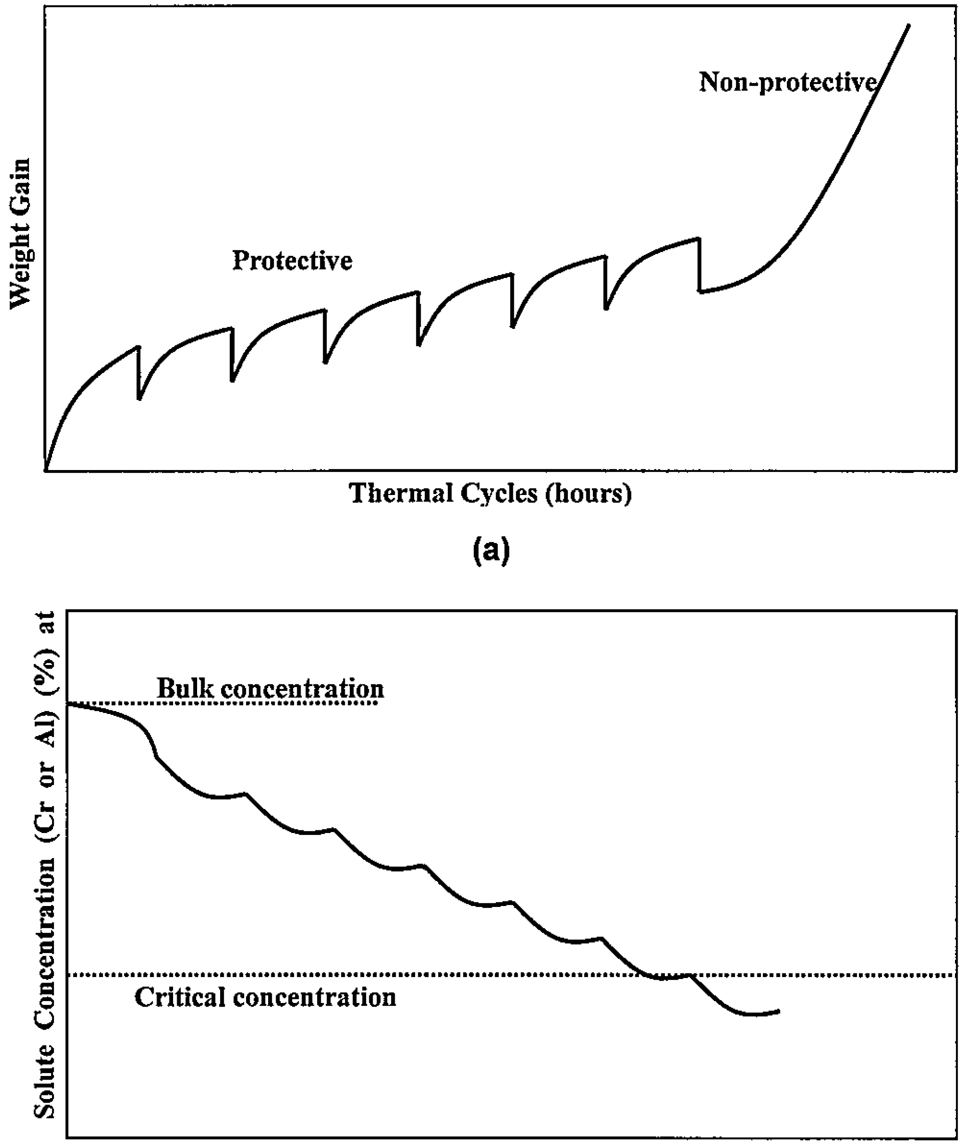

(a)

(b)

Figure 2.5 Spalling – Self-healing – Breakaway Model (Based on Nesbitt model) [24]: (a) Variation of weight gain with thermal cycles (time); (b) Variation of the solute concentration at oxide-metal interface with thermal cycles (time)

Nicholls et al [3] described and defined the growth—spalling&self-healing –breakaway process as a "birth"-"life"-"death" cycle using the following terminology:

"Birth"—Following an initial period of oxide nucleation and transient oxidation, a protective oxide scale grows with parabolic or sub-parabolic oxidation kinetics.

"Life"— Continued growth and effectiveness of the protective scale. Damaged areas, caused by mechanical failures, can be healed on re-exposure to oxidant by the formation of new oxide. This self-healing process may involve the formation of scales, which may or may not have a similar composition to that of the protective scale depending on the availability of protective scale forming elements within the alloy.

"Death"-- Once the near surface concentration of scale forming elements is depleted below a critical level, as a result of the continued oxidation, non-protective oxidation ensues, forming rapidly growing base metal oxides. These grow in a catastrophic manner at high temperatures, leading to what is term "breakaway oxidation". The formation of the non-protective oxides defines the end of the useful lifetime of the component.

When stainless steels or heat resistant alloys are exposed to an atmosphere containing SO_2, although the oxygen pressure is high enough for the formation of a protective Cr_2O_3 layer on the alloys, internal sulfidation often occurs and sulfides are often found to form beneath the oxide layer and /or within the alloy substrate [5,30]. Although the detailed mechanism for transport of sulfur through oxides is still poorly understood, it has been extensively discussed empirically and theoretically in the literature [5,30,40-52]. Two mechanisms are possible: (1) sulfur solubility and diffusion in oxides; (2) molecular transport of SO_2 via physical defects Detailed thermodynamic treatments of sulfur transport were made by Singh and Birks [40], who reported that the minimum partial pressure of SO_2 required to promote sulfide formation at the metal-scale interface by molecular transport of SO_2 is very low while that for formation of sulfides at the metal-scale interface by the solution-diffusion mechanism is high.

The formation of internal sulfides can modify the corrosion rates by one of the following mechanisms [53]:

- The sulfides are chromium sulfides and deplete the matrix of chromium, permitting its rapid oxidation and sulfidation.

- The sulfides are chromium sulfides and oxidize much more rapidly than metal, releasing sulfur that diffuses further inward to form new sulfides.
- The sulfides are liquid sulfides that either flux the protective chromium oxide or penetrate rapidly into the metal developing the irregular interface that is seen in many alloys.
- The sulfides lead to spalling of the protective Cr_2O_3 scale on thermal cycling because of different thermal-mechanical properties.

Even for high temperature corrosion under isothermal conditions, the presence of sulfur in the gas mixture could accelerate breakaway corrosion of alloys. Choi et al [5] studied the breakaway corrosion of Fe-20%Cr alloy at 950°C in a CO-CO_2-SO_2-Ar atmosphere and found that sulfur causes rapid breakaway of the protective Cr_2O_3 layer (Figure 2.6). The breakaway corrosion involves the development of a "critical microstructure" characterized by considerable intrusions of relatively coarse Cr_2O_3 fingers into the metal substrate. The formation of these coarse Cr_2O_3 fingers involves the progressive oxidation of the internal sulfides CrS that is formed beneath the outer Cr_2O_3 layer by SO_2 penetration (Figure 2.7).

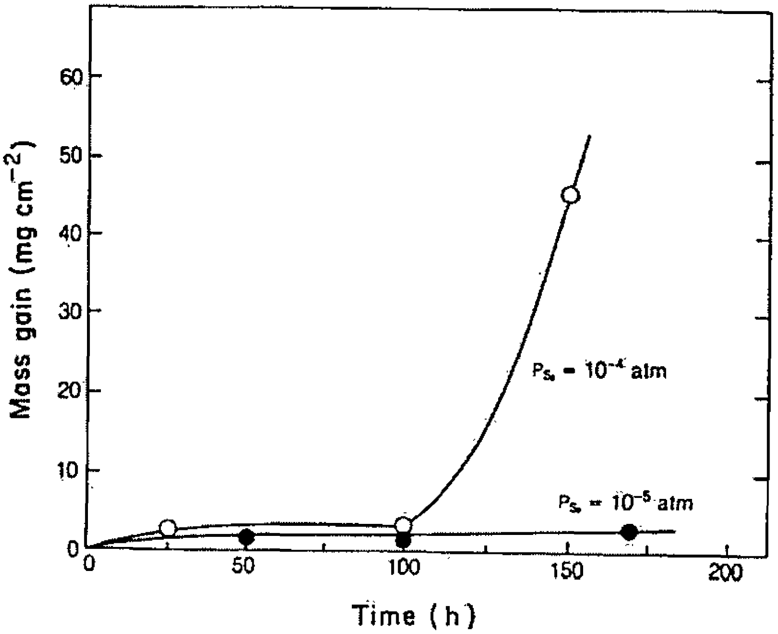

Figure 2.6 The isothermal corrosion of Fe-20%Cr at 950°C in CO-CO_2-SO_2-Ar atmosphere [5]

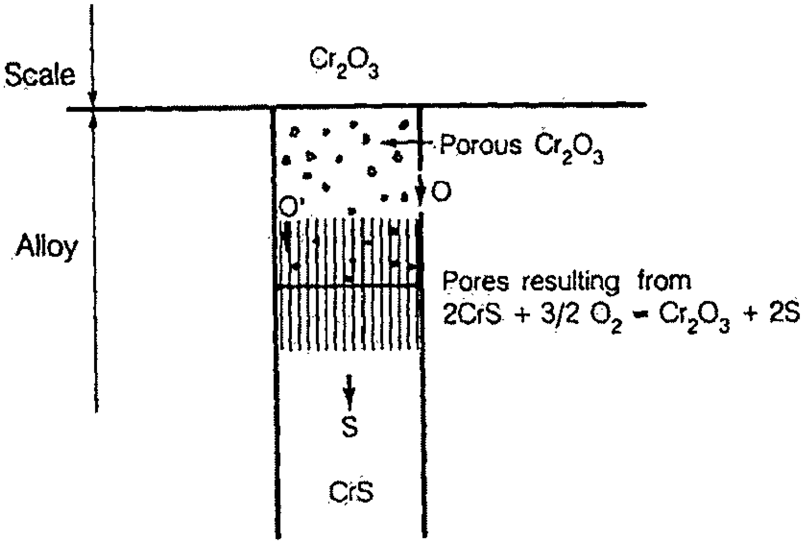

Figure 2.7 A schematic representation of the mechanism of the development of a porous Cr_2O_3 intrusion by the progressive oxidation of a CrS "leader" [5]

The cyclic oxidation of alloys in SO_2 containing atmospheres has been rarely reported. Basu et al [30] studied cyclic oxidation of austenitic Fe-18Cr-20Ni-1.5Mn alloys (containing 0,0.6, and 1.5wt. % Si) in a SO_2-O_2(50ppm) gas mixture at 900°C. All the large-grained, conventionally processed alloys exhibited breakaway oxidation during cyclic oxidation because these alloys had poor self-healing characteristics due to their large grain size and severe depletion of Cr near the surface of the alloy. However, the rapidly solidified, fine-grained alloys that contained less than 1.5wt%Si exhibited very protective oxidation behavior. The breakaway corrosion was caused by molecular SO_2 penetration through iron oxides formed on spalled area of Cr_2O_3 on the alloy and the subsequent formation of sulfides within substrate of alloy. This process accelerates depletion of Cr near the surface of alloys. The breakaway mechanism is shown in Figure 2.8.

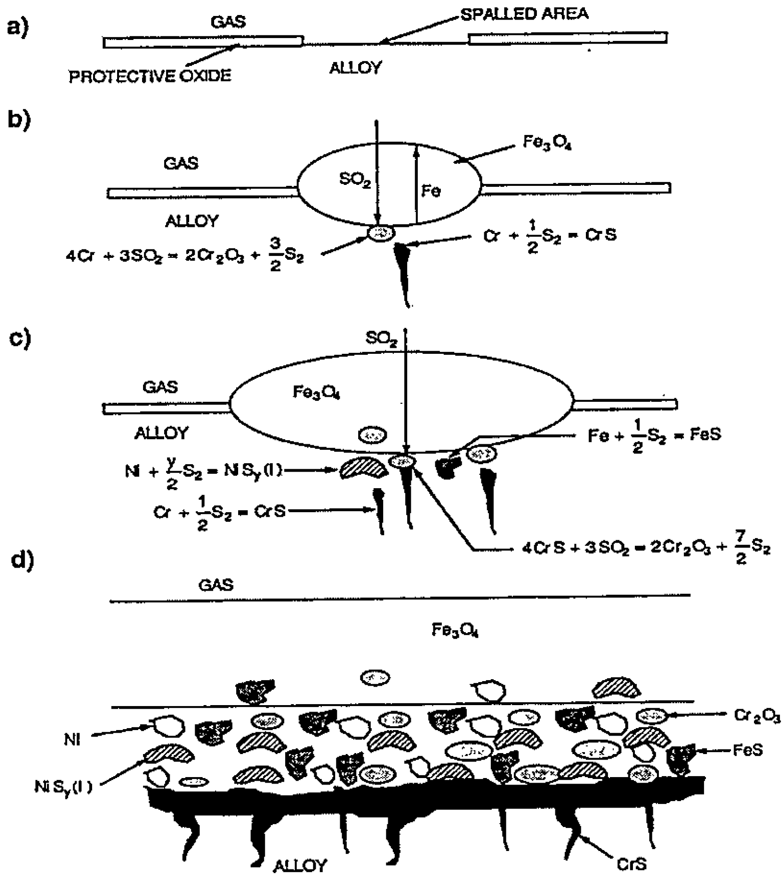

Figure 2.8 Mechanism of breakaway corrosion of alloy (Fe-18Cr-20Ni containing 1.45% Mn and 1.62%Si) during cyclic oxidation in SO_2-O_2 (50ppm O_2) gas mixture at 900°C[30]

2.4 Internal Oxidation

When oxygen dissolves and diffuses into the alloy phase during oxidation, the less noble alloying elements may react to form oxide particles and precipitate at an advancing reaction front within the base metal matrix; this precipitation process is called internal oxidation [54]. The internal oxidation of alloys occurs through the dissolution and diffusion of atomic oxygen into the base metal at the external surface (in the absence of an external oxide scale) or at the metal/external scale interface.

The criteria for internal oxidation are [54]: (1) The free energy of the formation of the solute oxide must be more negative than that of the solvent oxide; (2) The solvent metal must exhibit a significant solubility and diffusivity of the oxidant;(3) The solute concentration must be lower than that required to cause a transition from internal to external oxidation; and (4) Surface-oxide layers must not prevent oxygen diffusion into the substrate.

Previous studies of internal oxidation focused on dilute binary alloys (i.e. A-B alloys). Although, internal oxidation was studied a long time ago, significant progress was made by Wagner, and then, many studies have been done by Rapp

[54], Gesmundo et al [55]. The mechanism of internal sulfidation is similar to that of internal oxidation, and both internal oxidation and internal sulfidation take the same form [56].

Simultaneous internal oxidation by two or more oxidants (such as O, S, N etc.) has also been studied [57-62]. This is considerably more complex, but practically important.

2.4.1 Internal Oxidation in the Absence of External Scale Formation

In the case of exclusive internal oxidation of a binary A-B alloy, according to Wagner, if diffusion control is maintained, the depth ξ of the internal oxidation zone is a parabolic function of the time t, so that

$$\xi = 2\gamma(D_O t)^{1/2} \qquad (2\text{-}8)$$

and the velocity of reaction front motion is

$$\frac{d\xi}{dt} = \gamma\left(\frac{D_O}{t}\right)^{1/2} \qquad (2\text{-}9)$$

Where D_O is the diffusivity of oxygen in the base metal A, and γ is a dimensionless parameter. Assuming that previously precipitated particles do not interfere with the diffusion of oxygen in the base metal A, the diffusion equation for the one-dimensional diffusion of oxygen, namely,

$$\frac{\partial N_O}{\partial t} = D_O \frac{\partial^2 N_O}{\partial x^2} \qquad (2\text{-}10)$$

may be solved for the boundary conditions

$$x=0, t>0, N_O = N_O^{(S)} \qquad (2\text{-}11)$$

$$x \geq \xi, t>0, N_O = 0 \qquad (2\text{-}12)$$

where x -- distance from the outer surface;

N_O -- mole fraction of oxygen in the base metal;

$N_O^{(S)}$ -- mole fraction of oxygen at the external surface.

Analogously, the solution of the diffusion equation for the less noble alloying element B, namely,

$$\frac{\partial N_B}{\partial t} = D_B \frac{\partial^2 N_B}{\partial x^2} \qquad (2\text{-}13)$$

may be solved for the boundary conditions

$$x>0, t=0, N_B = N_B^{(0)} \qquad (2\text{-}14)$$

$$x \leq \xi, t>0, N_B = 0 \qquad (2\text{-}15)$$

where N_B -- Mole fraction of B in the base metal;

$N_B^{(0)}$ -- Mole fraction of B in the bulk alloy.

Thus, the solutions are

$$N_O = N_O^{(S)} \left\{ 1 - \frac{erf[x/2(D_O t)^{1/2}]}{erf(\gamma)} \right\} \qquad (2\text{-}16)$$

$$N_B = N_B^{(0)}\left\{1 - \frac{erf[x/2(D_B t)^{1/2}]}{erfc(\gamma\phi^{1/2})}\right\} \qquad (2\text{-}17)$$

where $\phi = D_O/D_B$.

At the precipitation front of the zone of internal oxidation, the flux of oxygen atoms arriving from the external surface must be equivalent to the flux of B atoms arriving from the bulk alloy if an insoluble and stoichiometric BO_v oxide particle is precipitated, so that,

$$\lim_{\varepsilon \to 0}\left[-D_O\left(\frac{\partial N_O}{\partial x}\right)_{x=\xi-\varepsilon} = vD_B\left(\frac{\partial N_B}{\partial x}\right)_{x=\xi+\varepsilon}\right] \qquad (2\text{-}18)$$

where v – the number of oxygen ions per B ion in the oxide BO_v.

Substitution of Eq. (2-16) and (2-17) into (2-18) gives:

$$\frac{N_O^{(S)}}{vN_B^{(O)}} = \frac{G(\gamma)}{F(\gamma\phi^{1/2})} \qquad (2\text{-}19)$$

The auxiliary functions G and F are defined by

$G(u) = \pi^{1/2} u \exp(u^2) erf(u)$ and $F(u) = \pi^{1/2} u \exp(u^2) erfc(u)$

Therefore the parameter γ may be obtained from a graphical or numerical solution of Eq. (2-19). Two limiting case exist.

(i) If $\gamma \ll 1$ and $\gamma\phi^{1/2} \gg 1$, which is equivalent to $\frac{D_B}{D_O} \ll \frac{N_O^{(S)}}{N_B^{(0)}} \ll 1$,

$$\gamma \cong \left[\frac{N_O^{(S)}}{2\nu N_B^{(0)}}\right]^{1/2} \qquad (2\text{-}20)$$

In this case, the movement of the precipitation front is essentially completely determined by the diffusion of oxygen in the base metal.

(ii) If $\gamma \ll 1$ and $\gamma\phi^{1/2} \ll 1$, which is equivalent to $\frac{N_O^{(S)}}{N_B^{(0)}} \ll \frac{D_B}{D_O} \ll 1$,

$$\gamma \cong \frac{\pi^{1/2}\phi^{1/2}N_O^{(S)}}{2\nu N_B^{(0)}} \qquad (2\text{-}21)$$

In this case, the rate of outward diffusion of the alloying element as well as the rate of inward diffusion of oxygen are important in determining the oxidation kinetics.

2.4.2 Transition From Internal to External oxidation

Wagner further calculated the solute enrichment in the internal oxidation zone, and the solute enrichment, α, is defined as [54-55]

$$\alpha = \frac{f}{N_B^{(0)}} \qquad (2\text{-}22)$$

If f is the mole fraction of solute B present as BO_V in the internal oxidation zone and V is the molar volume of the base metal, then f/V is the molar concentration of the oxide BO_V per unit volume. Consider the advance by a distance $d\xi$ of the precipitation front of area A in a time dt; in the volume element A $d\xi$, the number of moles of oxides BO_v precipitated, which by definition equals (f/V) A dξ, must also equal the number of moles of B arriving at the front through diffusion from $x>\xi$, i.e. [54].

$$\left(\frac{f}{V}\right)Ad\xi = \lim_{\varepsilon\to 0}\left[\frac{D_B A}{V}\left(\frac{\partial N_B}{\partial x}\right)_{x=\xi+\varepsilon}\right]dt \qquad (2\text{-}23)$$

Substituting $\frac{d\xi}{dt}$ (from Eq.2-9) and $\frac{\partial N_B}{\partial x}$ (from Eq.2-17) gives [54-55]

$$\alpha = \frac{1}{F(\gamma\phi^{1/2})} \qquad (2\text{-}24)$$

Wagner proposed that the transition from internal to exclusive external oxidation occurs when the solute content in a binary alloy is sufficient to form a critical volume fraction of internal oxide precipitate at the reaction front, f_v^*, under which BO_v forms directly on the alloy surface. The critical volume fraction of BO_v is related to the critical mole fraction of oxide, f^*, by the form [55]

$$f_v^* = f^*\psi \qquad (2\text{-}25)$$

where ψ is the fraction of the molar volume of BO_v to that of the alloy, so that the corresponding critical value of the mole fraction of B in the alloy, $N_B^{(0)*}$, becomes [55]

$$N_B^{(0)*} = \frac{1}{\psi}f_v^* F(\gamma\phi^{1/2}) \qquad (2\text{-}26)$$

and may be calculated if f_v^* and the other parameters required are known.

2.4.3 Internal Oxidation in the Presence of an External Scale

In most practical applications of alloys at high temperatures the internal oxidation zone is formed below an external oxide scale of the base metal. Analytical solutions for the kinetics of internal oxidation in combination with a parabolically thickening external scale have been given by Rhines et al and Maak, whose work was summarized and treated by Rapp [54] and Gesmundo et al [55].

Retaining the same symbols as above, except that $N_O^{(S)}$ now equals the oxygen mole fraction at the metal/scale interface. ξ is the position of the internal oxidation front measured from the original alloy surface; X, the thickness of the metal consumed, is given in the form

$$X^2 = 2k_c t \qquad (2\text{-}27)$$

where k_c is the parabolic rate constant related to the growth of the external scale. Thus, the effective thickness of the internal oxidation zone is given by ξ-X (see Figure 2.9).

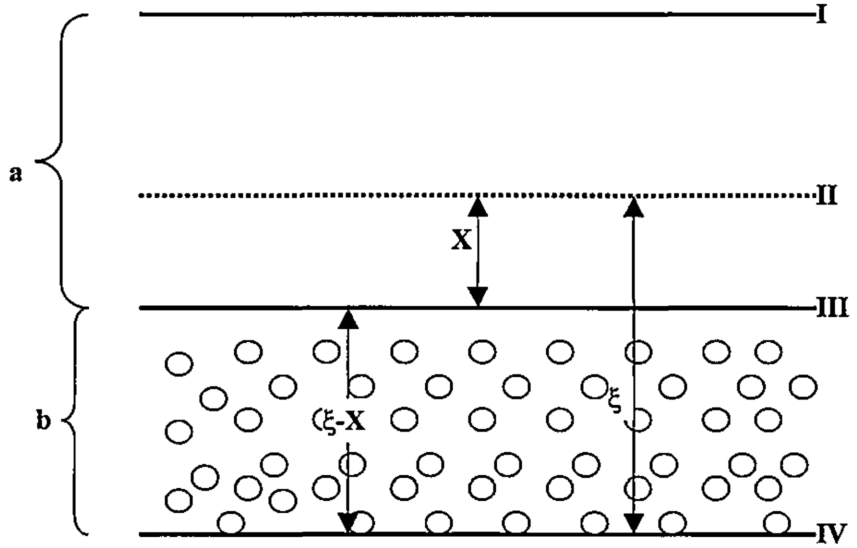

Figure 2.9 Schematic illustration of an oxidized sample. I, actual scale/gas interface; II, original alloy/gas interface; III, actual alloy/scale interface; IV, internal oxidation precipitation front; a, external scale (oxide AO); b, internal oxidation zone; X, thickness of alloy consumed; ξ, position of the internal oxidation front measured from the original alloy surface; (ξ-X), actual thickness of the internal oxidation zone [55]

The boundary conditions for diffusion equations (the same as above) are as follows [54]:

$x \geq \xi$, t>0, $N_O=0$ (2-28)

x=X, t>0, $N_O = N_O^{(S)}$ (2-29)

$x \leq \xi$, t>0 , $N_B = 0$ (2-30)

$x \geq 0$,t=0 , $N_B = N_B^{(0)}$ (2-31)

The solution gives the concentration profiles [54-55]:

$$N_O = N_O^{(S)} \left\{ \frac{erf(\gamma) - erf[x/2(D_O t)^{1/2}]}{erf(\gamma) - erf(k_c/2D_O)^{1/2}} \right\} \tag{2-32}$$

$$N_B = N_B^{(0)} \left\{ 1 - \frac{erf[x/2(D_B t)^{1/2}]}{erfc(\gamma\phi^{1/2})} \right\} \tag{2-33}$$

Substituting Eq. (2-32) and (2-33) into Eq.(2-18), an expression for γ , comparable to Eq. (2-19) but more involved, was obtained. Following Wanger's treatment, one obtains [55]:

$$\frac{N_O^{(S)}}{\nu N_B^{(O)}} = \frac{erf(\gamma) - erf[(k_c/2D_O)^{1/2}]}{erf(\gamma)} \frac{G(\gamma)}{F(\gamma\phi^{1/2})} \tag{2-34}$$

2.4.4 Multiple Internal Oxidation

Industrial process gases commonly contain multiple oxidants, such as oxygen, sulfur, and nitrogen etc. Thus, oxygen, sulfur, and nitrogen can diffuse into the alloy, and internal oxidation, internal sulfidation, and internal nitridation might take place simultaneously.

Meigering [57] proposed the concept of simultaneous internal oxidation of alloys by two different oxidants and developed some mathematical treatment. Recently, much more attention has been paid to this area [58-61], and Gesmundo et al [58] have refined the analysis and made it more general. The formalism given by Gesmundo et al is used in this text. A schematic diagram of the model is shown in Figure 2.10. The Model is based on the following assumptions [59]:

(a) The more stable precipitate forms immediately beneath the alloy surface and the less stable product is formed at greater depths where oxidant (1) is at a very low activity but oxidant (2) retains a high activity;

(b) Neither precipitate significantly affects the inward oxidant diffusion rates;

(c) The less stable precipitate is converted to the more stable one via a displacement reaction involving dissolved oxidant (1);

(d) The displacement reaction goes rapidly to completion at precisely defined oxidant activity values, i.e. no intersolubility exists between the two precipitate compounds;

(e) No thermodynamic or kinetic interaction of importance takes place in

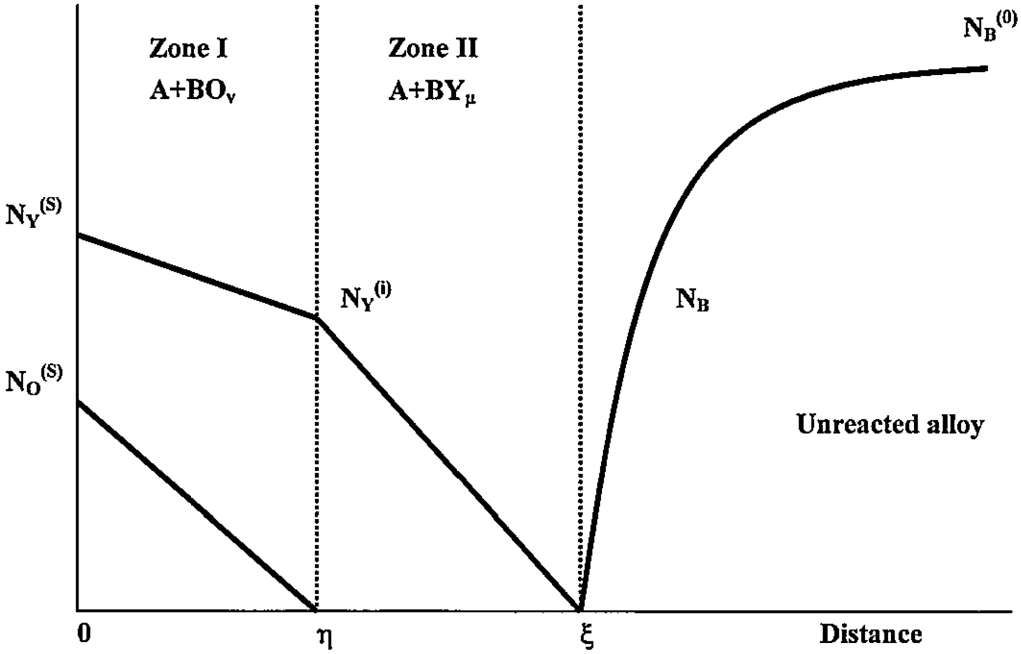

Figure 2.10 Schematic concentration profiles for the simultaneous internal oxidation of a binary A-B alloy by two oxidants (O and Y) in the absence of external AX scales [58]

the solution phase;

(f) Precipitates are extremely stable, and $N_M \cong 0$ throughout the two precipitate zones.

According to Gesmundo et al [58], the two internal oxidation fronts are assumed to move inward according to the parabolic rate law in the form

$$\eta = 2\gamma_1 (D_O t)^{1/2} \tag{2-35a}$$

or $$\eta = 2\gamma_2 (D_Y t)^{1/2} \tag{2-35b}$$

and $$\xi = 2\delta \; (D_Y t)^{1/2} \tag{2-36}$$

At the interface between two internal oxidation zones ($x=\eta$), oxygen will displace Y from BY_μ according to the reaction:

$$\nu O + BY_\mu = \mu Y + BO_\nu \tag{2-37}$$

Gesmundo et al's treatment [51] gives following equations:

$$\frac{N_O^{(S)}}{\nu N_B^{(0)}} = \frac{G(\gamma_1)}{F(h_2)} \tag{2-38}$$

and $$\frac{N_Y^{(S)}}{\mu N_B^{(0)}} = \frac{G(\delta) - G(\gamma_2)}{F(h_2)} \tag{2-39}$$

where $h_2 = \gamma \phi_2^{\;1/2}$, and $\phi_2 = D_Y / D_B$.

If $N_B^{(0)}, N_O^{(S)}, N_Y^{(S)}, D_O, D_Y$, and D_B are known, then the simultaneous solution of Eq. (2-38) and (2-39) will give the two kinetic parameters γ_1 (or γ_2) and δ for a given system.

However, Gesmundo et al's mathematical treatment of simultaneous internal oxidation by two oxidants was not verified by experiment, and cannot be applied to the formation of two internal compounds mixed together in the same region, which has been encountered in the oxidation-sulfidation situation [59,62].

In addition, Gesmundo et al's mathematical treatment is limited to A-B binary alloys in the absence of external oxides. Guan et al [63-65] extended the mathematical treatment of internal oxidation by a single oxidant from A-B binary alloys to A-B-C ternary alloys. Therefore, although the mathematical treatment is very complex, combining Guan's work, it is possible to extend Gesmundo et al's treatment to A-B-C ternary alloy in absence or presence of external oxides, and this work has not been reported yet.

Thus multiple internal oxidation (by two or more oxidants) is still poorly understood. Further research, both theoretical and experimental, is very necessary in the future.

2.5 Summary

Thermal stress greatly contributes to the cracking & spalling of protective oxide layers (e.g. Cr_2O_3). Repeated spalling and self-healing eventually causes the depletion of Cr near the surface of chromia-forming alloys and therefore leads to breakaway corrosion of the alloys.

The presence of SO_2, and therefore penetration of molecular SO_2 via physical defects and the formation of sulfides at the substrate/scale interface, causes quick breakaway corrosion during the cyclic oxidation of chromia-forming alloys. However, cyclic oxidation behavior of chromia-forming alloys, especially commercial alloys, in $SO_2/SO_3/O_2$ atmosphere have been rarely reported, and the corrosion mechanism in this atmosphere, especially under thermal cyclic conditions is still poorly understood.

The breakdown of protective oxides (e.g. Cr_2O_3), exposing the base metal, eventually leads to internal oxidation. Previous studies mainly focus on internal oxidation of binary alloys by a single oxidant. Internal oxidation by multiple oxidants is still poorly understood, and further research, both theoretical and experimental, is very necessary and of practical significance.

CHAPTER 3

EXPERIMENTAL METHODS

AND

ANALYTICAL TECHNIQUES

3.1 Experimental Objective

The experimental objective is to determine the breakaway corrosion mechanism in SO_2+ air (non-equilibrium gas: major SO_2) and SO_3+air (equilibrium gas: major SO_3) atmospheres typical of sulfuric acid production.

3.2 Experimental Preparation

3.2.1 Sample Preparation

304H (UNS. S30409) and A611 (UNS.S30601) stainless steels are used for test. 304H is the common construction material used in the gas converter in sulfuric acid plants. A611 stainless steel has higher silicon content compared to 304H. The chemical composition of the alloys is shown in table 3.1. Test specimens of 2.5cm × 2.5cm × thickness were prepared, and polished by SiC #220, #1200, #4000.

Table 3.1. Chemical composition of commercial stainless steels

Alloys	Cr	Ni	Mn	Si	C	N	S	P
304H	18.43	8.53	1.35	0.45	0.058	0.0057	0.003	0.027
A611	17.30	17.33	0.61	5.26	0.01	0.017	0.001	0.017

After the experiment was finished, exposed samples were cooled down to room temperature, and transferred to a desiccator prior to analysis.

3.2.2 Gas Environment

A 7%SO_2 + air gas mixture was used in this study. If the gas mixture is equilibrated converting SO_2 to SO_3 in the furnace, the resulting gas composition is mainly SO_2, SO_3, O_2, and N_2. Gas equilibrium partial pressures (at 420°C, 620°C,and 720°C), calculated by use of the FactSage software, are shown in table3.2. However, the compositions of the gas mixture entering and leaving the reaction tube were checked by a portable Reich Test (Figure 3.1). It was found that gas equilibrium was not achieved when using gold catalyst (Figure 3.2) and the majority of sulfur species was SO_2.

The portable Reich test, shown in Figure 3.1, consists of aspirating the gas through standard iodine solution (starch indicator added) until it is decolorized. Water which flows out from the graduated cylinder by lowering the aspirating bottle produces suction, and the amount measures the volume of the aspirated gas. From the amount of iodine used in the test and the volume of the aspirated gas, the percentage of SO_2 can readily be calculated ($SO_2 + 2I + 2H_2O = H_2SO_4 + 2HI$). Details are given in reference 66.

Since the presence of SO_3 in the exit gas, the gas was passed through solid NaCl [16] to remove SO_3 before it entered into the Reich test apparatus. The difference of SO_2 between ingoing and outgoing gas is used to determine the amount of SO_3 in the exit gas.

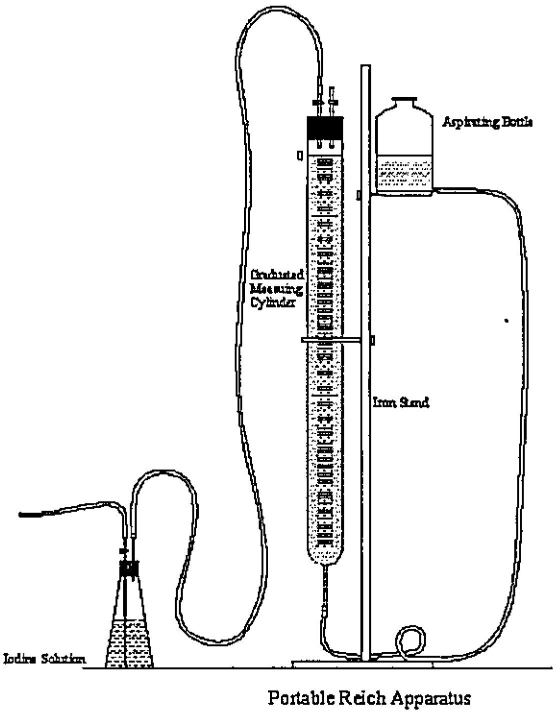

Figure 3.1 Portable Reich test apparatus [66]

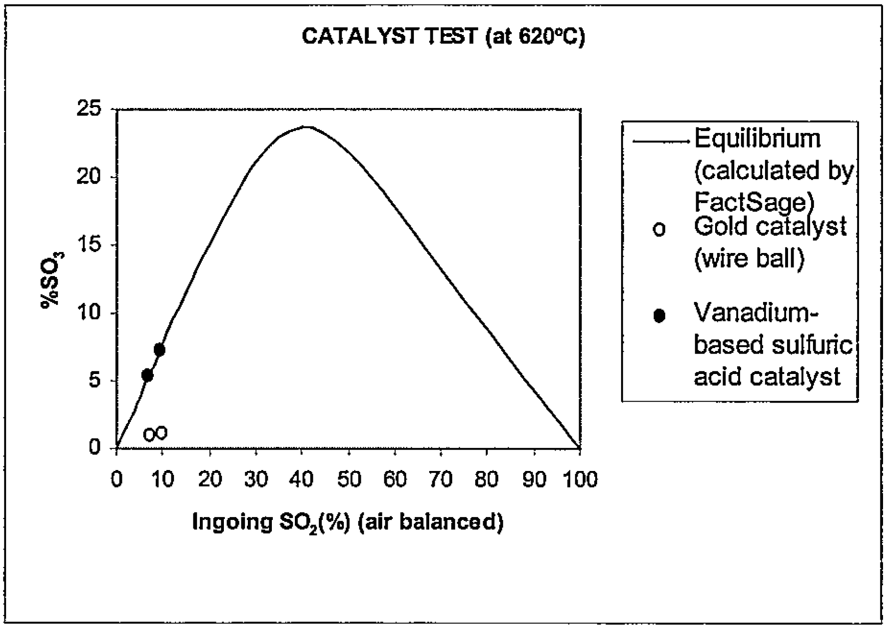

Figure 3.2 Reich test results for catalyst (620°C)

Table 3.2. Gas equilibrium partial pressure (1atm)

Temp.	Equilibrium Partial Pressure (atm)				
(°C)	N_2	O_2	SO_2	SO_3	S_2
420	0.7612	0.1663	5.158×10^{-4}	0.072	1.15×10^{-52}
620	0.75446	0.17342	0.017516	0.054387	2.046×10^{-37}
720	0.74665	0.18218	0.038582	0.032558	1.6539×10^{-32}

3.3 Experimental Methods

In sulfuric acid production plants, stainless steels are subject to both thermal cycling and SO_2/air or SO_3+air. Therefore, it is of practical importance to investigate cyclic oxidation behavior, and especially breakaway corrosion mechanisms of stainless steels. To simulate actual situations in sulfuric acid production plants, the discontinuous cyclic oxidation test is employed.

"Discontinuous cyclic oxidation " involves periodically removing samples from a furnace, cooling from exposure temperature to room temperature, weighing (an electro-balance of 0.1mg readability was used), and then putting them back into the furnace to continue the exposure.

Provided that the specimens are contained in ceramic crucibles, both the total extent of attack (gross mass gain) and of scale spallation can be determined separately. Spalled scales were collected to evaluate weight change.

The discontinuous cyclic oxidation experimental apparatus used in this study is shown schematically in Figure 3.3.

Thermal cycling performance is illustrated in Figure 3.4.

Advantages of discontinuous cyclic oxidation are as follows:

- Suitable for long-term thermal cycle duration: e.g. 20 ~5000h
- Suitable for manual operation
- Simulate actual situations in plants (i.e. shut down)

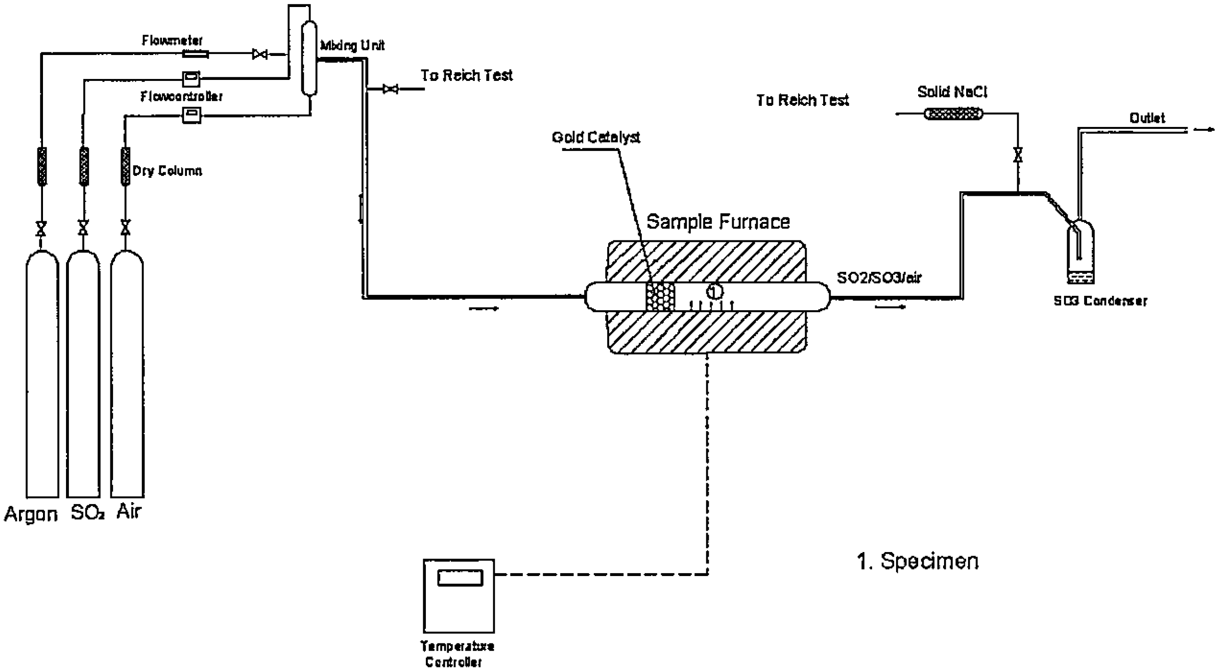

Figure 3.3 Schematic representation of discontinuous cyclic oxidation test apparatus

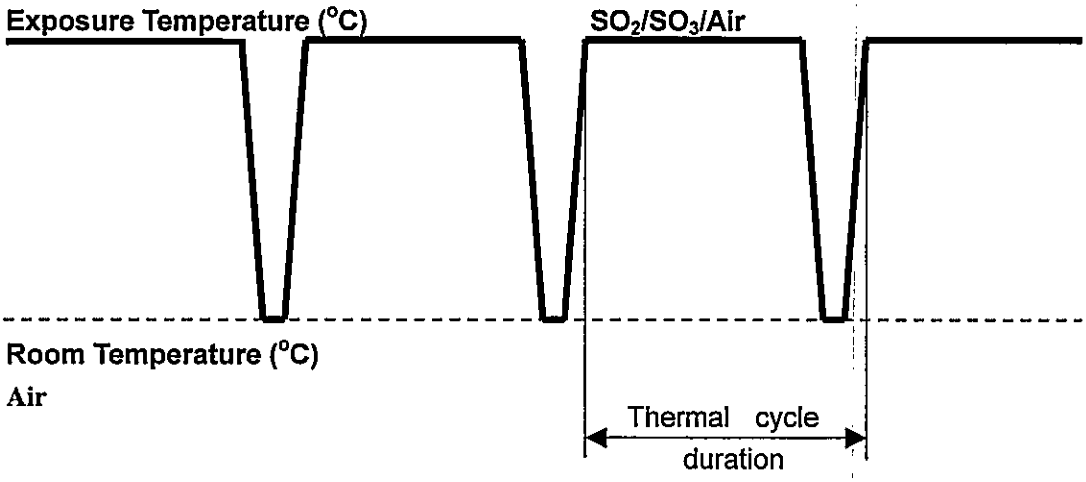

Figure 3.4 Schematic illustration of thermal cycling performance in SO_2 +air atmosphere

3.4 Analytical Techniques

To understand detailed breakaway mechanisms of stainless steels, work should be done on analysis of samples after cyclic or isothermal oxidation in SO_2 +air atmospheres. Analytical techniques, which are used to examine exposed samples (longer term or short term), should be employed. In this study, SEM (Scanning Electronic Microscopy) and XRD (X-Ray Diffraction) were used for this purpose.

3.4.1 Scanning Electron Microscopy (SEM)

Scanning Electron Microscopy (SEM) was used to examine the morphological features of samples after exposure (including surface morphology, and cross-section micrograph). For analysis of cross-section of samples, the samples were mounted in epoxy under vacuum, polished and coated with gold to avoid electrical charge build up. An energy dispersive X-ray analyzer (EDAX) attached to the SEM is used to identify the elements and their distribution in the samples after exposure.

3.4.2 X-Ray Diffraction (XRD) Analysis

XRD provides a powerful technique for phase identification. Depending on compound and number of phases, only the phases present in relatively high concentration (≥**5%** [67]) can be detected. Because of this detection limit, some phases of very small amounts might not be identified by XRD, although they do exist.

In this study, XRD was mainly used for analyzing spalled scales (or removed scales) to identify phases.

CHAPTER 4

EXPERIMENTAL RESULTS

4.1 Introduction

The cyclic oxidation behavior of stainless steels (304H & A611) was investigated in SO_2 + air. In this chapter, the results of the cyclic oxidation behavior of these alloys are presented, and results of analysis of exposed samples by SEM and XRD are given.

4.2 Experimental Results

4.2.1 Cyclic Oxidation Behavior

When 304H stainless steel was isothermally exposed to 7%SO_2 + air atmosphere at 620°C, the alloy exhibited slow corrosion kinetics (Figure 4.1, and Figure 4.2), protection lasting for several hundreds of hours. However, by shutting down the furnace twice, breakaway corrosion occurred and protectiveness of the alloy was lost. In this case the SO_2 and air were shut off, and samples were kept in the furnace and cooled to room temperature. After the first shutdown, the samples

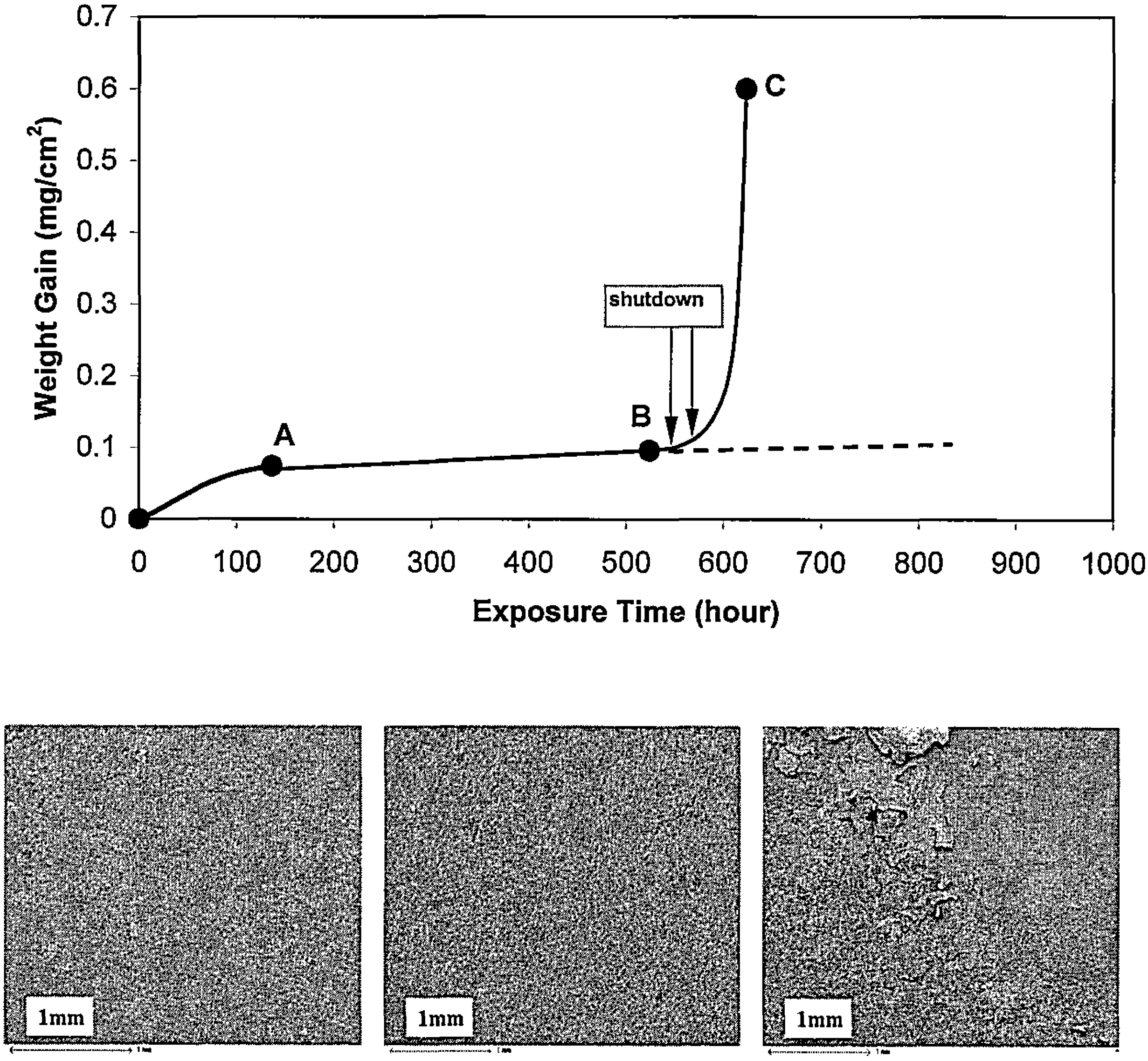

A B C

Figure 4.1 Isothermal oxidation of 304H in 7%SO_2+air at 620°C (+2 shutdowns). First shutdown: hold for 12 hours; second shutdown: hold for 76 hours (Samples were kept in furnace during shutdown)

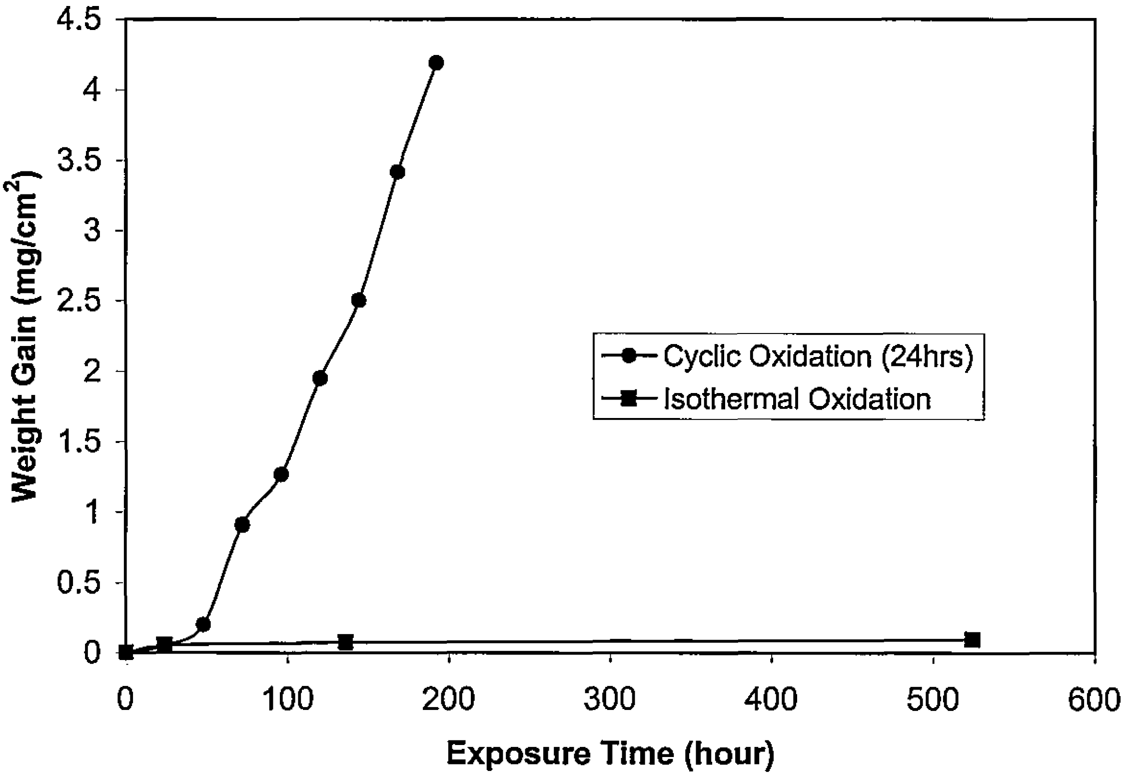

Figure 4.2 Isothermal & cyclic oxidation of 304H in 7%SO_2+air at 620°C (Cyclic oxidation: 24-hour thermal cycle, cooled to room temperature)

remained at room temperature in the furnace for 12 hours. After the second shutdown, samples remained at room temperature in the furnace for 76 hours,

Figure 4.2 shows the effect of a series of 24-hour thermal cycles on the corrosion of alloy 304H in 7%SO_2 + air at 620°C. After two thermal cycles, breakaway corrosion occurred, and a very high corrosion rate was observed. However, for isothermal exposure (no thermal cycling), there was no breakaway corrosion observed and the alloy was protected for 524 hours.

Figure 4.3 puts together the effects of shutdown, 24-hour cyclic oxidation, and temperature fluctuation, to show the influence of temperature stability on the corrosion behavior of 304H stainless steel. In addition, as shown Figure 4.3, if the temperature is not well controlled (temperature fluctuation occurred and lasted for about 2 hours: about 595 ±50°C) after starting the experiment (595°C), the alloy was not protective and showed a high corrosion rate compared to isothermal exposure (the temperature was well controlled, and there was no temperature fluctuation after starting furnace). It appears that a protective oxide layer failed to form on the alloy surface

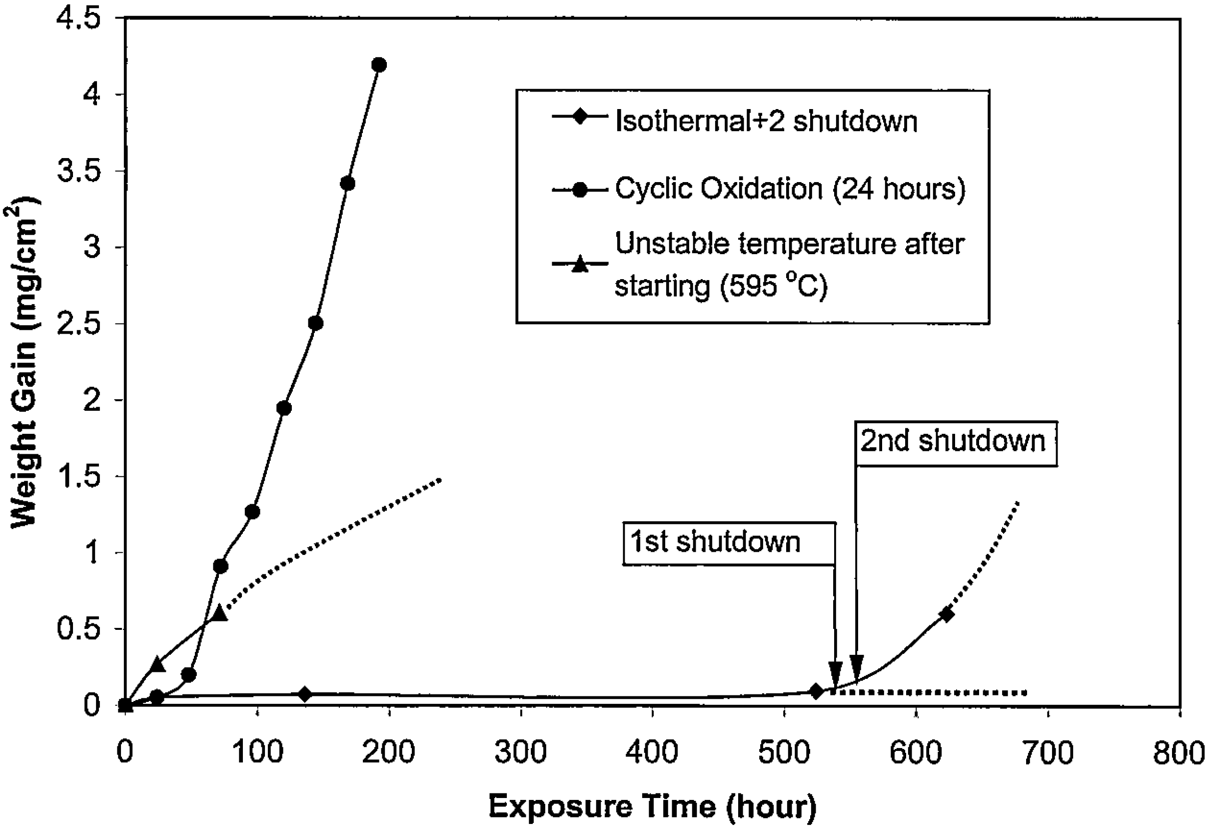

Figure 4.3 Effects of 24-hour thermal cycle, temperature fluctuation, and shutdown on corrosion behavior of 304H in 7%SO_2+air at 620°C (Cyclic oxidation: 24-hour thermal cycle, cooled to room temperature)

under unstable temperature at the beginning of the experiment. Figure 4.3 clearly demonstrates significant effects of temperature stability on corrosion behavior of 304H stainless steel in 7%SO_2+air atmosphere.

Although there are significant effects of thermal cycling on the corrosion behavior of 304H in a 7%SO_2+air atmosphere, no breakaway corrosion was observed on cyclic oxidation of 304H in air alone after 12 thermal cycles at 620°C (Figure 4.4). A better self-healing process was observed during cyclic oxidation in air compared to SO_2 containing atmospheres.

Compared to 304H, A611 stainless steel shows good corrosion resistance, and no breakaway corrosion under cyclic oxidation in a 7%SO_2+air atmosphere at 620°C, as shown in Figure 4.5. From the appearance of samples after exposure, there was almost no cracking & spalling on the sample surface. At all test temperatures (420°C, 620°C, and 720°C), A611 showed no breakaway corrosion (as shown in Figure 4.6), and good adherence of scales, with almost no spalling.

Cyclic oxidation behavior of 304H in 7%SO_2+air atmosphere at different

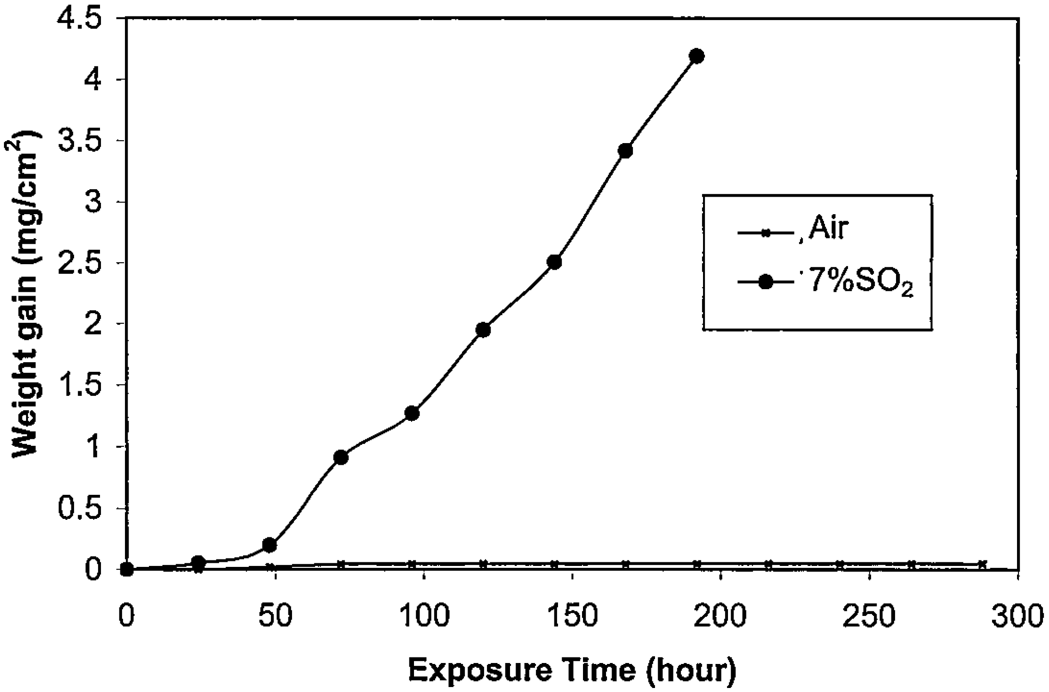

Figure 4.4 24-hour cyclic oxidation of 304H in air or 7%SO_2+air at 620°C

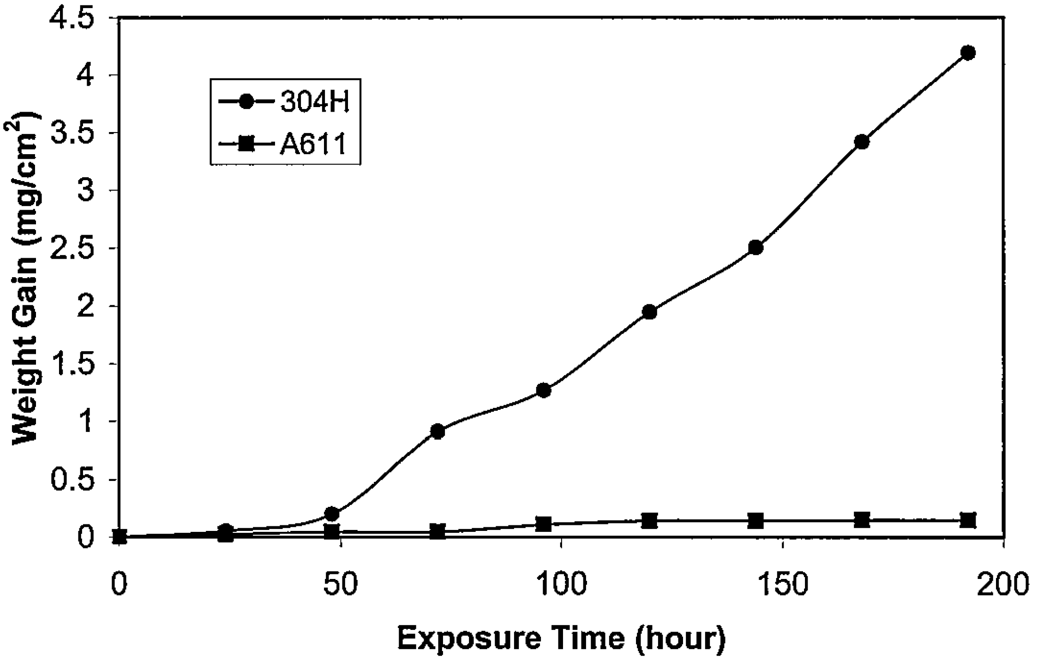

Figure 4.5 24-hour cyclic oxidation of 304H and A611 in 7%SO_2+air at 620°C

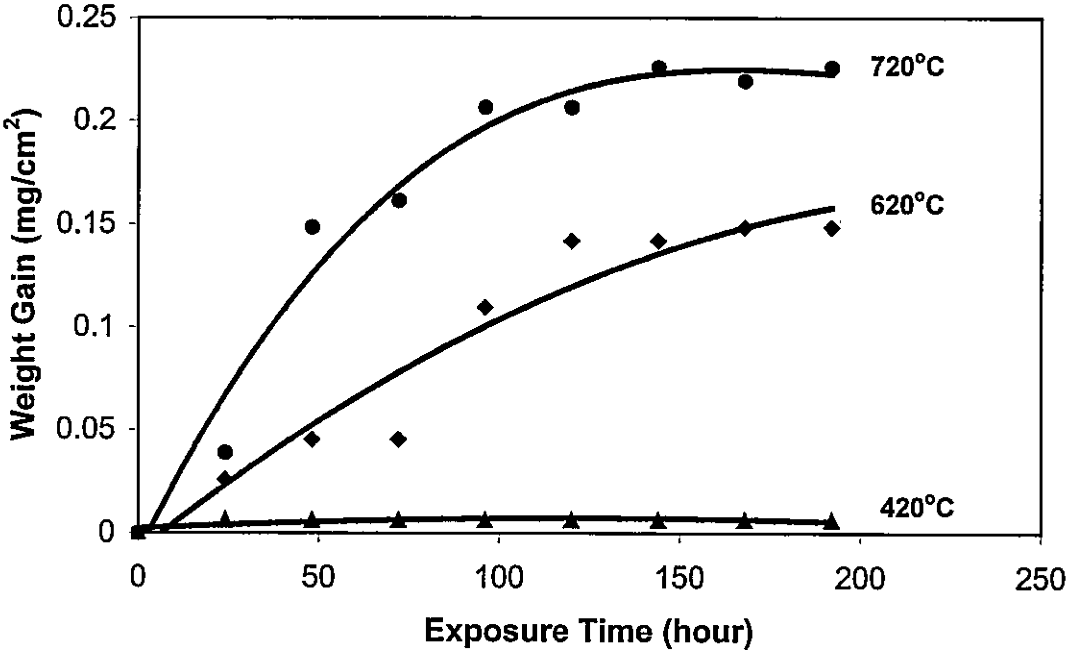

Figure 4.6 24-hour cyclic oxidation of A611 in 7%SO_2 +air at 420°C, 620°C, and 720°C

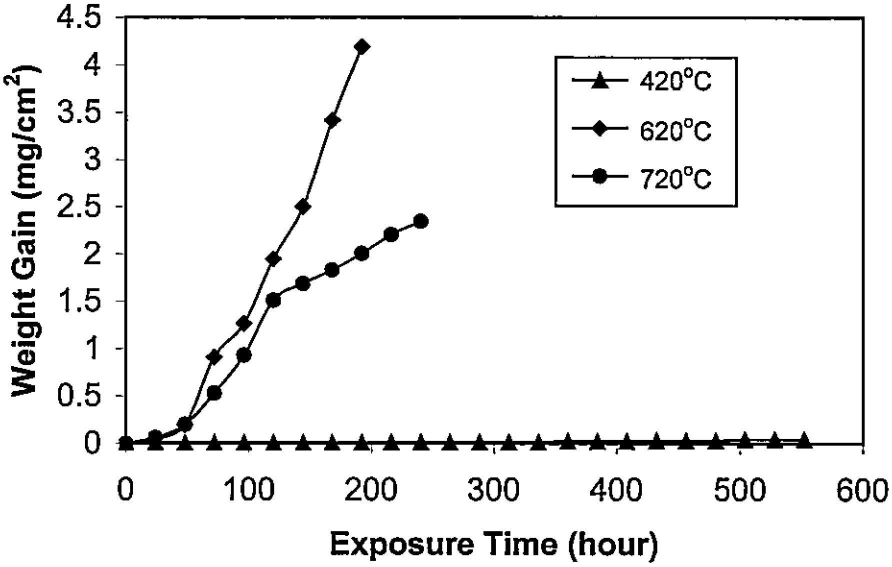

(a)

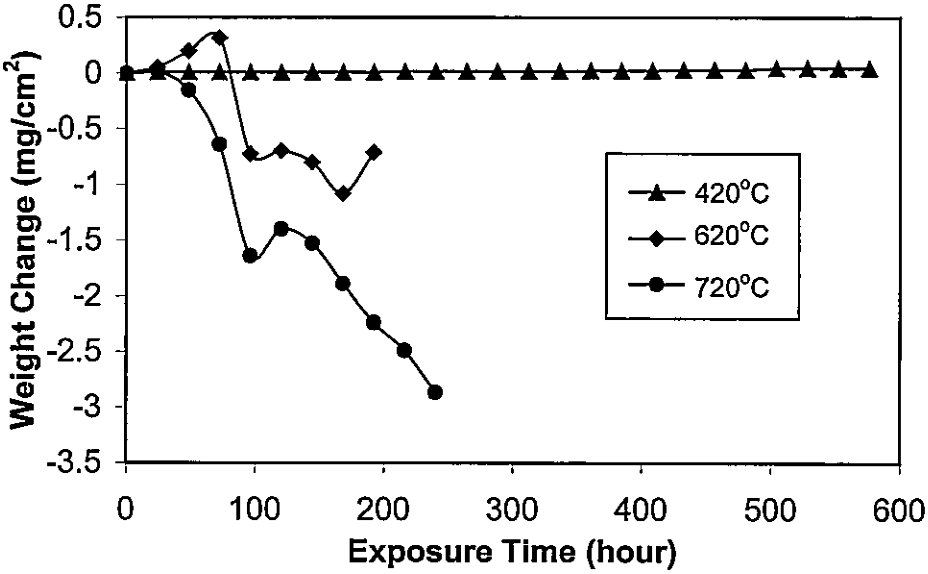

(b)

Figure 4.7 24-hour cyclic oxidation of 304H in 7%SO_2 +air at 420°C, 620°C, and 720°C, (a) including spalled scales; (b) not including spalled scales temperatures is very complex. Weight gain presented in Figure 4.7a includes spalled scales (collected in a crucible). From Figure 4.7a, for cyclic oxidation at 420°C, there was almost no spalling and breakaway corrosion; for both 620°C and 720°C, there was spalling and breakaway corrosion present in cyclic oxidation. However, weight gain for 720°C is lower than that for 620°C. Weight change presented in Figure 4.7b does not include spalled scale. From Figure 4.7b, we see no spalling during cyclic oxidation at 420°C, but spalling is observed at both 620°C and 720°C. However, spalling is worse at 720°C than at 620°C. During cyclic oxidation at 720°C, scales spalled almost completely; however for cyclic oxidation at 620°C, only partial spalling occurred, and the majority of scale remained on the alloy surface after cooling to room temperature.

4.2.2 SEM and XRD analysis

When both 304H and A611 were exposed to cyclic oxidation in air at 620°C, no breakaway corrosion was observed on either alloy, and the alloys showed good self-healing ability during cyclic oxidation in air after twelve 24-hour thermal cycles. Figure 4.8 and Figure 4.9 show, respectively, SEM micrographs of 304H and A611 sample surfaces. The scale on 304H is mainly Fe and Cr oxide, and the scale showed some cracking and spalling on the surface. The scale on A611 is

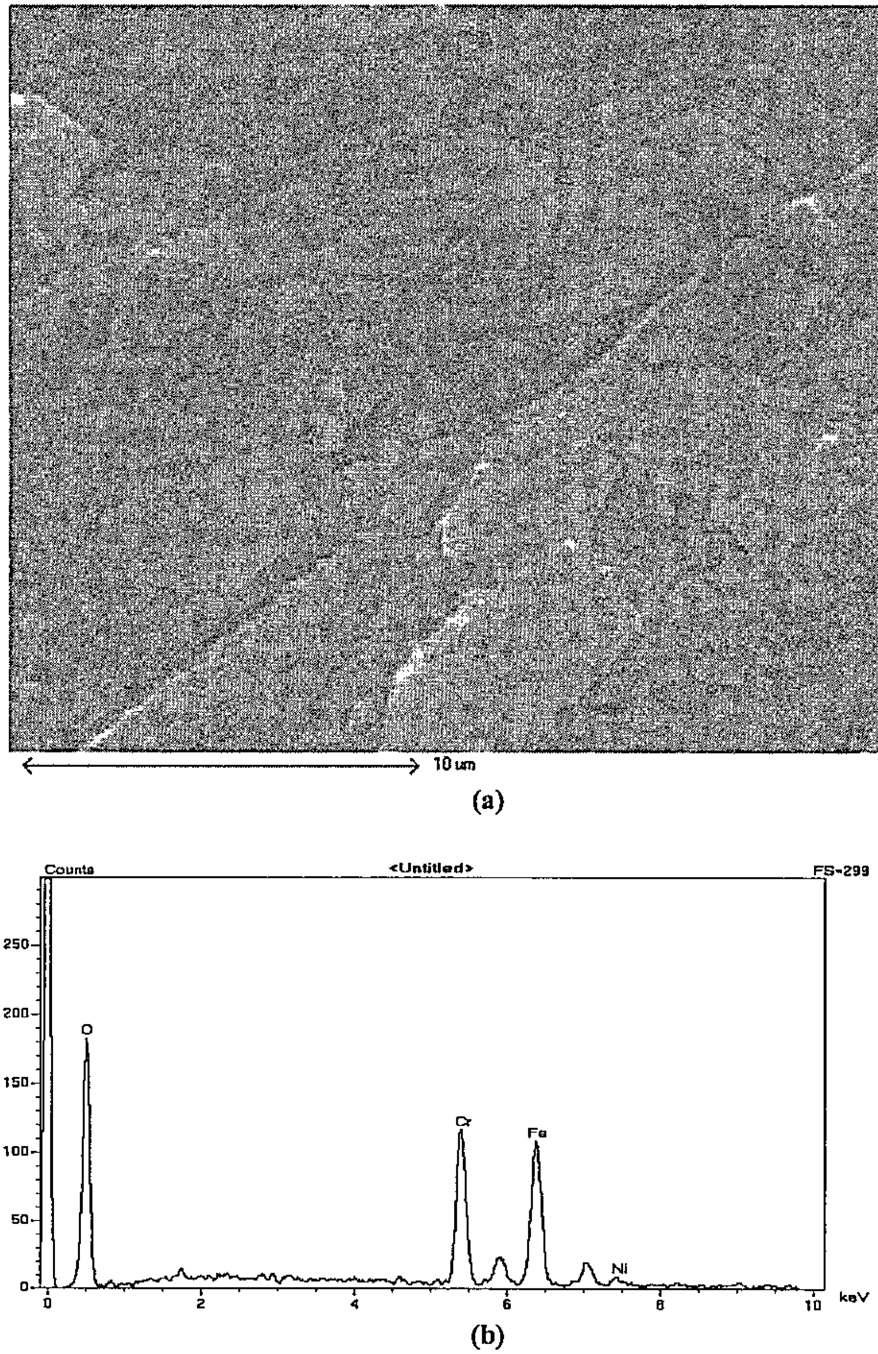

Figure 4.8 24hr-cyclic oxidation of 304H in air at 620°C (Total exposure time: 288hours): (a) SEM micrograph of surface; (b) EDAX analysis

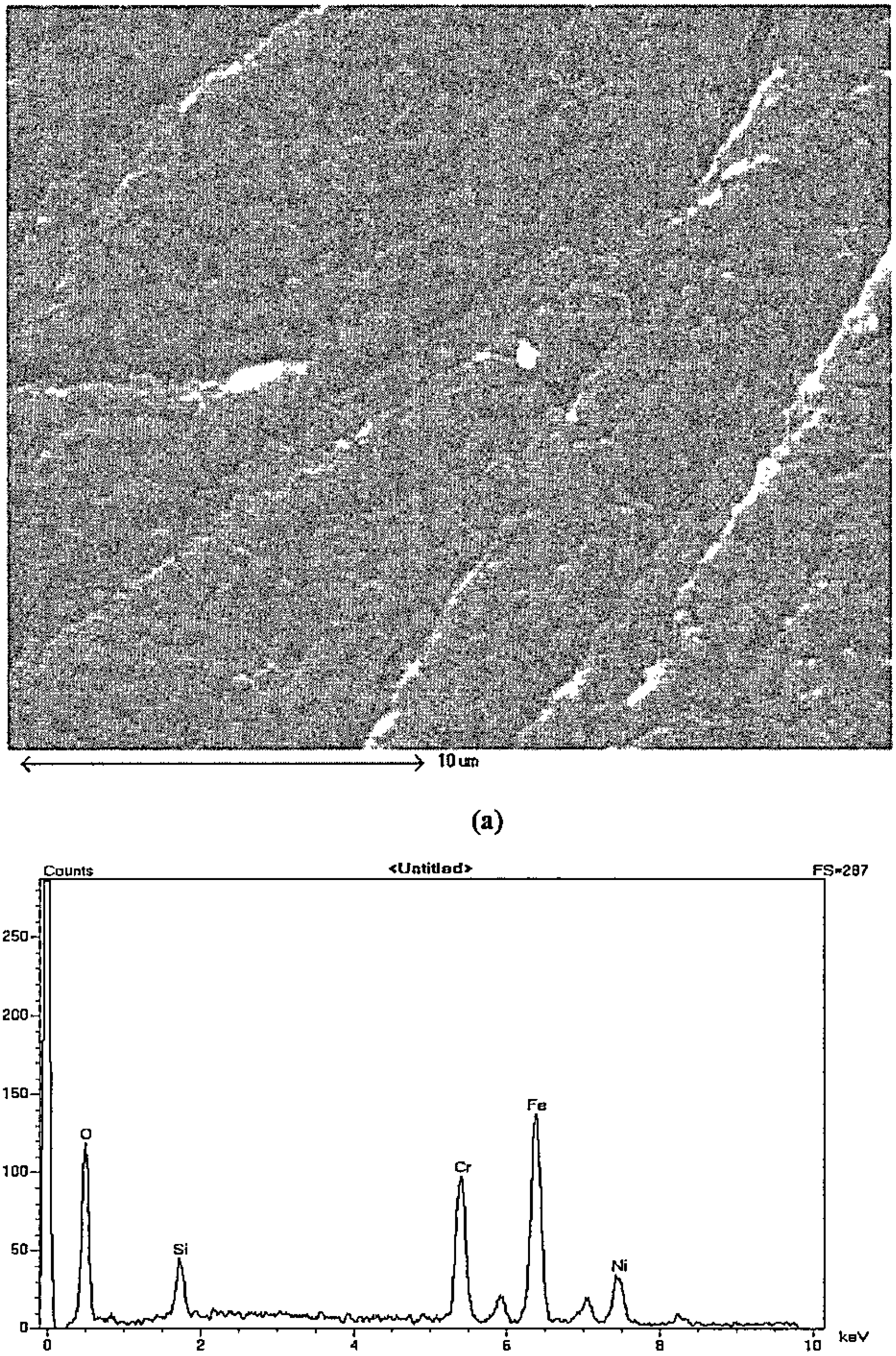

(a)

(b)

Figure 4.9 24-hour cyclic oxidation of A611 in air at 620°C (Total exposure time: 288hours): (a) SEM micrograph of surface; (b) EDAX analysis also mainly Fe and Cr oxide, but Si is incorporated into scales (may be present as SiO_2). No obvious cracking or spalling was observed on A611 during cyclic oxidation in air at 620°C.

Protective oxides failed to form on 304H in 7%SO_2+air at 595°C (the temperature was unstable after starting furnace: about 595 ±50°C for 2 hours periods). Figure 4.10a shows an SEM micrograph of a cross-section of the sample after 72-hour exposure. From Figure 4.10, it is clear that sulfur (S) penetrated into the 304H alloy substrate. XRD analysis of spalled external scales showed the presence of mainly Fe_2O_3 and a little Fe_3O_4 (Figure 4.10c). No sulfides or sulfates were detected by XRD.

When 304H was isothermally exposed to 7%SO_2+air atmosphere at 620°C for 524 hours, the alloy was protective. However, after two shutdowns, breakaway corrosion occurred. Figure 4.11a shows an SEM micrograph of a cross-section of the sample. Although sulfur concentration is relatively low, it is clear that sulfur (S) concentrated at the alloy-scale interface and in the alloy substrate. External scales are mainly iron oxides. XRD analysis of spalled scales showed the presence of Fe_2O_3, Fe_3O_4, and Cr_2O_3 (Figure 4.11b). No sulfides or sulfates were detected by XRD.

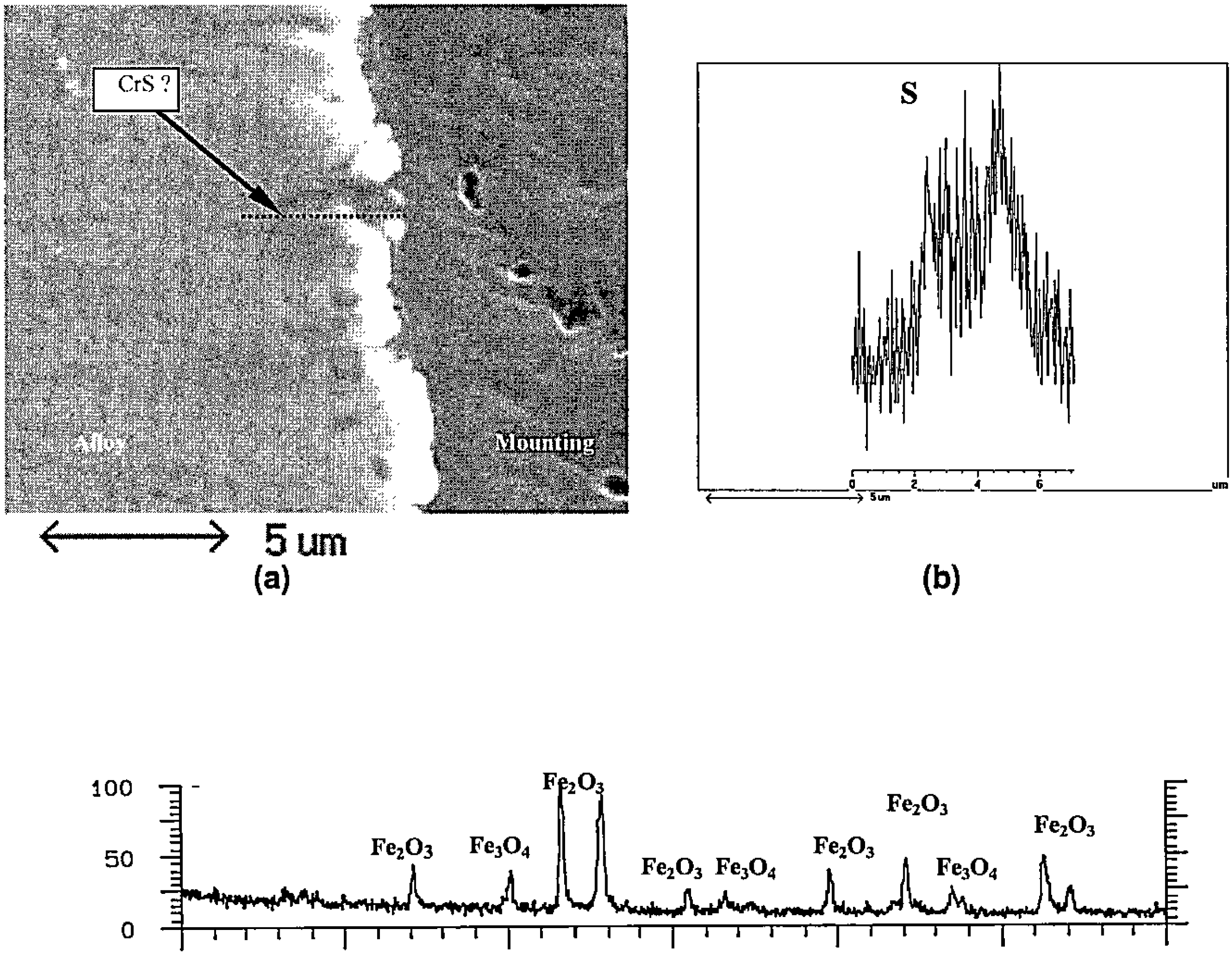

(a)

(b)

(c)

Figure 4.10 SEM analysis of 304H after 72 hours exposure to 7%SO_2+air at 595°C (Unstable temperature after starting furnace): (a) SEM micrograph of cross-section; (b) Sulphur (S) line scan; (c) XRD analysis of spalled scales

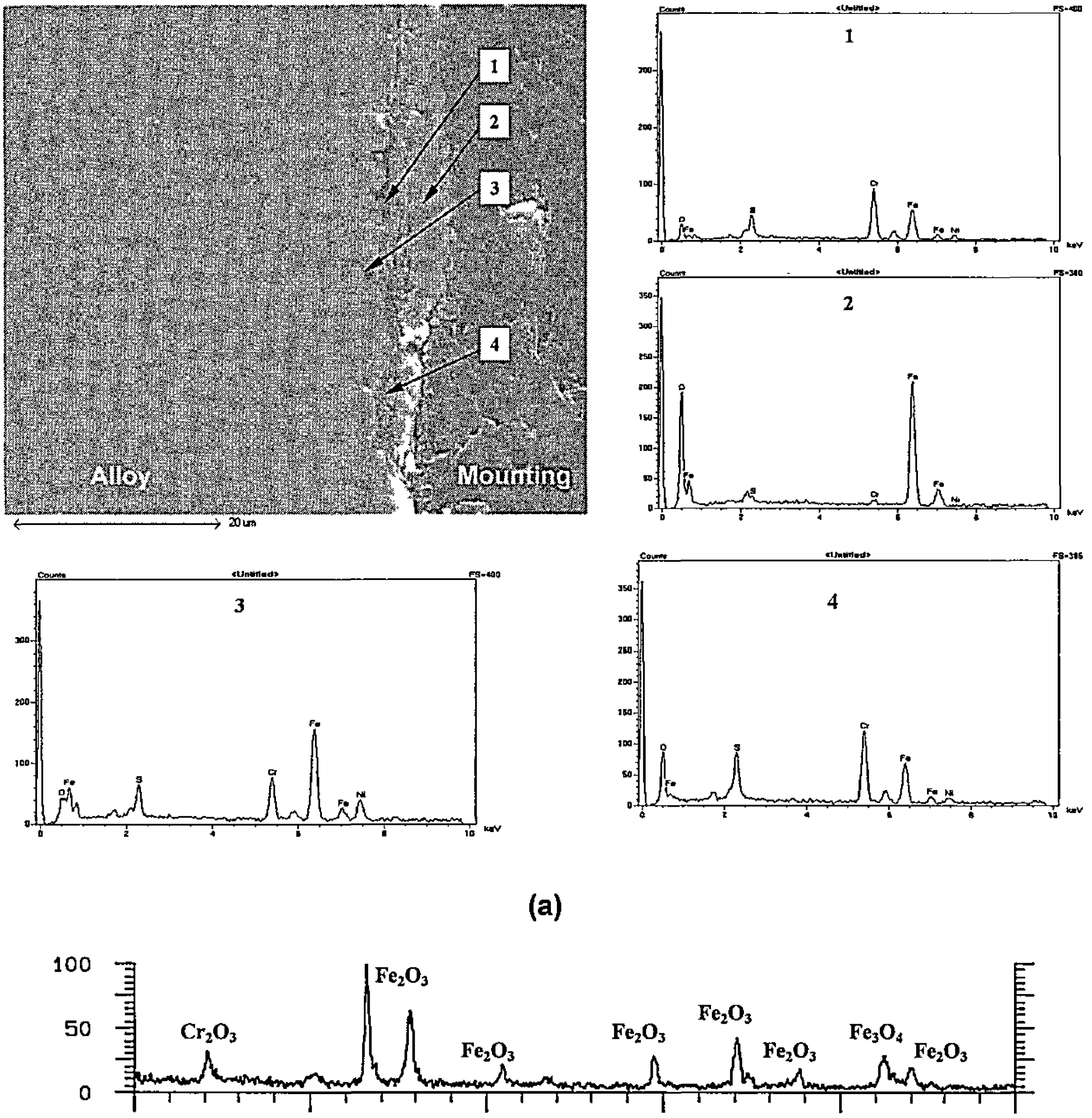

(a)

(b)

Figure 4.11 (a) SEM cross-section and EDS analysis of 304H after isothermal oxidation + shutdowns in 7%SO_2 +air at 620°C (Total exposure time: 623 hours+ 2 shutdowns after 524 hours); (b) XRD analysis of spalled scales

SEM results from 24–hour cyclic oxidation of 304H in SO_2+air at 620°C and 720°C show the presence of internal oxidation and sulfidation at both temperatures (Figures 4.12a, 4.13a). At 720°C, the internal oxidation and sulfidation are very clear. However, at 620°C, since the presence of a large amount of the external scale creates a good environment for the penetration of SO_2 into interface, the area of internal oxidation and sulfidation near interface quickly becomes a part of external scale during cyclic oxidation. Therefore, the front of internal oxidation and sulfidation evenly advances into alloy. In both cases, XRD analysis of spalled scales showed the presence Fe_2O_3, Fe_3O_4, and Cr_2O_3 (Figures 4.12b, 4.13b), and no sulfides or sulfates were detected by XRD.

It is possible that sulfur detected by EDAX at the alloy/scale interface or within the substrate is associated with CrS, but this sulfide was not found using XRD. Probably the sensitivity of the XRD method is too low for so small an amount of CrS. Basu et al [30] and Gilewicz-Wolter et al [68] also reported that XRD analysis failed to detect the presence of chromium sulfides at the alloy-scale interface.

Although sulfates are the most stable phases in the atmosphere under study,

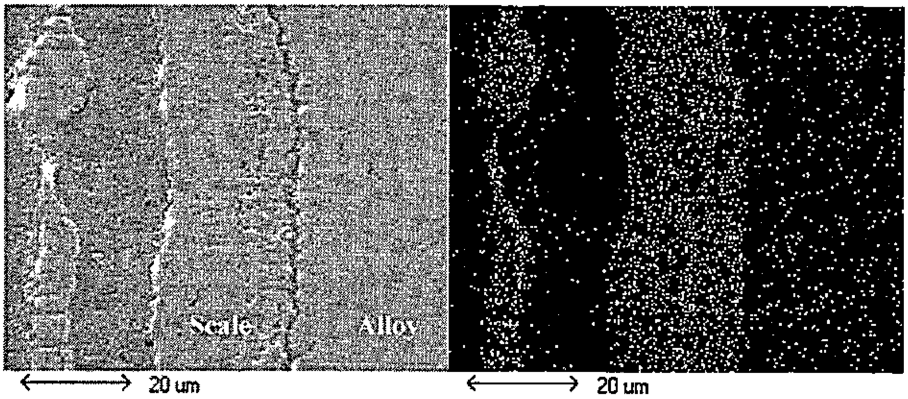

SEM image O Kα X-ray

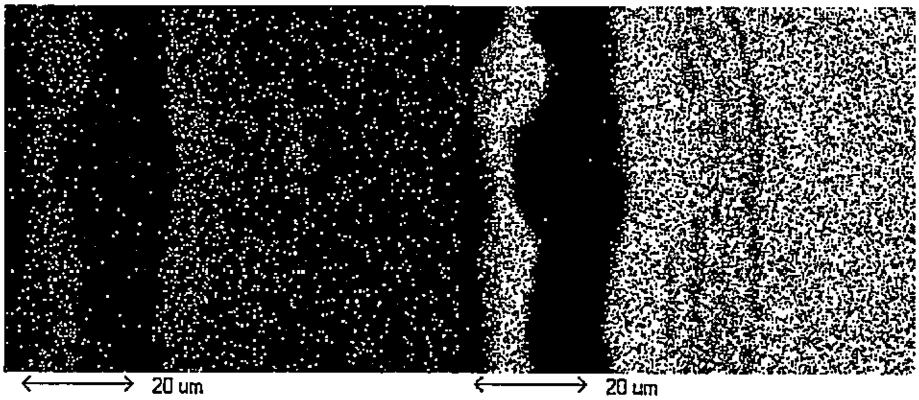

S Kα X-ray Fe Kα X-ray

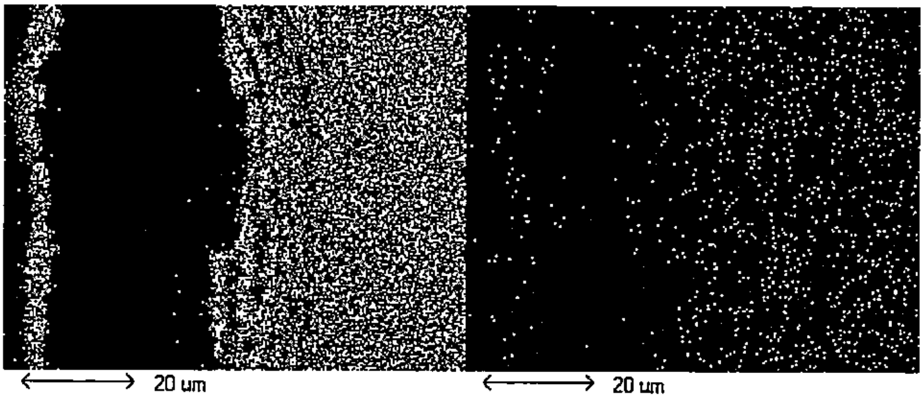

Cr Kα X-ray Ni Kα X-ray

Figure 4.12a 24-hour cyclic oxidation of 304H in SO_2+air at 620°C (192hours): SEM cross-section image and X-ray mapping

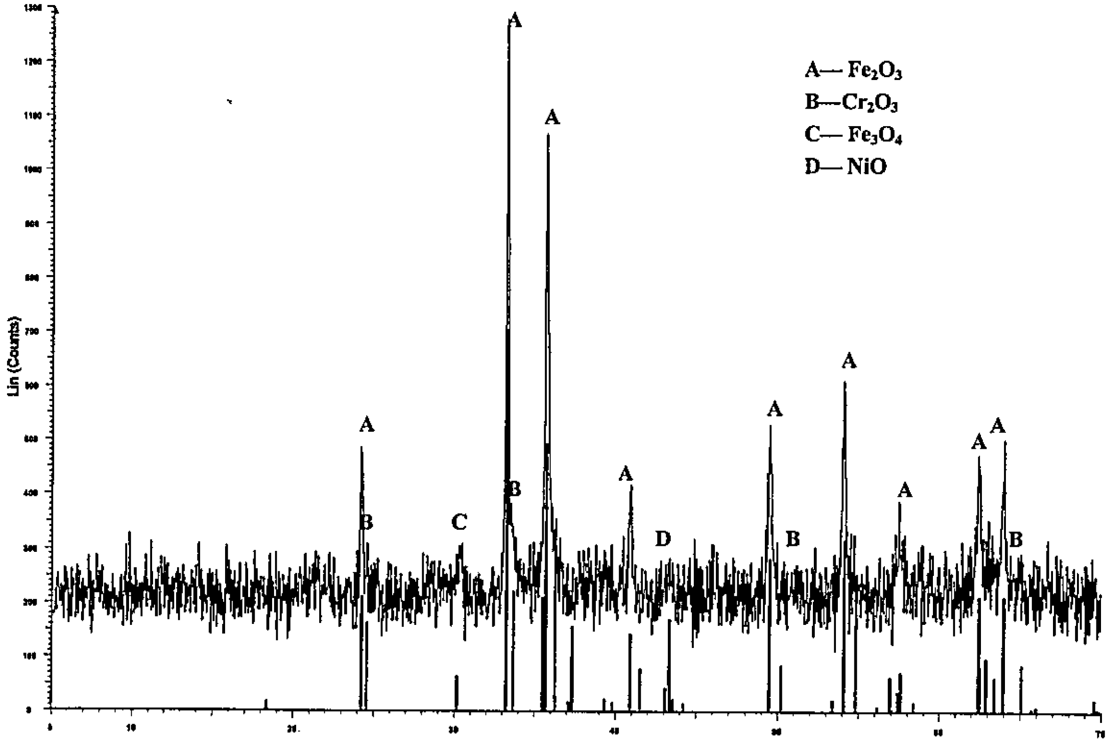

Figure 4.12b 24-hour cyclic oxidation of 304H in SO_2+air at 620°C (192hours): XRD analysis of spalled scales

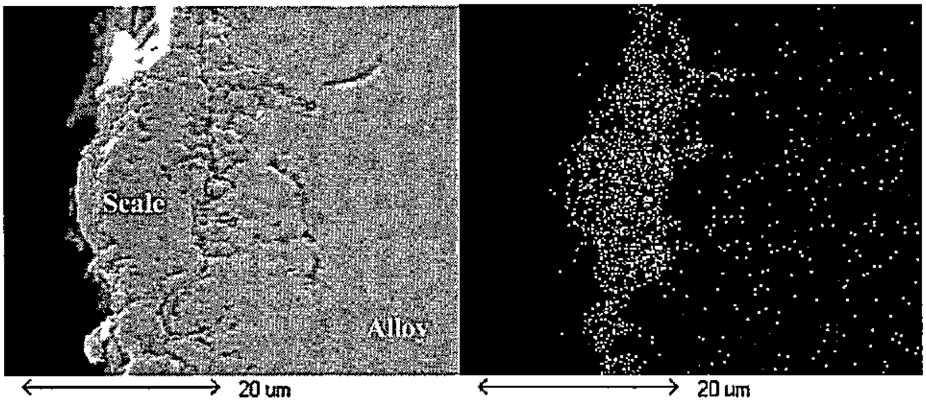

SEM image O Kα X-ray

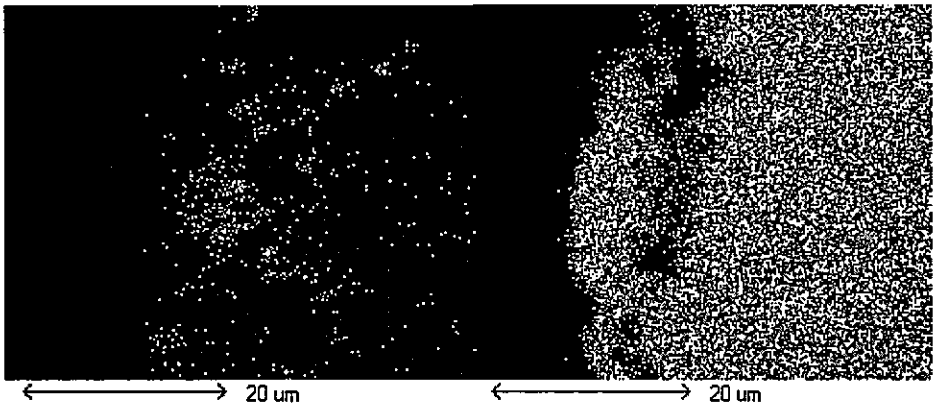

S Kα X-ray Fe Kα X-ray

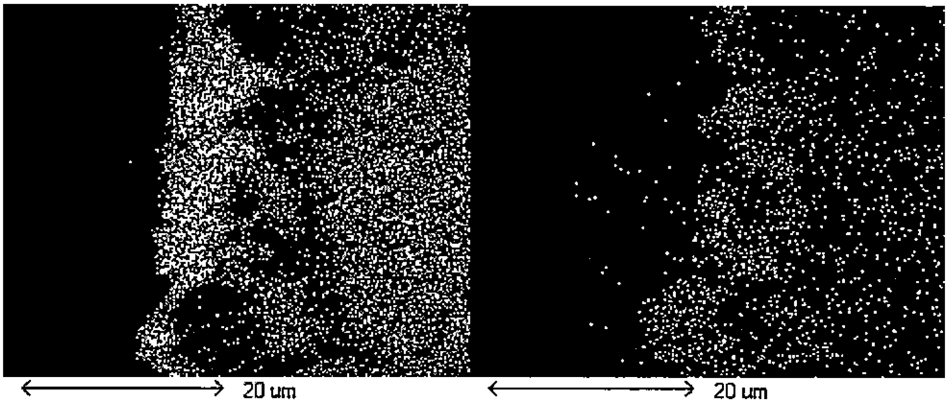

Cr Kα X-ray Ni Kα X-ray

Figure 4.13a 24-hour cyclic oxidation of 304H in SO_2+air at 720°C (240 hours): SEM cross-section image and X-ray mapping

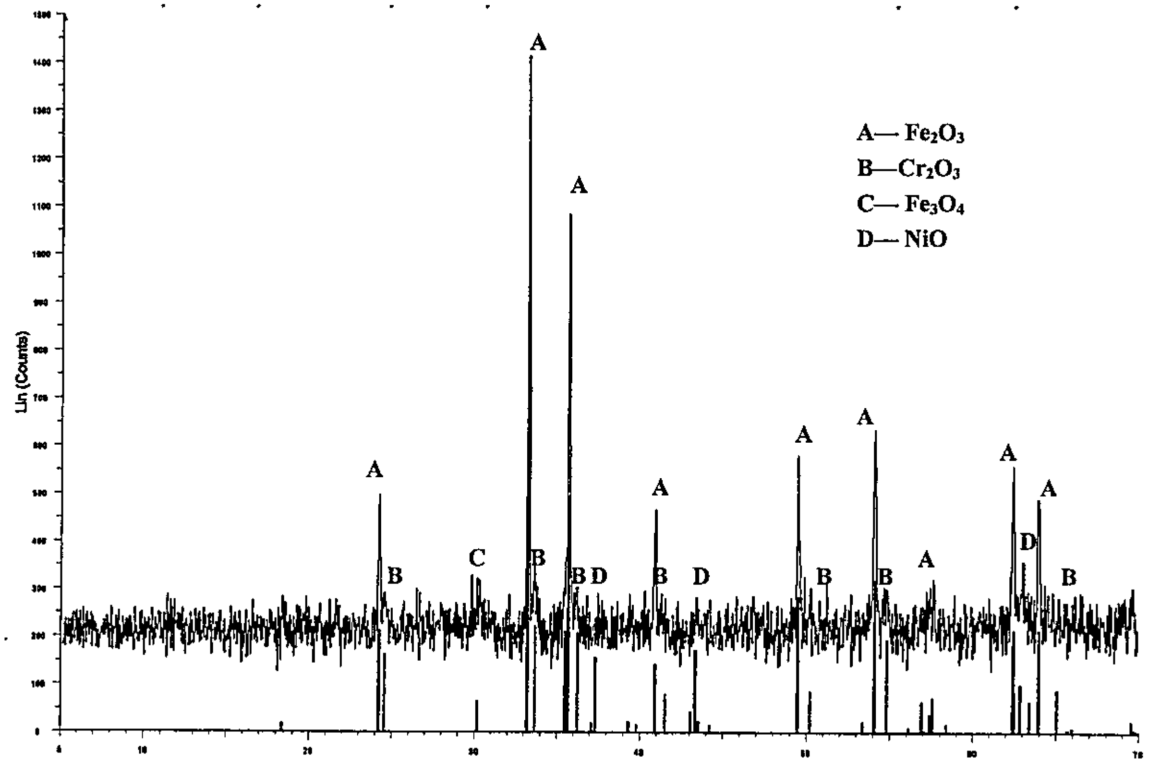

Figure 4.13b 24-hour cyclic oxidation of 304H in SO_2+air at 720°C (240 hours): XRD analysis of spalled scales

no sulfate was identified by XRD. Probably the amount of sulfate is too small for XRD to detect. Actually, in the literature, even for high temperature corrosion of pure metals in $SO_2/SO_3/O_2$ atmosphere, it was very difficult to detect sulfates, and the sulfates were suggested to form as a very thin outer layer on the scale surface and almost unobservable [6-16]. K.L. Luthra et al [10,16] reported no sulfate during the corrosion of pure Ni in $SO_2/SO_3/O_2$ atmosphere at 603°C. Some researchers used XPS (X-ray photoelectron spectroscopy) [6,15,19-21], or AES (Auger Electron Spectroscopy) [7] for detecting sulfates on the scale surface.

For A611, There is no breakaway corrosion when exposed to SO_2+air gas mixture at all test temperatures: 420°C, 620°C, and 720°C. From Figures 4.14 and 4.15, it is clear that silicon concentrates at the scale/metal interface after 24-hour cyclic oxidation of A611 in 7%SO_2 + air at 620°C (240 hours exposure). Also, there is some sulfur concentrated at the interface, but it is evident that no sulfur penetrated into the alloy substrate. From Figure 4.16a, b, at 420 °C, A611 shows almost no cracking & spalling after cyclic oxidation, but at 720°C, it is obvious that there is cracking (the cracking is not through the entire thickness of the scale), but almost no spallation was observed during the thermal cycling test. However, at all test temperatures, the alloy was protected and no breakaway corrosion occurred during the exposure to SO_2+air gas mixture.

In contrast with A611, 304H shows breakaway corrosion at both 620 °C and 720 °C. After 150 hours isothermal exposure to SO_2+air gas mixture at 620 °C, the 304H sample was taken out of the furnace and cooled to room temperature. From Figure 4.17, it is seen that through thickness cracking and spallation occurred and there are voids at the interface on the alloy side. These voids might greatly contribute to the poor adherence of scale on 304H and therefore the bad cyclic oxidation resistance of 304H compared to A611.

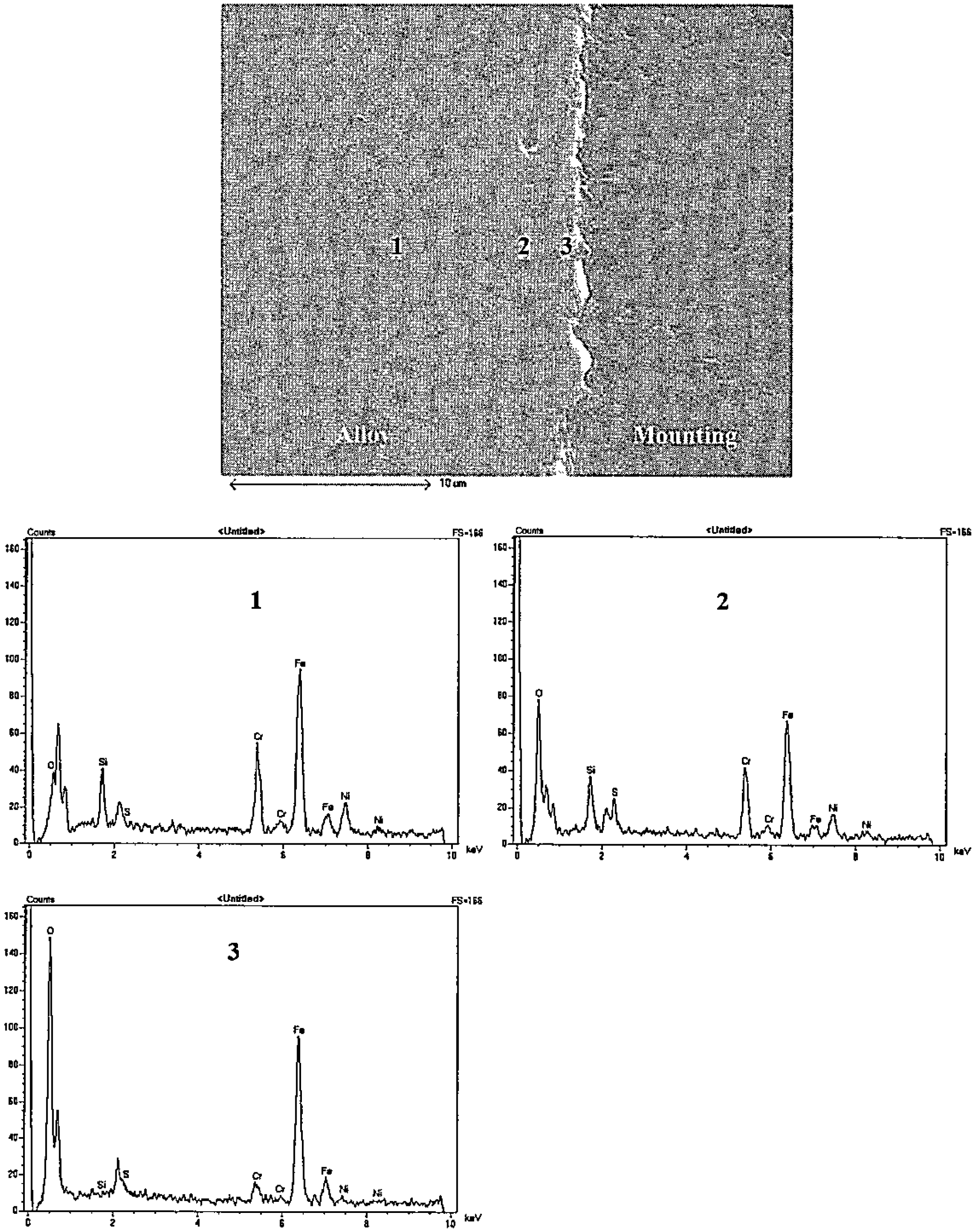

Figure 4.14 24-hour cyclic oxidation of A611 in SO_2+air at 620°C (240 hours): SEM cross-section image and EDS analysis

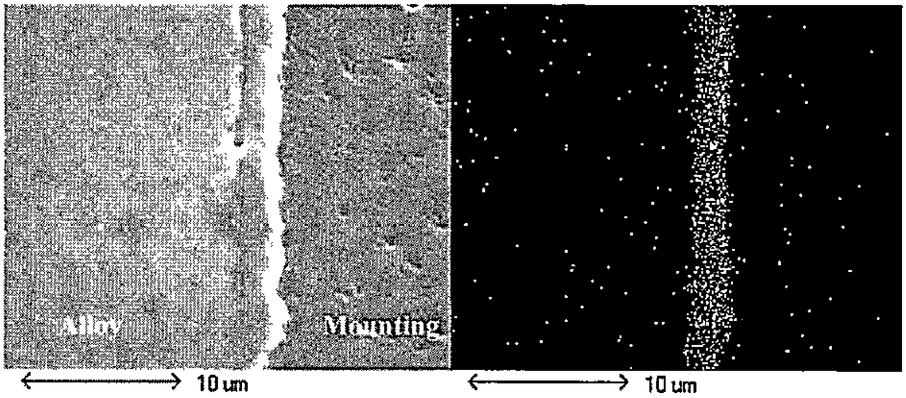

SEM image O Kα X-ray

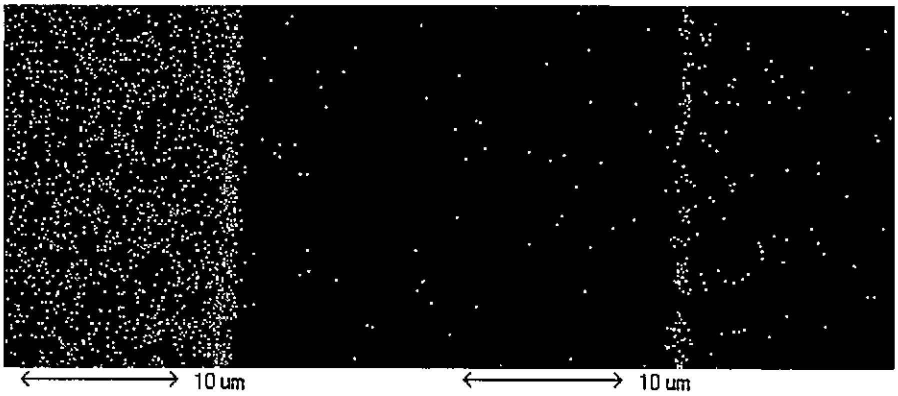

Si Kα X-ray S Kα X-ray

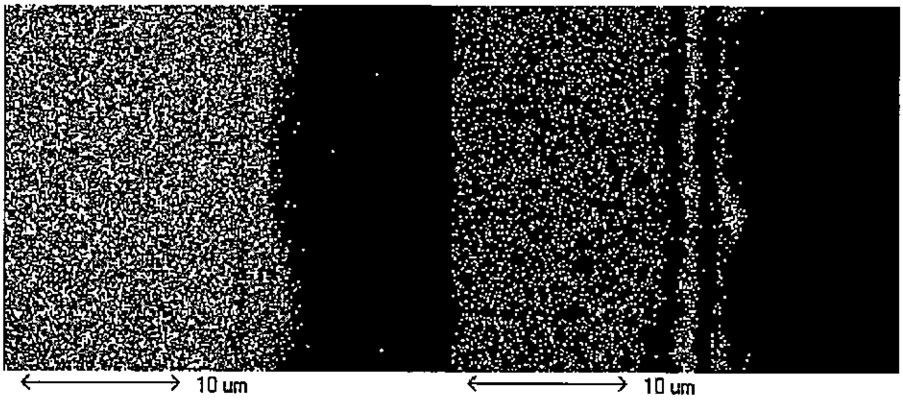

Fe Kα X-ray Cr Kα X-ray

Figure 4.15 24-hour cyclic oxidation of A611 in SO_2+air at 620°C (240 hours): SEM cross-section image and X-Ray mapping

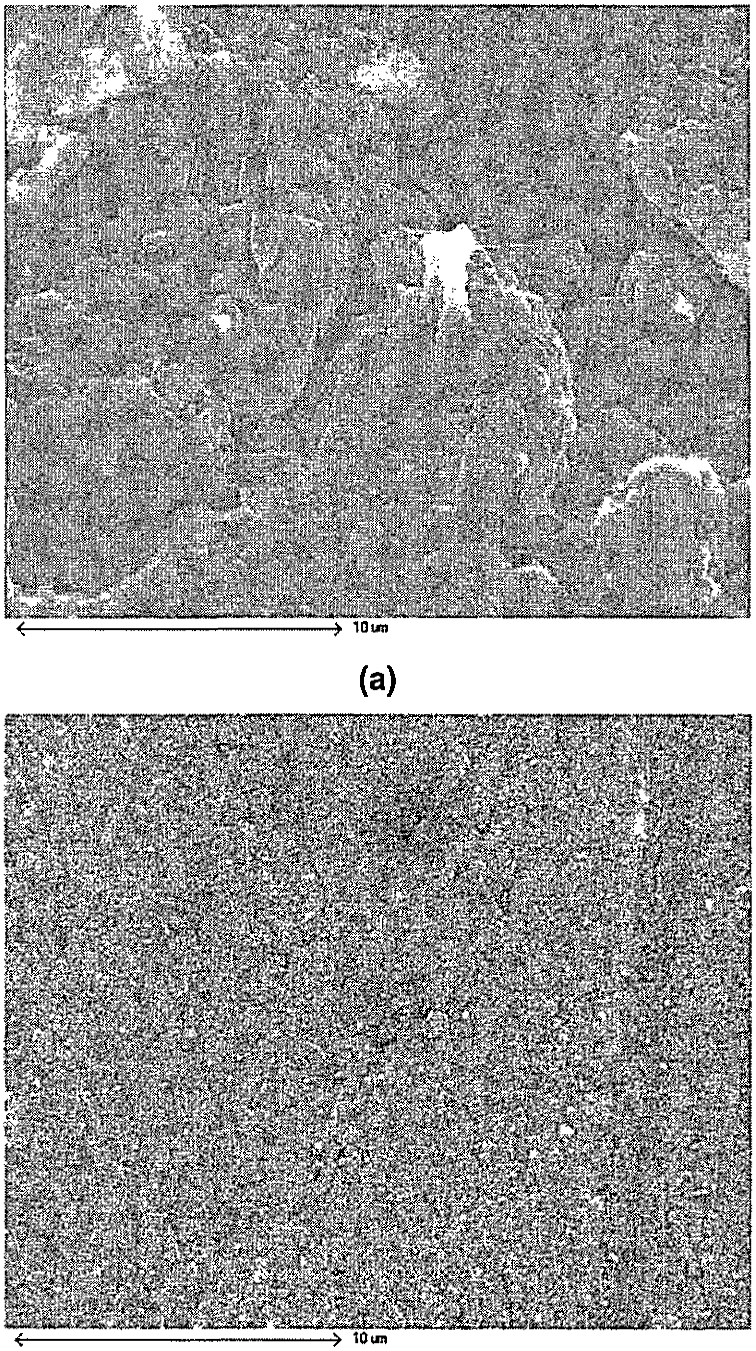

(a)

(b)

Figure 4.16 Surface morphology of A611 after 24-hour cyclic oxidation in 7%SO_2+air (240 hours): (a) 720°C, (b) 420°C

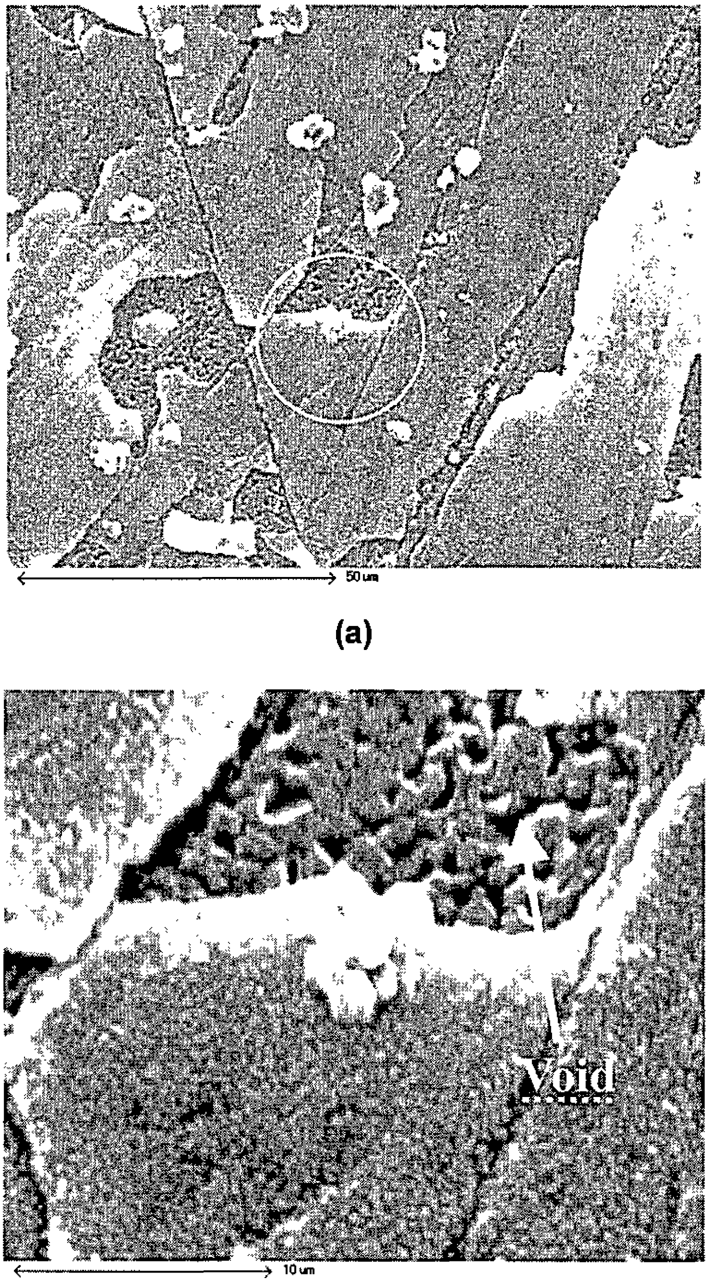

(a)

(b)

Figure 4.17 Surface morphology of 304H after 150-hour isothermal exposure to SO_2+air at 620°C (Taken out of furnace and cooled to room temperature in air): (b) is magnification of (a).

CHAPTER 5

ANALYSIS AND DISCUSSION

5.1 Introduction

In this chapter, experimental results on the cyclic oxidation behavior of 304H & A611 commercial stainless steels, obtained from either this study or the literature, are analyzed and discussed. A possible spalling and corrosion mechanism of 304H at different test temperatures, and a possible breakaway corrosion mechanism of stainless steels in SO_2 containing atmosphere are proposed. In addition, the effects of silicon on the adherence of oxide scale are discussed.

5.2 Thermodynamic Considerations

The thermodynamic stability diagrams for the Fe-S-O, Ni-S-O, and Cr-S-O systems at 420°C, 620°C, and 720°C (calculated by FactSage software) are shown in Figure 5.1, Figure 5.2, and Figure 5.3. (A point for 7%SO_2+air gas mixture was superimposed)

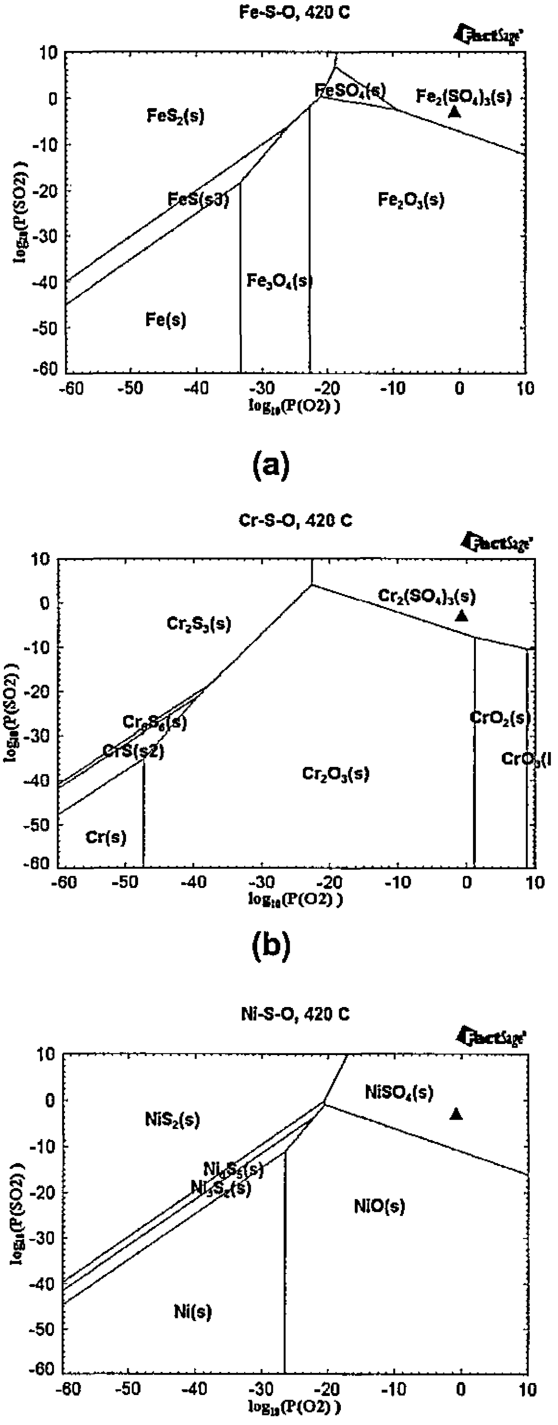

(c)

Figure 5.1 Thermodynamic stability diagrams for (a) Fe-S-O; (b) Cr-S-O; (c) Ni-S-O at 420°C (▲indicates equilibrium gas condition for 7%SO_2+air)

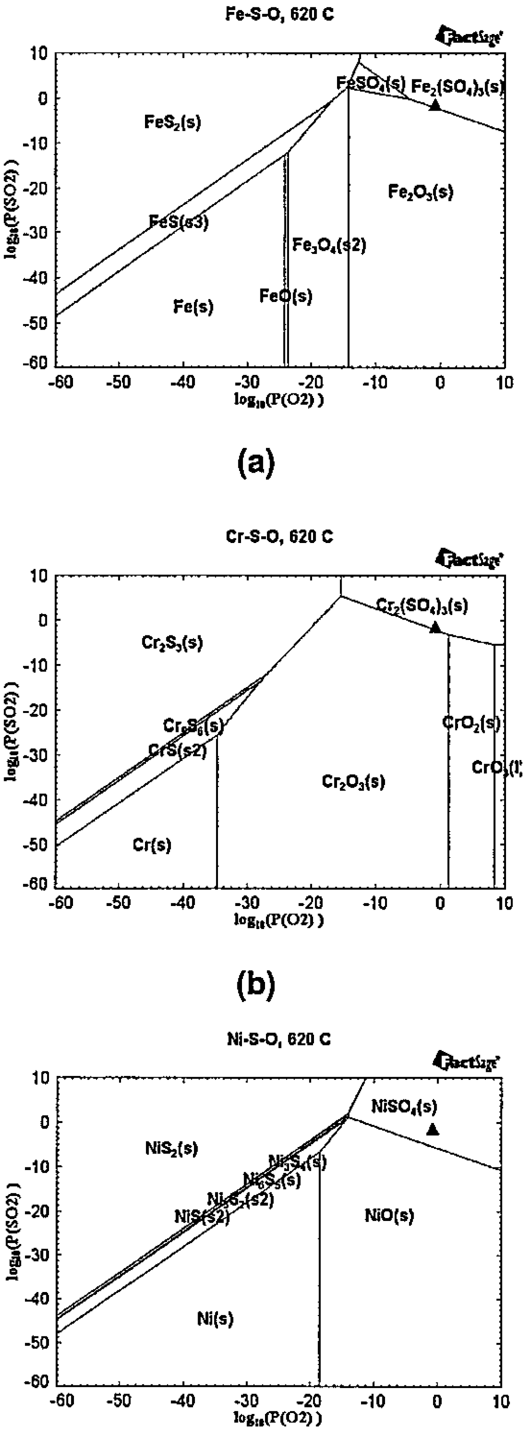

Figure 5.2 Thermodynamic stability diagrams for (a) Fe-S-O; (b) Cr-S-O; (c) Ni-S-O at 620°C(▲indicates equilibrium gas condition for 7%SO_2+air)

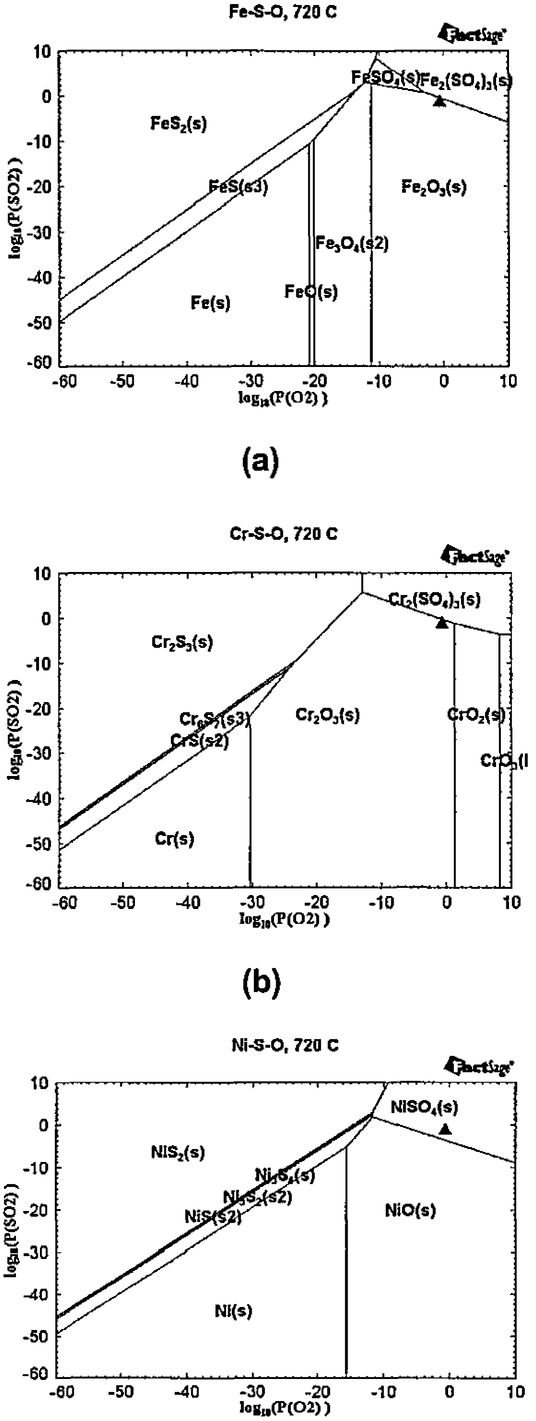

Figure 5.3 Thermodynamic stability diagrams for (a) Fe-S-O; (b) Cr-S-O; (c) Ni-S-O at 720°C(▲indicates equilibrium gas condition for 7%SO_2+air)

Table 5.1 Sulfate identification for corrosion of pure metals in $SO_2/SO_3/O_2$ gas mixture

Metal	Researcher	Date	Gas Mixture	Catalyst Used	Temperature	Sulfate/ Analytical Technique
Fe	Holt et al [6]	1989	O_2+4%SO_2	Platinum	500~800°C	$Fe_2(SO_4)_3$ detected and identified by XPS; No XPS data provided
Ni	Alcock et al [9]	1969	SO_2:O_2=2:1; 12:1; 1:9 etc.	Platinum	500~750 °C	$NiSO_4$ was assumed to be a thin outer layer; no evidence for $NiSO_4$ identification
	Luthra et al [10,16]	1979	SO_2:O_2=2:1; 1:9 etc.	Ceramic honeycomb coated with Platinum	603 °C	No $NiSO_4$ was found (by XRD,TEM)
	Haflan et al [8]	1983	SO_2:O_2=2:1;18:1;1:9; 1:4;1:24 etc.	Platinum	500~900 °C	$NiSO_4$ was assumed to be a thin outer layer; no evidence for $NiSO_4$ identification
	Rishel et al [13]	1990	Air+2256ppmSO_2+68ppm SO_3	Not available	600 °C	$NiSO_4$ was assumed to be a thin outer layer; no evidence for $NiSO_4$ identification
	Roslik et al [15]	1995	SO_2+0.2% O_2	V_2O_5 powder	600~850 °C	$NiSO_4$ detected and identified by XPS; XPS data provided
	Lillerud et al [7]	1984	O_2+4%SO_2	Pt-10Rh	700~900°C	$NiSO_4$ detected and identified by AES; AES data provided
Cr	Andersen et al [14]	1995	SO_2:O_2=2:1	Not available	600 °C	$Cr_2(SO_4)_3$ was assumed to be a thin outer layer; no evidence for $Cr_2(SO_4)_3$ identification

Although sulfates are stable phases in equilibrium with the gas mixture (at 420°C, 620°C), only oxides and sulfides (formed at alloy/scale interface) have been observed in the scales. No sulfate was identified by XRD in spalled scales (304H). Two possibilities are responsible for this: (1) the amount of sulfate in spalled scales is too low for XRD to identify (normally the detection limit of XRD is 5%[67]), or (2) no sulfate formed at all.

Actually, in the literature, even for high temperature corrosion of pure metal (Fe, Cr and Ni) [6-16] in $SO_2/SO_3/O_2$ atmosphere, the formation of sulfates has been controversial, particularly in the case of pure Ni, which was extensively studied [7-13,15-16]. For a clear comparison, examples of sulfate phase identification are summarized in Table 5.1 for the corrosion of pure metals in an $SO_2/SO_3/O_2$ gas mixture.

Although some investigators have postulated the presence of a thin, unobservable $NiSO_4$ layer, no researchers have provided strong, convincing evidence for the formation of $NiSO_4$. Luthra et al [10,16] studied corrosion of Ni at 603°C in $SO_2/SO_3/O_2$ atmosphere, and reported that no sulfate formed and also the corrosion rate decreased with the partial pressure of SO_3. Luthra et al explained that local equilibrium was not reached at the scale-gas interface, and probably the SO_2 molecule was preferentially chemisorbed on the scale surface, compared to SO_3 or O_2. Only Holt et al [6] studied corrosion of pure Fe in $SO_2/SO_3/O_2$ atmosphere (500~800°C), and claimed the formation of a thin layer of iron sulfate ($Fe_2(SO_4)_3$) on the scale surface. However, Holt et al did not provide any results of phase identification in the paper. Also, Andersen et al [14] studied corrosion of pure Cr in $SO_2/SO_3/O_2$ atmosphere, and postulated the presence of a very thin layer of chromium sulfate ($Cr_2(SO_4)_3$) on the scale surface (but no XRD or other analysis result was provided).

Since the sulfate layer was believed to be very thin and unobservable, Holt et al [6], Otero et al [20], Xu et al [19,21], and Roslik et al [15] used XPS (X-ray photoelectron spectroscopy), a surface technique that can provide chemical state information for the outermost atom layers of samples, to identify sulfate phases on the scale surface. Xu et al [19] and Otero et al [20] provided XPS analysis results in their papers. Lillerud et al [7] used another surface technology, AES (Auger Electron Spectroscopy), to identify $NiSO_4$ and provided analysis results.

Actually, metals are relatively unreactive toward dry SO_3 at room temperature

[69], and often a layer of reaction products is formed on the surface, which hinders further reaction [69]. This mechanism may also apply to the reaction of metal oxides with dry SO_3. If a layer of sulfate formed on the surface of an oxide scale, the layer could separate metal oxide from SO_3, and therefore hinder further formation of sulfates, as in the way that oxides protect alloys from oxidation.

From the above analysis, although the formation of sulfate cannot be excluded in this study, we may conclude that if an outer layer of sulfate forms on the surface of an oxide scale, the layer would be very thin and almost unobservable. In the case of pure Ni, the $NiSO_4$ layer was estimated to be 0.05 ~0.7μm [8], and 0.6nm [15]. In addition, in this study the SO_2 was not fully converted to SO_3 prior to entering the furnace, and equilibrium was not reached (Figure 3.4). In this study, no conclusion can be reached on the formation of sulfates, in small or large amounts. For further research, XPS could be employed for identification of sulfates.

5.3 Transport of Sulfur and Internal Sulfidation

Although XRD analysis of the spalled scale showed mainly Fe_2O_3, and a few Fe_3O_4 and Cr_2O_3 peaks, and could not identify sulfides or sulfates, SEM analysis clearly showed that sulfur concentrated at the interface and penetrated into the alloy substrate. Chromium sulfides are the most probable phases due to the high affinity of chromium for S and O (Si, Mn are minor additions, thus, Cr is primarily considered for analysis). The chromium sulfide formed will be referred to as CrS, which is expected to be stable in contact with the alloy. Two possible mechanisms are responsible for the formation of internal sulfides:

(1) Chemical dissolution and diffusion though scale

(2) Molecular transport of SO_2 via physical defects, e.g. grain boundary, micro-cracks, etc.

The formation of sulfides at the oxide/alloy interface by chemical dissolution and diffusion mechanism requires the P_{S_2} at the interface to be higher than that required for CrS/alloy equilibrium, which is referred to as $P_{S_2(cr/CrS)}$. This can be calculated from the following reaction:

$$Cr + \frac{1}{2}S_2 = CrS \qquad \Delta G_1^0 = -215310 + 65.0T \quad \text{(J) [40]}$$

Thus, $P_{S_2(cr/CrS)} = (a_{Cr})^{-2}\exp(\frac{2\Delta G_1^0}{RT})$ (assuming pure CrS, a_{CrS}=1)

Assuming a_{Cr}=X_{Cr}=0.18 (ideal solution), then:

At 420°C, $P_{S_2(cr/CrS)}$=6.63×10^{-25} (atm)

At 620°C, $P_{S_2(cr/CrS)}$=1.23×10^{-17} (atm)

At 720°C, $P_{S_2(cr/CrS)}$=4.24×10^{-15} (atm)

However, the equilibrium partial pressure of sulfur in the gas mixture (7%SO_2+air), denoted as $P^0_{S_2}$, was calculated by use of FactSage software. At 420°C, $P^0_{S_2}$ =1.15×10^{-52} (atm); at 620°C, $P^0_{S_2}$ =2.046×10^{-37} (atm); at 720°C, $P^0_{S_2}$ =1.654×10^{-32} (atm). Therefore, at all test temperatures, since $P^0_{S_2} < P_{S_2(cr/CrS)}$, it is not possible for CrS to form by the chemical dissolution and diffusion mechanism.

The second mechanism of sulfide formation is the penetration of molecular SO_2 into alloy/scale interface through the oxide via microcracks. In this case, sulfur may be generated by the following decomposition at the interface:

$$SO_2 = \frac{1}{2}S_2 + O_2 \qquad \Delta G_2^0 = 364000 - 72.6T \qquad \text{(J) [40]}$$

Since the oxygen potential at the interface is lower than in the bulk gas, locally, the sulfur potential can be high. If the sulfur partial pressure exceeds the P_{S_2} required for the formation of metal sulfides, sulfide formation will occur at the interface or within the alloy substrate. At comparable metal activities, the most stable oxide and sulfide will form first. For alloy 304H, chromium oxide and sulfide should form first. The reactions leading to the oxide and sulfide formation may be written respectively as:

$$SO_2 = \frac{1}{2}S_2 + O_2 \qquad \Delta G_2^0 = 364000 - 72.6T \quad \text{(J) [40]}$$

$$\frac{2}{3}Cr + \frac{1}{2}O_2 = \frac{1}{3}Cr_2O_3 \qquad \Delta G_3^0 = -373060 + 86.5T \quad \text{(J) [40]}$$

$$Cr + \frac{1}{2}S_2 = CrS \qquad \Delta G_1^0 = -215310 + 65.0T \quad \text{(J) [40]}$$

Adding the above reactions, gives:

$$\frac{7}{3}Cr + SO_2 = \frac{2}{3}Cr_2O_3 + CrS \qquad \Delta G_1^0 + \Delta G_2^0 + 2\Delta G_3^0 = -597430 + 165.4T \quad \text{(J)}$$

Assuming Cr_2O_3 and CrS are pure phases (unit activity), then the minimum partial pressure of SO_2 required for the formation of chromium sulfide is:

$$P_{SO_2}^{Min} = a_{Cr}^{-\frac{7}{3}} \times \exp(\frac{\Delta G_1^0 + \Delta G_2^0 + 2\Delta G_3^0}{RT})$$

Assuming $a_{Cr}=X_{cr}=0.18$ (ideal solution), then:

At 420°C, $P_{SO_2}^{Min}=2.2\times10^{-35}$ (atm)

At 620°C, $P_{SO_2}^{Min}=2.68\times10^{-25}$ (atm)

At 720°C, $P_{SO_2}^{Min}=8.86\times10^{-22}$ (atm)

The minimum partial pressure of SO_2 required for the formation of CrS is much lower than the partial pressure (P_{SO_2}) of gas mixture (7%SO_2+air) or even the equilibrium partial pressure after SO_3 formation (at 420°C, at $P_{SO_2}=5.158\times10^{-4}$ atm; at 620°C, P_{SO_2} = 0.017514 atm; at 720°C, P_{SO_2} = 0.03858 atm). Thus, in this study, the molecular transport of SO_2 is the only feasible mechanism of sulfur penetration.

Sulfur can diffuse into the alloy substrate and form more CrS, and thus the corrosion front can advance into alloy.

5.4 Possible Spalling and Breakaway Corrosion Mechanism

Although the gas mixture contains SO_2 and SO_3 after being catalyzed, the gas has a high oxygen potential, and therefore is still a strong oxidizing atmosphere. So, when stainless steels are exposed to this kind of gas mixture under stable temperatures, initially, a continuous chromia (Cr_2O_3) layer forms on the surface of stainless steel to provide protection. The chromia layer is dense and grows slowly by diffusion of Cr^{3+} through the dense chromia layer [32], and some believe O^{2-} diffusion also plays a role [32]. This chromia layer provides protection for stainless steels and most heat resistant alloys. In some cases, the spinel oxide may also be relatively protective [36-37] under isothermal conditions.

If the exposure temperature is stable, and almost no thermal stress is induced, the stainless steel will be protected by a chromia layer for a long time, e.g. several hundred hours. However, when stainless steels are subject to thermal cycling, especially during cooling, induced thermal stress might cause cracking and/or spalling of the chromia layer. Thermal stress is related to the temperature drop (ΔT) and the difference in coefficients of thermal expansion between oxides and metal

[34]. The fraction of spalled scales depends on the thickness of oxide scale, temperature drop (ΔT), and also the properties of the scale [23]. In this study, after 524 hours isothermal exposure of 304H to 7%SO_2 + air at 620 °C, two shutdowns caused breakaway corrosion. This clearly demonstrates that thermal stress greatly contributed to the breakdown of the protective oxide layer and therefore caused a high corrosion rate.

The oxide scale formed on A611 shows very good adherence under 24-hour thermal cycle at all test temperatures (420°C, 620 °C and 720 °C). Therefore, for cyclic oxidation of A611 in an air or SO_2 + air atmosphere, no breakaway corrosion takes place, and the alloy remains under protection. The good adherence of oxide scale on A611 may be attributed to the presence of Si or to the lack of penetration into alloy substrate by sulfur (to be discussed later) or to the relatively thinner scale causing less thermal stress.

For 24-hour cyclic oxidation of 304H in 7%SO_2 +air at 420 °C, there is almost no cracking and spalling of the oxide scale. This is believed to be due to the relatively thin oxide scale and low ΔT experienced during cooling. At 620 °C and 720 °C, there are cracking and spalling. At 620 °C, the oxide scale partially spalled during cooling, and some scale still remained on the alloy surface. However, at 720 °C, oxide scale almost completely spalled. At 420 °C, there was no breakaway corrosion, but breakaway corrosion took place at 620 °C and 720 °C, and therefore cause a high corrosion rate. However, the weight gain at 720 °C was lower than that at 620 °C.

A possible spalling and breakaway corrosion mechanism of 304H in SO_2+air at different test temperatures is shown in Figure 5.4. The mechanism is described as follows: **(1)** At the beginning of exposure, a continuous protective oxide layer (mainly Cr_2O_3) forms on the surface of 304H at 420 °C, 620 °C and 720 °C, and the higher the temperature, the thicker the oxide scale. **(2)** The first thermal cycle is performed after 24-hour exposure. For 420 °C, there is almost no cracking and spalling; for 620 °C, partial spalling occurs, and un-spalled scales are still on the alloy surface; however, for 720 °C, scales almost entirely spall off. After weighing, the samples are put back into furnace to continue exposure. **(3)** During the second exposure, at 420 °C, the protective oxide scale is still in good condition without cracking and spalling, and therefore the alloy is still under protection; At 620 °C, since cracking & partial spalling occurred, SO_2 can easily penetrate into the alloy/scale interface and cause the sulfur potential to be locally high. This

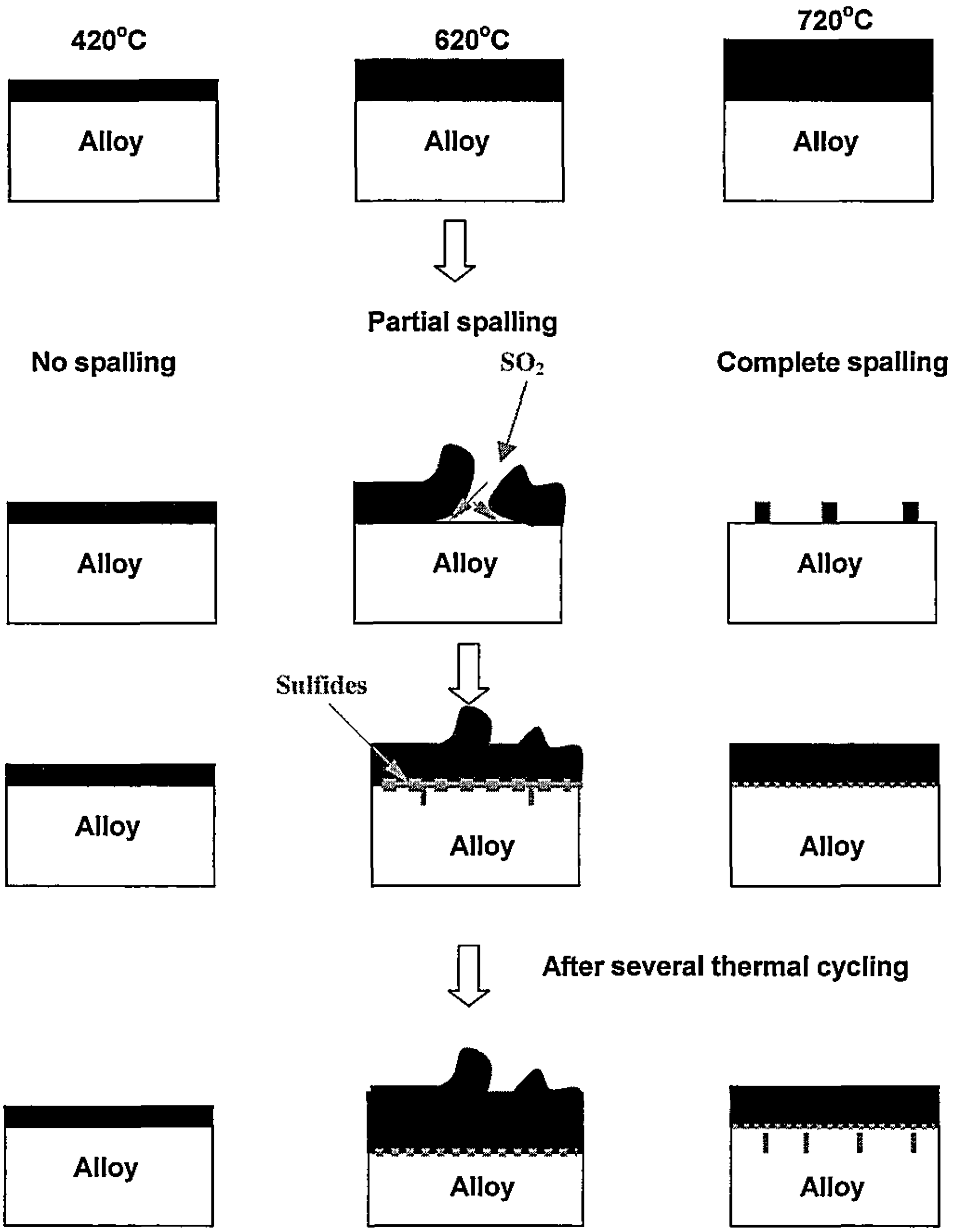

Figure 5.4 Schematic representation of possible spalling &corrosion mechanism of 304H in SO_2+air atmosphere at different temperatures

would lead to sulfide formation at the alloy/scale interface, and therefore a continuous protective chromia layer cannot form again. During cyclic oxidation, the sulfides will be oxidized when exposed by subsequent spalling. Continuation of this process eventually leads to only non-protective oxides (mainly iron oxides: Fe_2O_3, Fe_3O_4). However, at 720 °C, since almost all the initial protective oxide spalls off, a new protective oxide layer might form on the surface again if the Cr near the alloy surface is not depleted. The environment for the penetration of SO_2 and therefore sulfide formation is not good at 720 °C compared to 620 °C. **(4)** As 24-hour thermal cycling continues, eventually, after a certain number of thermal cycles, at 420 °C, the alloy is still protected by the protective oxide scale, but, at both 620 °C and 720 °C, the alloy loses protection. For 620 °C, since the presence of a large amount of external scale creates a good environment for the penetration of molecular SO_2, the area of internal oxidation and sulfidation is quickly converted into a part of external scale (fresh external scales), which also makes the internal oxidation region almost unobservable. This was also confirmed by Young [62], who reported that very much faster scaling rates of alloys and the consequently rapid recession of the alloy surface prevented internal oxidation occurring. Thus, compared to 720°C, at 620 °C the corrosion rate (weight gain) is higher. However, for 720 °C, because of depletion of Cr near the alloy surface, a continuous protective oxide layer cannot form repeatedly, and instead a non-protective oxide scale forms on the alloy surface. During thermal cycling at 720 °C, external scales almost entirely spall off and the base metal is exposed to the gas mixture. SO_2 can penetrate into the alloy along the rapid diffusion paths such as grain boundaries to form internal oxides and sulfides showing an obvious internal oxidation and sulfidation region, and also some sulfides might be found at alloy/scale interface.

Spalling eventually causes breakdown of the protective oxide scale at both 620 °C and 720 °C. Partial spalling creates a better environment for penetration of molecular SO_2 than complete spalling, and therefore results in a rapid recession of the alloy/scale interface. In this sense, partial spalling is worse than complete spalling.

However, for 24-hour cyclic oxidation of 304H in air at 620°C, the damaged area can be repaired, and good self-healing was observed. Thus there is almost no breakaway corrosion after twelve 24-hour thermal cycles, because Cr near alloy surface is not depleted yet.

Generally, a possible breakaway corrosion mechanism of stainless steels in a SO_2 +air atmosphere is shown in Figure 5.5. At the beginning, chromia (Cr_2O_3)

grows into a continuous layer to provide protection for stainless steels. During exposure, when reaching a critical thickness, cracking and/or spalling might initiate. Damaged areas can be repaired by self-healing, and therefore alloys are still under protection. Thermal cycling will accelerate the process of cracking and spalling—self-healing, rapidly reaching the critical concentration of chromium near alloy surface. After reaching the critical concentration of Cr, a continuous chromia layer cannot form again. In the presence of SO_2, because of the penetration of molecular SO_2, via through thickness cracks, a continuous chromia layer cannot be reformed even after only one thermal cycle. Thus, the presence of both thermal cycling and SO_2 causes very rapid depletion of Cr near the alloy surface, thereby causing rapid breakaway corrosion of stainless steels. Actually, even if the chromium (Cr) near the alloy surface is not depleted, the penetration of molecular SO_2 and therefore formation of sulfides (mainly CrS) at alloy/scale interface hinders the formation a continuous chromia layer. Therefore, the presence of both thermal cycling and SO_2 may cause very rapid breakaway corrosion of stainless steels in an SO_2 +air atmosphere even after only one thermal cycle. After breakaway corrosion, base metals are exposed and a non-protective scale of primarily iron oxides will form on alloy surface. Due to the presence of SO_3, sulfates, mainly iron sulfate, might form if there are proper

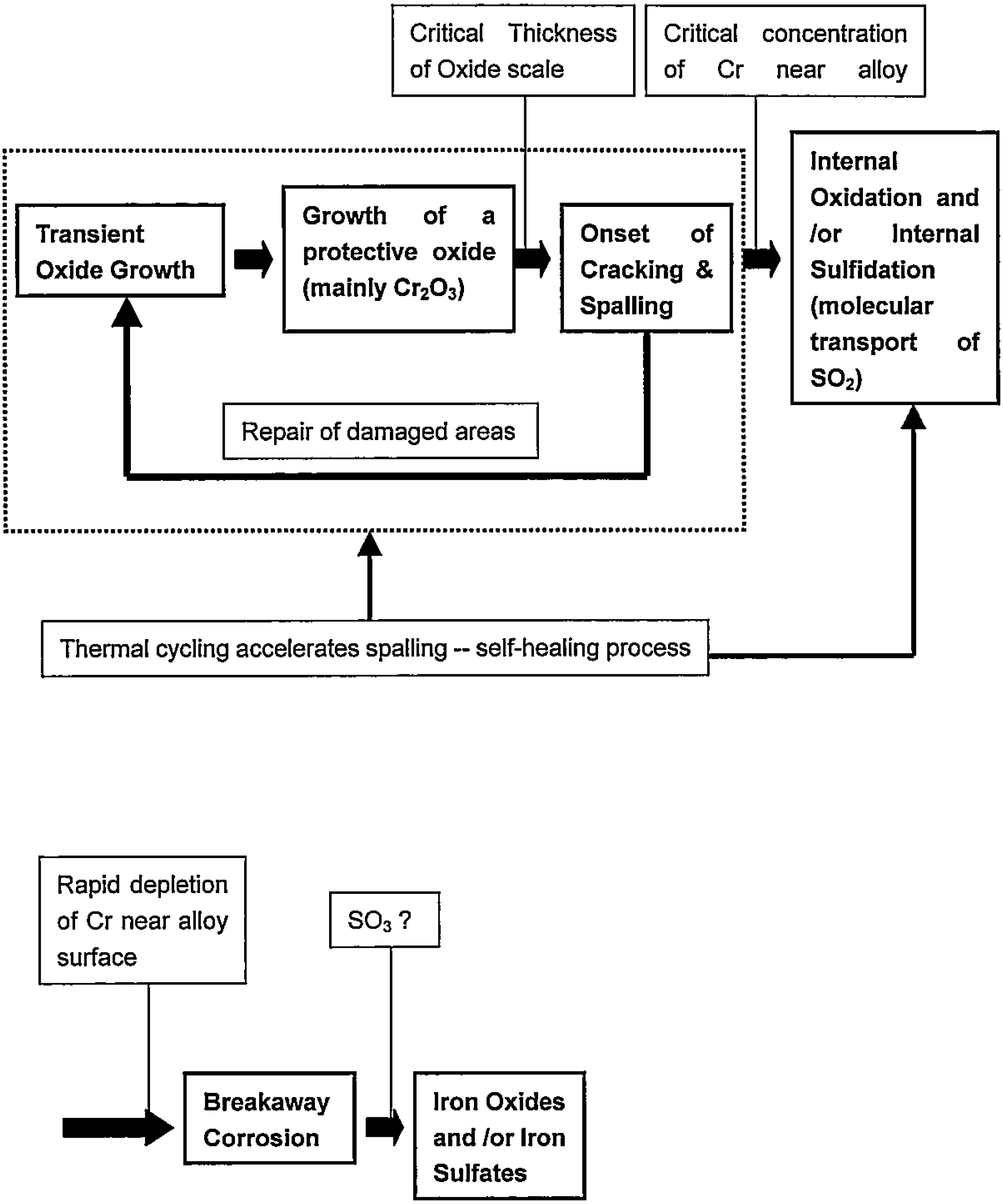

Figure 5.5 Illustration of possible breakaway corrosion mechanism of stainless steels in SO_2 +air atmosphere

kinetic conditions present for the formation of sulfates. Thus, final corrosion products of stainless steels in SO_2+air atmosphere will be mainly iron oxides and /or iron sulfates, and chromium sulfides and other sulfides (at the interface and within alloy substrate). Amounts of sulfides and sulfates might be too low to be detected by XRD.

In contrast with the lab experiments, a large amount of iron sulfate was found in field experiments, this might be attributed to some other factors in plants, which improved kinetic conditions for sulfate formation but were not recognized and simulated in the lab. For example, a layer of catalyst fines could have covered the oxide scale, or condensed acid on samples. In addition, the plant samples were exposed for at least one year (>7000h) (see APPENDIX I), and the immediate steps of corrosion were unknown and just the final corrosion products were seen.

After breakaway, the corrosion enters the stage of high corrosion rate, a period defined as post-breakaway (Figure 5.6). Non-protective external scales form, and simultaneous internal oxidation and internal sulfidation might take place and play a very important role in the corrosion process. Therefore, it is very

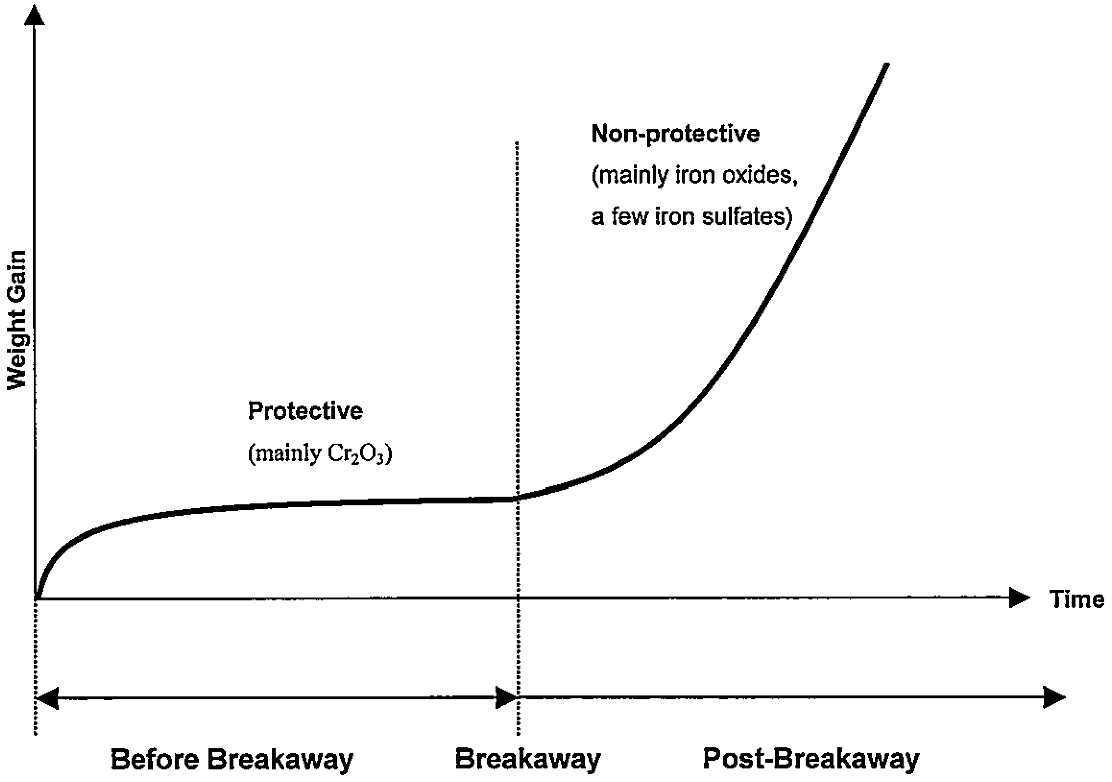

Figure 5.6 Schematic representation of corrosion kinetics of stainless steel

important to know the kinetics of internal oxidation and sulfidation, and also the morphologies and distribution of internal oxides and/or sulfides within alloy substrate. The understanding of the detailed mechanism of internal oxidation & sulfidation would be useful for developing and improving corrosion resistance of stainless steels in this atmosphere. In future work, more attention should be paid to the study of internal oxidation and sulfidation of stainless steels during post-breakaway corrosion.

5.5 Effects of Silicon on Oxide Adherence

Spalling and failure of self-healing eventually cause the breakdown of the protective oxide scale and therefore breakaway corrosion. Good adherence of protective oxide scale on the alloy surface is directly related to good corrosion resistance under thermal cycling conditions. Thus, improving adherence of the protective oxide scale is one of the important measures to improve resistance to corrosion under thermal cycling conditions.

There have been controversial conclusions about the effect of Si on the adherence of protective oxide. Basu et al [30] reported that Si addition can cause spallation. However, promising effects were also often reported [25-27,38,70-75].

Although the detailed mechanism is still poorly understood and should be further investigated, beneficial effects of Si addition to stainless steels can be summarized as:

(1) Silicon does not act directly but decreases or suppresses the incorporation of iron into the chromia scale [70].

(2) A continuous or non-continuous SiO_2 layer forms at the interface to act as a diffusion barrier to Fe and Cr, thus promoting the formation of a thin, more protective Cr_2O_3 layer [27,38,72-75].

(3) The formation of SiO_2 along high diffusivity paths (grain boundaries and triple points) near the scale-alloy interface to act as both a diffusion barrier and pegs extended into the alloy [25-26]

In this study, compared to 304H (0.45%Si), A611 has higher silicon content (5.26%Si). From the experiments and the results, A611 showed good resistance to cyclic oxidation in SO_2 +air at all test temperatures (420°C, 620°C, 720°C), and there was no breakaway corrosion. From the kinetic results, the exposed A611 has a significantly lower weight gain than 304H, and therefore the scale on the A611 is considerably thinner than the scale on the 304H. In addition, voids are clearly observed at the scale/metal interface of exposed 304H (Figure 4.17) while almost no obvious void can be found at the scale/metal interface of exposed A611 (Figures 4.14 -16). Thus, high silicon in A611 might contribute to both the thinner scale and the good cyclic oxidation resistance.

From Figures 4.14 -15, the silicon is clearly observed to be concentrated at the scale-metal interface of the exposed A611, and may be attributed to a layer of silica (SiO_2) adjacent to the metal. Although the layer was claimed to be a continuous or noncontinuous film [27,38,72-75], the evidence for the physical presence of the silica layer is difficult to prove using SEM. In addition, sulfur is also found at the interface, but no sulfur penetration is observed through the high silicon layer and within the alloy substrate. So, these results and observations suggest that the Si might be present at the interface as a layer of silica that acts as a diffusion barrier (Figure 5.7b).

From Figure 4.17, the voids were found at the scale-metal interface of 304H, but almost no voids were found at the interface of A611. This in itself might lead to improved adherence. Although the diffusion of Cr from the alloy substrate to the surface requires the flux of vacancies away from the oxide-metal interface, voids could be formed in alloy grain boundaries, and in particular at the grain triple points. Therefore the voids will most likely nucleate along the substrate grain boundaries, as observed in Figure 4.17. Thus for 304H, it is very easy for a through-thickness cracking & spalling to take place upon cooling, thus exposing the alloy substrate to SO_2 containing gas. Since 304H has lower silicon (0.45%Si) compared to A611 (5.26%Si), it seems that the high silicon concentration contributes to the destruction of vacancies caused by the outward diffusion of chromium and therefore avoid the agglomeration of vacancies into voids at the interface and substrate and improve the oxide adherence. Schematic illustration is shown in Figure 5.7. However, the detailed mechanism needs to be further understood.

For further research, TEM should be used to detect the physical presence of the silica layer, and SIMS can be used to obtain the Si profile across the scale, to elucidate the exact mechanism of A611 having good cyclic oxidation resistance in both air and SO_2 containing atmosphere.

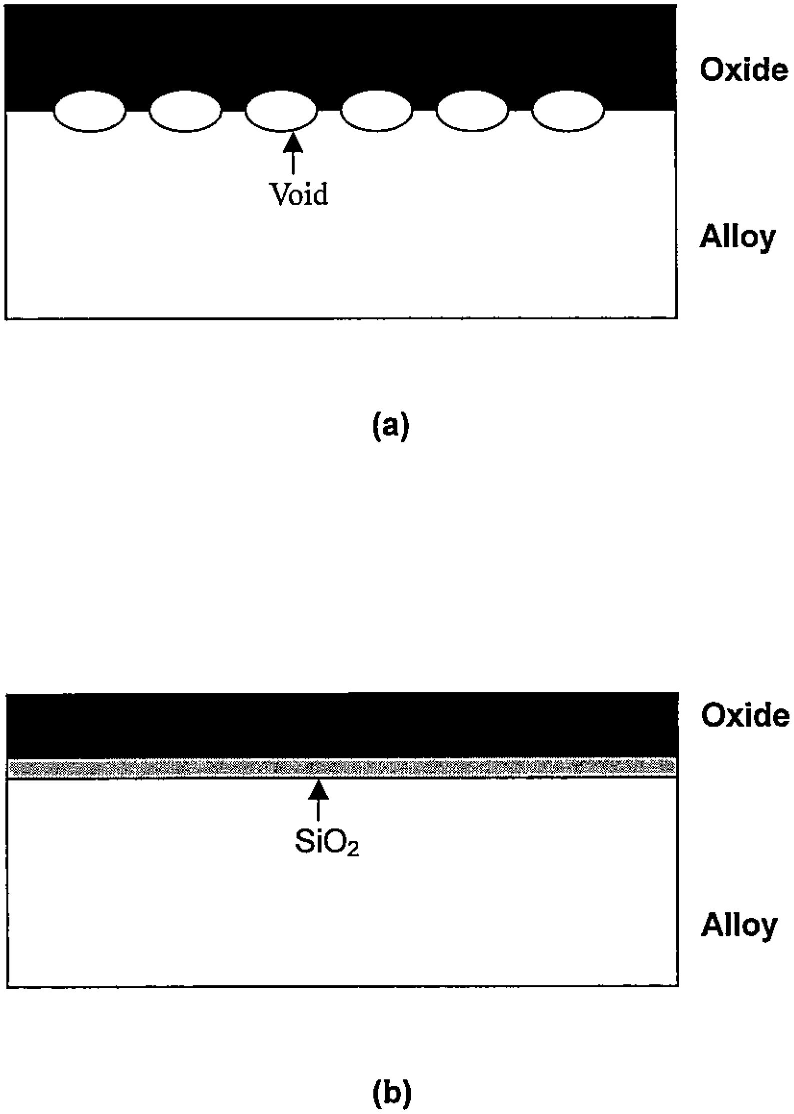

Figure 5.7 Schematic comparison of scale –metal interface of exposed alloys before spalling/cracking: (a) 304H(0.45%Si), (b) A611 (5.26%Si)

CHAPTER 6

CONCLUSIONS

6.1 Conclusions

Although sulfates are most stable phases, no sulfate was identified by XRD in either this study or the literature. Probably the amount of sulfate formed on the oxide scale surface was too small for XRD to detect. Although a large amount of iron sulfate was found in the field experiments, no conclusion was reached on whether or not sulfate can be formed in high or low amount, due to complex conditions in plants, which cannot be simulated in the lab.

For 304H, although no breakaway corrosion occurred during cyclic oxidation in air at 620°C (after twelve 24-hour thermal-cycles), the breakaway corrosion occurred after only two 24 h-thermal cycles in SO_2 +air at both 620°C and 720°C. This suggests that under thermal cycling conditions the penetration of molecular SO_2 and therefore formation of sulfides at interface or alloy substrate contributes to rapid breakaway corrosion of 304H exposed to 7%SO_2 + air atmosphere.

For the cyclic oxidation behavior of 304H in SO_2+air, it was found that a lower weight gain was obtained at 720 °C compared to the higher weight gain at 620 °C, and partial spallation and complete spallation of the scale were observed at 620 °C, 720 °C respectively. Compared to the clear internal oxidation and sulfidation region within alloy at 720 °C, no obvious internal oxidation and sulfidation area was observed at 620 °C. It is suggested that the partial spallation creates a good environment for the penetration of molecular SO_2 and therefore the oxidation and sulfidation reactions at the interface cause a rapid interface recession leaving no obvious internal oxidation area observed.

For A611, at all test temperatures: 420 °C, 620°C, and 720 °C, no breakaway corrosion occurred during thermal cycling in 7%SO_2 +air atmosphere. Silicon is observed to be concentrated at the scale/metal interface and sulfur is also found at the interface but no sulfur penetrating into the alloy substrate. It is assumed that silicon is present as a layer of silica at the interface, both improving the adherence of scale and acting as a barrier to diffusion.

6.2 Suggestions for Future Work

6.2.1 Discontinuous Cyclic Oxidation in SO_2+air and SO_3+air

Discontinuous Cyclic Oxidation in SO_2+air (non-equilibrium)

Results of 304H and A611 exposed to SO_2 +air atmosphere have been achieved and a possible breakaway corrosion mechanism for 304H has been proposed according to current experimental and analytical results. Detailed breakaway corrosion mechanisms of 304H in SO_2 +air atmosphere should be further investigated.

Discontinuous Cyclic Oxidation in SO_3+air (equilibrium)

Future work should be focused on the study of cyclic oxidation and breakaway corrosion mechanism of 304H and A611 stainless steels in SO_3 + air atmosphere (at 420°C, 620°C, and 720°C). The result can be compared to that in SO_2 +air atmosphere to determine the difference (and/or similarity) in corrosion mechanism of the alloys between SO_2+air and SO_3 +air atmosphere.

To guarantee gas equilibrium by a catalyst, a vanadium –based sulfuric acid catalyst (used in sulfuric acid plants) (Figure 6.1), will be used for the catalyst, and an additional furnace will be used for housing the catalyst (Figure 6.2), and the

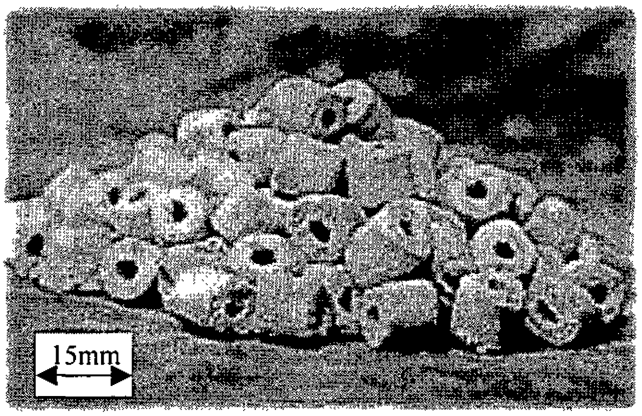

Figure. 6.1 Vanadium –based sulfuric acid catalyst: the vanadium is present as a complex sulfated salt mixture (http://www.enviro-chem.com/plant-tech/3rdtier/sulfcat.html)

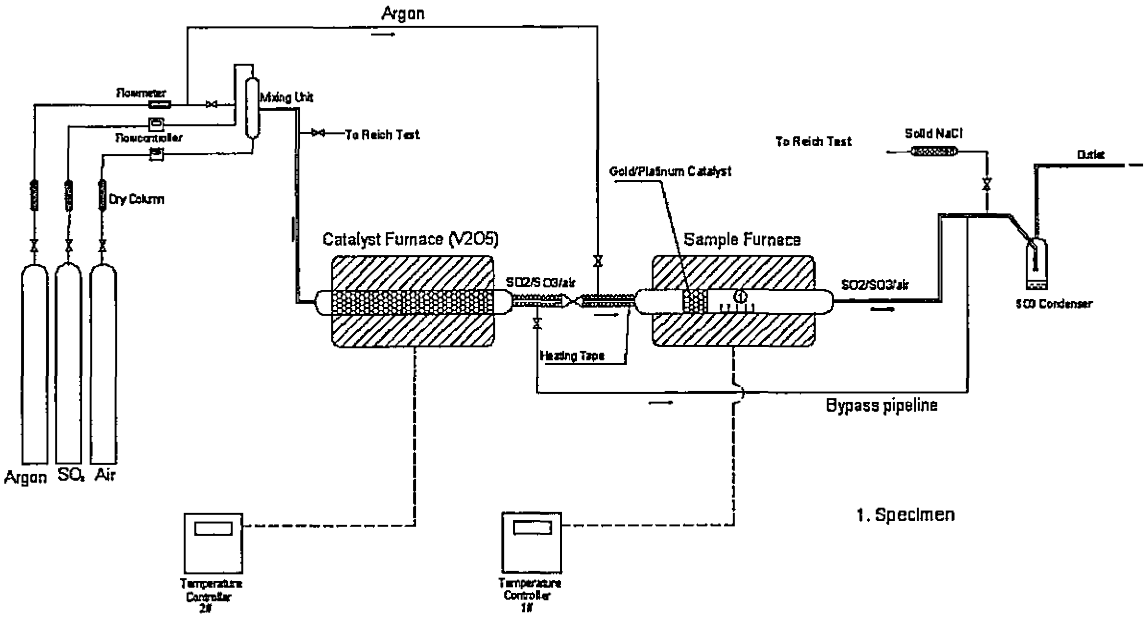

Figure. 6.2 Modified discontinuous cyclic oxidation test apparatus (for SO_3/SO_2/Air gas mixture)

gas equilibrium is to be achieved in the catalyst furnace. The connection tube between the two furnaces will be heated to above 100°C [16] to avoid SO_3 condensation. The effectiveness of the catalyst furnace has been demonstrated by the Reich Test (Figure 3.1), and the gas equilibrium has been achieved in the catalyst furnace to produce SO_3/SO_2/air gas mixture (the majority of sulfur species is SO_3 in this case) (Figure 3.2). Another catalyst (gold or platinum) will be placed before specimens to compensate for the possible loss of SO_3 when the gas mixture goes into the sample furnace via the connection tube.

In the lab studies of corrosion of metals in $SO_3/SO_2/O_2$ (most under isothermal condition), whether or not a metal sulfate could be formed has been controversial. In the literature, although no strong and convincing evidence was provided, most researchers agreed that a thin outer layer of sulfate could be formed on scale surface. So, it is clear that in the lab experiments, as far as I can find, nobody got a large amount of sulfate as one of main corrosion products. However, from the plant experimental results [31,76-77] (the samples were exposed for 1~3 years to SO_3/SO_2/air gas mixture in the gas converter in sulfuric acid plants), for both 304H and A611 stainless steel samples, a large amount of sulfates (mainly $Fe_2(SO_4)_3$ or /and $FeSO_4$) was found after 1~3 years' exposure in hot gas converter in sulfuric acid production plants. For further research, it should be elucidated why the large amount of sulfate is formed in the plant experiments and whether or not a large or small amount of sulfate could be formed in lab experimental conditions.

6.2.2 Silicon Effect on Adherence of Protective Oxide

Compared to 304H, A611 has high Si content and shows a good cyclic resistance in both air and SO_2-air atmosphere. Whether or not is Si responsible for the good cyclic resistance? And how? In other words, what is the mechanism for A611 showing a good cyclic resistance in SO_2 and/or SO_3 containing atmosphere?

SEM, TEM, SIMS and XPS will be used to obtain extensive information and answer the above questions.

SEM (Scanning Electron Microscopy) will be used for the analysis of morphology of exposed A611 samples.

TEM (Transmission Electron Microscopy) will be mainly used for the analysis of the scale/alloys interface of A611 after exposure to SO_2-air or SO_3/SO_2/air gas mixture to find out the distribution of the possible SiO_2 at the interface.

SIMS (Secondary Ion Mass Spectrometry) will be used to determine the depth profiling of oxide scale formed on A611 after exposure, especially to find out the distribution of Si across the scale and the interface

XPS (X-ray Photoelectron Spectroscopy) will be used to determine chemical state information from the outermost atom layers of scales on the exposed A611, mainly for the identification of possible sulfates.

6.2.3 Internal Oxidation and Sulfidation of 304H after Breakaway

Thermal cycling eventually lead to loss of the protection of stainless steels, and the stainless steels will undergo simultaneous internal oxidation and sulfidation within alloy substrate during post-breakaway corrosion. This has been observed in exposed 304H in the experiments, especially at 720°C. The internal oxidation and sulfidation will dominate after breakaway corrosion, especially during long period exposure in practical applications. To elucidate overall corrosion mechanism of stainless steels (especially 304H), it is of interest and practical significance to investigate the simultaneous internal oxidation and sulfidation:

(1) To find out the kinetics of internal precipitates (oxide and/or sulfide) within alloy substrate (penetration depth vs exposure time)

(2) To find out the morphology and distribution of internal oxides and internal

sulfides within alloy substrate. SEM and /or TEM will be used for this purpose.

(3) Although complex, it is of interest to do some mathematical treatment of simultaneous internal oxidation & sulfidation of 304H, which could be used to evaluate the internal precipitation kinetics.

6.2.4 Critical Temperature Drop Test

Spalling greatly contribute to the breakdown of protective oxide scale. Although it will not be a priority, testing of the critical temperature drop to initiate spalling, ΔT_c, would help provide information for evaluating adherence of protective oxide scale and to understand spalling and breakaway corrosion mechanism. Following ΔT_c can be determined:

- ΔT_c in air
- ΔT_c in SO_2 +air atmosphere

APPENDIX I

PLANT EXPERIMENTAL RESULTS

In field experiments, in the SO_3/SO_2/air gas mixture (the majority of sulfur containing species is SO_3) in hot gas converters the samples were exposed for 1~3 years. Corrosion kinetics in term of weight loss of 304H and A611 is given in Figure A, B respectively. Both 304H and A611 underwent a breakaway corrosion, but it is hard to know when the breakaway, the loss of protection, took place during the long time exposure in plants. Compared to A611, 304H shows a higher corrosion rate. Although, for 304H, the corrosion rate at 525°C is higher than that at 430°C, generally, the corrosion rate of the alloys increases with temperature, and this was also confirmed by this studies. In lab experiments, although no breakaway corrosion observed on A611 (short exposure time might be the reason), breakaway corrosion occurred on 304H at both 620 °C and 720 °C.

ESEM image of exposed 304H and A611 is given in Figure C, D respectively. XRD analysis of scales from the exposed 304H and A611samples showed that the scales are composed mainly of iron oxides and iron sulfates [31,76-77]. However no large amount of sulfate was found by XRD in this studies and the literature.

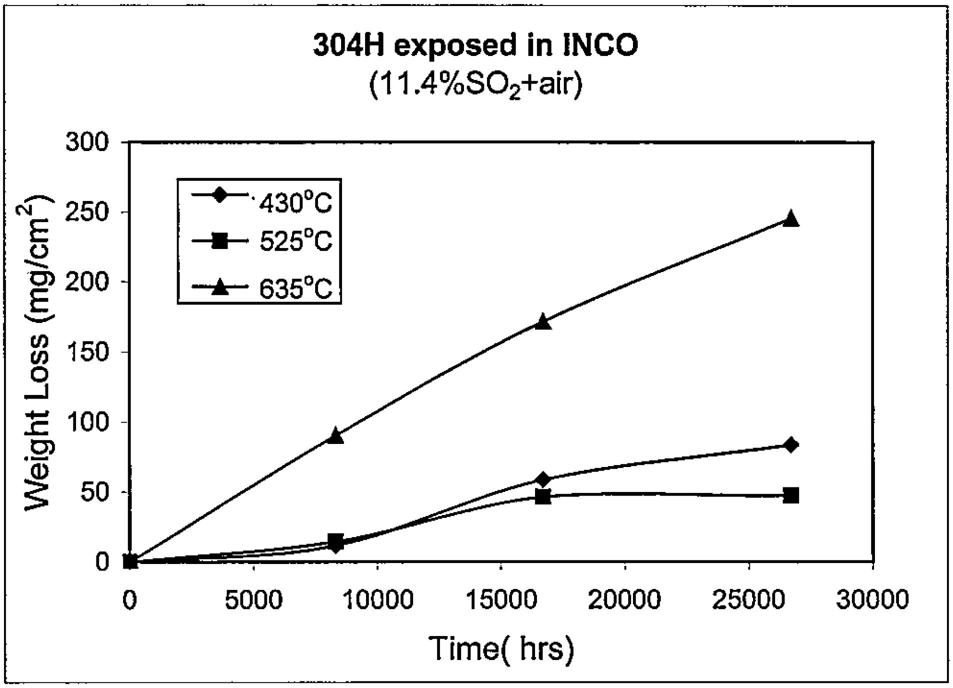

Figure A. Weight loss vs time for 304H exposed at INCO (11.4%SO_2+air)[31]

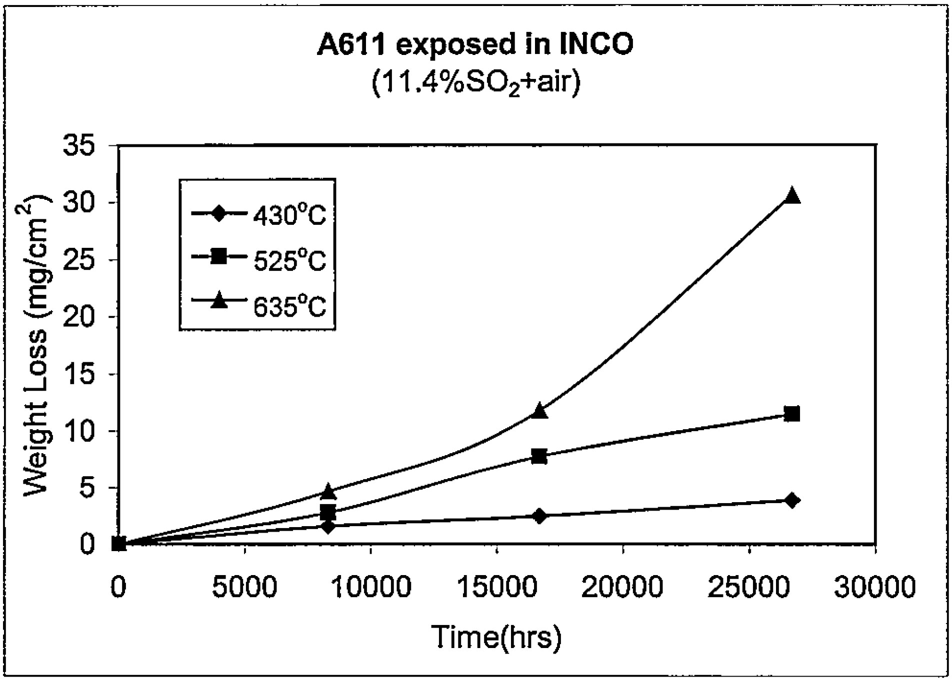

Figure B. Weight loss vs time for A611 exposed at INCO (11.4%SO_2+air)[31]

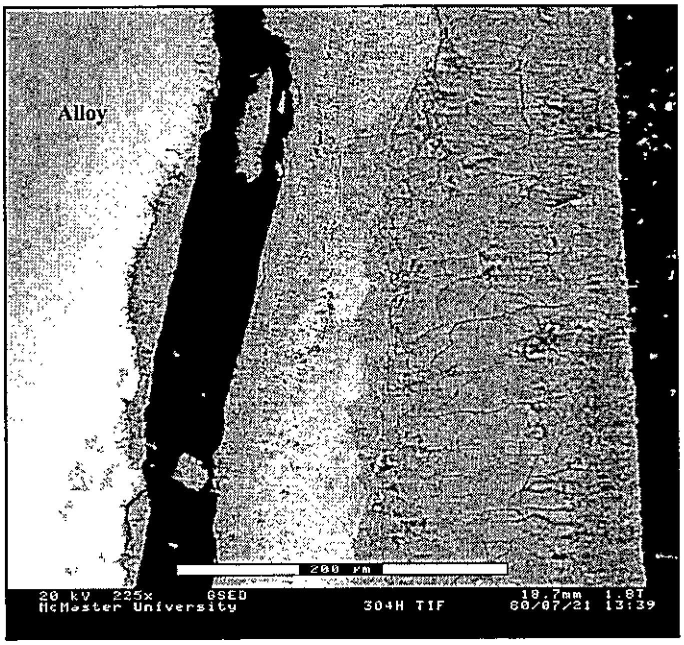

Figure C. 304H exposed at INCO for 1year (640 °C) [77]

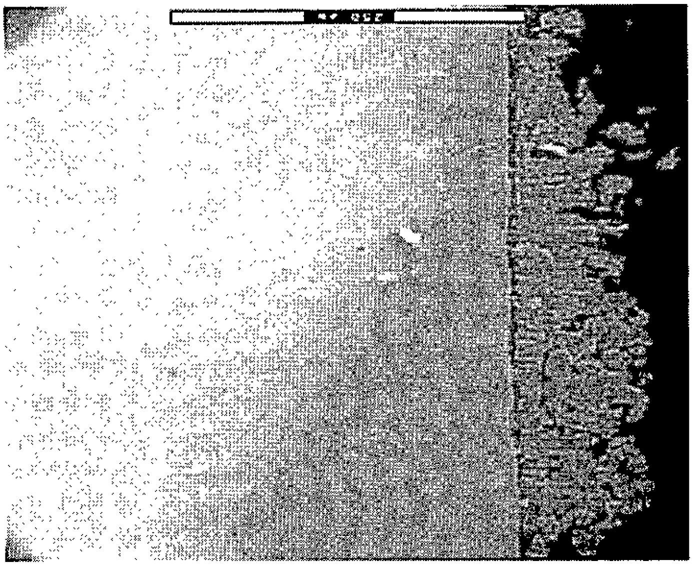

Figure D. A611 exposed at INCO for 1year (640 °C) [31]

REFERENCES

1. **M.Walter, M.Schutze, and A. Rahmel**, Behavior of Oxide Scales on 12Cr-1Mo Steel During Thermal Cycling, Oxidation *of Metals, Vol.39, Nos.5/6,1993, p389~411*

2. **F.J.Pérez, M.J.Cristóbal, and M.P.Hierro**, High Temperature Oxidation Studies of Low-Nickel Austenitic Stainless Steel. Part II: Cyclic Oxidation, *Oxidation of Metals, Vol.55, Nos.1/2,2001, p165~175*

3. **J.R.Nicholls and M.J. Bennett**, Cyclic Oxidation—Guidelines for test standardization, aimed at the assessment of service behavior, *Materials at High Temperatures, 17(3), 2000,p413~428*

4. **D. L. Deadmore and C. E. Lowell**, The effect of ΔT (Oxidizing Temperature Minus Cooling Temperature) on Oxide Spallation, *Oxidation of Metals, Vol. 11, No.2, 1977*

5. **S.H. Choi and J.Stringer**, The breakaway corrosion of Fe-Cr alloys in atmospheres containing sulphur and oxygen, *Materials Science and Engineering, 87 (1987) 237-242*

6. **A. Holt and P.Kofstad**, High Temperature Corrosion of Iron in $O_2+4\%SO_2/SO_3$ at 500~800°C, *Materials Science and Engineering, 1989,A120, p101-104*

7. **K.P. Lillerud, B.Haflan, and P.Kofstad**, On the Reaction Mechanism of Nickel with SO_2+O_2/SO_3, *Oxidation of Metals, Vol. 21, Nos. 3/4, 1984*

8. **B. Haflan, and P. Kofstad,** The reaction of Nickel with SO_2+O_2/SO_3 at 500~900°C, *Corrosion Science, Vol.23, 1983,p1333~1353*

9. **C.B. Alcock, M.G. Hocking, and S. Zador**, The Corrosion of Ni in $O_2 + SO_2$ Atmospheres in The Temperature Range 500-750°C, *Corrosion Science, Vol.9, 1969, p111-120*

10. **K.L. Luthra and W.L.Worrell**, Simultaneous Sulfidation-Oxidation of Nickel at

603 °C in SO_2-O_2-SO_3 Atmospheres, *Metallurgical Transactions A, Vol.10A,1979, p621-630*

11. **V.Vasantasree and M.G. Hocking,** Hot Corrosion of Ni-Cr Alloys in SO_2/O_2 Atmospheres –1. Kinetics, *Corrosion Science, 1976,Vol.16, p261-277*

12. **M.G. Hocking and V.Vasantasree**, Hot Corrosion of Ni-Cr Alloys in SO_2/O_2 Atmospheres –2. Visual Observations, Analyses and mechanisms, *Corrosion Science, 1976,Vol.16, p279-295*

13. **D.M. Rishel, F.S.Pettit, and N.Birks,** Erosion and Corrosion of Nickel in Sulphurous Atmospheres, *High Temperature Science, Vol.27, 1990,P393~411*

14. **A. G. Andersen, and P.Kofstad,** Reaction of Chromium in SO_2-Cintaining Atmospheres, *Oxidation of Metals, Vol. 43, Nos. 3/4, 1995, p301~315*

15. **A.K.Roslik, V.N.Konev, and A.M.Maltsev**, Some Aspects of the Mechanism of High Temperature Oxidation of Nickel in SO_2, *Oxidation of Metals, Vol. 43, Nos.1/2, 1995,P59~82*

16. **K.L. Luthra**, Corrosion of Nickel in Mixed Sulfidizing-Oxidizing Gas Atmosphere at Elevated Temperatures, *Ph.D. Dissertation, University of Pennsylvania,1976*

17. **P.S.Sidky and M.G.Hocking**, The Hot Corrosion of Nickel-Based Ternary Alloys and Superalloys for Gas Turbine Applications-I. Corrosion in SO_2/O_2 Atmospheres, *Corrosion Science, Vol.27, No.2, 1987, p183-203*

18. **M.G.Hocking and P.S.Sidky**, The Hot Corrosion of Nickel-Based Ternary Alloys and Superalloys for Gas Turbine Applications-II. The Mechanism of Corrosion in SO_2/O_2 Atmospheres, *Corrosion Science, Vol.27, No.2, 1987, p205-215*

19. **H.Xu, M.G. Hocking, and P.S.Sidky,** Sulphidation-Oxidation Behavior of a Ni-Co-Cr-Si Alloy in an SO_2+O_2 atmosphere, *Oxidation of Metals, Vol. 39, Nos.5/6, 1993,P371~388*

20. **E.Otero, A.Pardo, F.J.Pérez, F.J.Perosanz, A.Parra and T.Levi,** Corrosion of Several Steels after their Exposure at High Temperature to Oxygen and Sulfur Mixtures, *Materials Science Forum, Vols. 251-254, 1997, p615~624*

21. **H.Xu, M.G. Hocking, and P.S.Sidky,** Sulfidation-Oxidation Behavior of Alloy 800H in SO_2-O_2 and H_2-H_2S-CO-CO_2 Atmosphere, *Oxidation of Metals, Vol. 41, Nos. 1/2, 1994,P81~101*

22. **B.Gleeson and M.A. Harper,** The Long-Term Cyclic Oxidation Behavior of Selected Chromia –Forming Alloys, *Oxidation of Metals, Vol. 49, Nos. 3/4, 1998*

23. **C.O.Moon and S.B. Lee,** Analysis on Failures of Protective-Oxide Layers and Cyclic Oxidation, *Oxidation of Metals, Vol. 39, Nos.1/2, 1993*

24. **J. A. Nesbitt,** Scale Formation on Ni-Basae Alloys- II. Cyclic Oxidation, *J.Electrochem.Soc.,Vol.136,No.5, May 1989, P 1518~1527*

25. **D. E. Alman** et al, Improved Austenitic Steels for Power Plant Applications, *U.S. Department of Energy, Albany Research Center, 2002*

26. **J.S.Dunning, D.E.Alman, and J.C.Rawers**, Influence of Silicon and Aluminum Additions on the Oxidation Resistance of a Lean-Chromium Stainless Steel, *Oxidation of Metals, Vol. 57, Nos. 5/6, 2002,P409~425*

27. **L.Antoni,** Comparison of the Cyclic Oxidation Behavior between AISI 304H and Low-Nickel Austenitic Stainless Steels, *Materials Science Forum, Vols.369-372 (2001), p 345~352*

28. **C. A. Barrett and C. E. Lowell,** Comparison of Isothermal and Cyclic Oxidation behavior of Twenty-Five Commericial Sheet Alloys at 1150°C, *Oxidation of Metals, Vol. 9, No.4, 1975,P307~354*

29. **C. A. Barrett and C. E. Lowell,** The Cyclic Oxidation Resistance of Cobalt-Chromium-Aluminum Alloys at 1100 and 1200°C and a Comparison with the Nickel-Chrium-Aluminum Alloys System, *Oxidation of Metals, Vol. 12, No.4, 1975,P293~311*

30. **S.N.Basu and G.J. Yurek**, Effect of Alloy Grain Size and Silicon Content on the oxidation of Austenitic Fe-Cr-Ni-Mn-Si Alloys in a SO_2-O_2 Gas Mixture, *Oxidation of Metals, Vol. 35, Nos.5/6, 1991,P441~469*

31. Development of Improved Materials for Sulphuric Acid Production [NSERC-CRD 2rd Report], *The Walter W.Smelzter Corrosion Laboratory, McMaster University, January 16, 2002, Internal Report*

32. **P. Kofstad**, High Temperature Corrosion, (Elsevier Applied Sience, Lodon and New York 1988)

33. **C. Wagner**, Diffusion and High Temperature oxidation of Metals, *Atom Movements, American Society for Metals,Cleveland,Ohio, P153~173, 1951*

34. **H.E.Evans**, Stress effects in high temperature oxidation of metals, *International Materials Reviews, 1995,Vol.40, No.1*

35. **H.E.Evans and R.C. Lobb**, Conditions for The Initiation of Oxide-Scale Cracking and Spallation, *Corrosion Science, Vol.24, 1984,p209-222*

36. **A.J. Sedriks**, Corrosion of Stainless Steels, A Wiley-Interscience Publication, *1979*

37. **G.C. Wood**, The Oxidation of Iron-Chromium Alloys and Stainless Steels at High Temperatures, *Corrosion Science, Vol.2, 1962, P173~183*

38. **G.C.Wood , M.G.Hobby and B. Vaszko**, Electron Probe Microanalysis of a Nodular Scale Growth on an Austenitic Stainless Steel, *Journal of The Iron and Steel Institue,Vol.203, P685~695,1964*

39. **M.E. Evans, A.T.Donaldson, and T.C.Gilmour**, Mechanism of Breakaway Oxidation and Application to a Chromia-Forming Steel, *Oxidation of Metals, Vol. 52, Nos. 5/6, 1999,P379~402*

40. **P.Sigh and N.Birks**, Penetration of Sulphur Through Preformed Protective Oxide Scales, *Oxidation of Metals, Vol. 19, Nos. 1/2, 1983, p37~52*

41. **P.Kofstad and G. Akeson**, High Temperature Corrosion of Nickel in SO_2, *Oxidation of Metals, Vol. 12, Nos. 6, 1978,p503~527*

42. **T. Flatley and N.Birks**, Oxidation of Iron in Atmospheres Containing Sulphur Dioxide, *Journal of Iron and Steel Institute, July 1971, P523*

43. **R.P.Salisbury and N.Birks**, Oxidation of Iron-Chromium Alloys in Sulphurous Atmospheres, *Journal of The Iron and Steel Institute, July 1971,Vol.209, p534~540.*

44. **K.N. Stafford, and P.J.Hunt,** The Mechanism of Transport of Sulphur Across Scales and The Corrosion of Materials in Bi-Oxidant Oxygen-Sulphur Environment, *High Temperature Corrosion, March 2-6,1981,San Diego, California, P 380~386*

45. **J.Gilewicz-Wolter and M.Ciechanowski**, Transport of Sulphur in the Scale growing on Nickel in Sulphur Dioxide Atmosphere at 873K, *Oxidation of Metals*, Vol. *34, Nos. 1/2, 1990,p151~159*

46. **M.C.Pope and N.Birks**, The Penetration by Sulphur of NiO Scales Growing on Nickel, *Oxidation of Metals, Vol.12, No.2, 1978, p173~181*

47. **M.C.Pope and N.Birks**, Sulphur Solubility of NiO and CoO at 1000°C, *Oxidation of Metals, Vol.12, No.2, 1978, p191~204*

48. **A. Rahmel**, The Scaling of iron in Oxygen and Sulphur Containing gases, *Oxidation of Metals, Vol. 9, No. 5, 1974, P401-409*

49. **J. Gilewicz-Wolter and Z.Zurek**, Corrosion of Iron in Sulphur Dioxidae at 0.1MPa, *Oxidation of Metals, Vol. 45, Nos. 5/6, 1996*

50. **J.Gilewicz-Wolter**, Study of Iron Oxidation in Sulphur Dioxide Atmospheres by Means of the ^{35}S Radioisotope, *Oxidation of Metals, Vol. 11, No. 2, 1977*

51. **M.F. Stroosnijder and W.J. Quadakkers**, Review of High temperature Corrosion of Metals and Alloys in Sulphidizing/Oxidizing Environments: I. Corrosion of Metals, *High Temperature Technology, Vol.4, No.2, May, 1986, P83~96*

52. **M.F. Stroosnijder and W.J. Quadakkers**, Review of High temperature Corrosion of Metals and Alloys in Sulphidizing/Oxidizing Environments: I. Corrosion of Alloys, *High Temperature Technology, Vol.4, No.3, August, 1986, P141~151*

53. **S.K.Verma,** Oxidation/Sulphidation Behavior of Some Ferritic Stainless Steels in High Temperature Coal Gasification Atmospheres, *Ferritic Steels for High Temperature Applications, 1983*

54. **R. A. Rapp,** Kinetics, Microstructures and Mechanism of Internal Oxidation-Its Effect and Prevention in High temperature Alloy Oxidation, *Corrosion, Vol.21, 1965, p382~401*

55. **F. Gesmundo and F. Viani,** Transition from Internal to External Oxidation for Binary Alloys in the Pressure of an Outer Scale, *Oxidation of Metals, Vol. 25, Nos. 5/6, 1986,P269~283*

56. **P.C. Patnaik**, High Temperature Sulfidation Properties of Fe-Al Alloys, *Ph.D. Dissertation, McMaster University, Feb. 1984*

57. **L.Meijering**, Internal oxidation in Alloys, *Adances in Materials Research, vol.5, edited by H.Herman, Wiley, New York, 1971, p1~81*

58. **F.Gesmundo, and Y.Niu,** The Formation of Two Layers in The Internal Oxidation oc Binary Alloys by Two Oxidants in The Absence of External Scales, *Oxidation of Metals, Vol. 51, Nos. 1/2, 1999,P129~157*

59. **D.J. Young**, Internal Oxidation Processes Under Non-ideal Conditions, *Materials at High Temperatures, 17(4) 465~470*

60. **S.Han and D.J. Young**, Simultaneous Internal Oxidation and Nitridation of Ni-Cr-Al Alloys, *Oxidation of Metals, Vol. 55, Nos. 3/4, 2001,P223~242*

61. **M.Udyavar and D.J.Young**, Precipitate Morphologies and Growth Kinetics in

The Internal Carbonization and Nitridation of Fe-Ni-Cr Alloys, *Corrosion Science,Vol.42, 2000,p861-883*

62. **D.J. Young and S.Watson,** High temperature Corrosion in Mixed gas Environments, *Oxidation of Metals, Vol. 44, Nos. 1/2, 1995,P235~265*

63. **S.W.Guan,** Ph.D thesis, McMaster University, 1993

64. **S.W.Guan, H.C.Yi, and W.W.Smeltzer**, Internal Oxidation Alloys. Part I: Kinetics in the Absence of an External Scale, *Oxidation of Metals, Vol. 41, Nos. 5/6, 1994,P377~387*

65. **S.W.Guan, H.C.Yi, and W.W.Smeltzer**, Internal Oxidation Alloys. Part II: Kinetics in the Presence of an External Scale, *Oxidation of Metals, Vol. 41, Nos. 5/6, 1994,P389~401*

66. Standard Methods of Chemical Analysis, Vol.2, 5th Edition by N.Howell Furman, D.Van Nostrand Company Inc. New York, p 2399~2402, 1939(reprinted in 1945)

67. **A. Y. Borisevich**, Analysis of Phase Distribution in the Li_2O-Nb_2O_5-TiO_2 system by piezoresponse imaging, *J. Mater. Res., Vol.16, No.2, Feb 2001, p329-332*

68. **J.Gilewicz-Wolter and Z.Żurek,** Mechanism of Chromium Oxidation in SO_2 at 3×10^4Pa and 10^5Pa, *Oxidation of Metals, Vol. 58, Nos.1/2, 2002,P217~233*

69. **P. W. Schenk and R. Steudel**, Oxides of Sulphur, Inorganic Sulphur Chemistry (edited by G. Nickless), *Elsevier Publishing Company, 1968, P367~418*

70. **A.M.Huntz, M.K.Loudjani, C.Séverac, C.Haut and F.Ropital**, Effect of Silicon on the Protective Character of Cr_2O_3 Scales Analysis by "In Situ" XPS, *Materials Science Forum, Vols.251-254 (1997), p 243~250*

71. **J.F. Norton, M. Maier and W.T. Bakker,** The Influence of Si Content Upon the Corrosion Resistance of Fe-12%Cr and Fe-12%Cr-12%Ni Alloys Exposed in a Reducing/Sulphidising Atmosphere at 450°C, *Materials Science Forum,*

Vols.251-254 (1997), p 607~614

72. **H.E.Evans, D.A.Hilton, R.A.Holm, and S.J.Webster,** Influence of Silicon Additions on the Oxidation Resistance of a Stainless Steel, *Oxidation of Metals, Vol. 19, Nos. 1/2, 1983,P1~18*

73. **A.Kumar and D.L.Douglass**, Modification of the Oxidation Behaviour of High-Purity Austenitic Fe-14Cr-14Ni by the addition of Silicon, *Oxidation of Metals, Vol. 10, No. 1, 1976,P1~23*

74. **G.C.Wood and M.G.Hobby**, Compostion Changes During the Healing of Oxide Scales on an Austenitic Stainless Steel, *Journal of The Iron and Steel Institue,Vol.203 ,1965, P54~63*

75. **G.C.Wood and M.G.Hobby**, Composition Changes During the Healing of Oxide Scales on an austenitic Stainless Steel, *Journal of The Iron and Steel Institue,Vol.203, P54~63,1965*

76. Improved Materials for Sulphuric Acid Production [NSERC-CRD Project, 3rd Report], *The Walter W.Smelzter Corrosion Laboratory, McMaster University, February, 2003, Internal Report*

77. Improved Materials for Sulphuric Acid Production [NSERC-CRD Project, 1st Report], *The Walter W.Smelzter Corrosion Laboratory, McMaster University, January, 2001, Internal Report*

78. **S. J. B. Reed**, Secondary Ion Mass Spectrometry, Analysis of High Temperature Materials (edited by O.Van Der Biest), *Applied Science Publishers, London and New York, 1983, p129~140*

79. **T. A. Carlson**, X-ray Photoelectron Spectroscopy, *Dowden, Hutchingson & Ross Inc., 1978*

80. http://www-personal.engin.umich.edu/armoore/SIMS.html
81. http://www.uwo.ca/ssw/services/SIMS.html
82. http://www.mcpf.ust.hk/surface/xpsmain.htm